Testing the New Applications of Luminescence Dating in Archaeology.

Dissertation

zur Erlangung des Doktorgrades eingereicht

am Fachbereich Geschichts- und Kulturwissenschaften der Freien

Universität Berlin

im Jahr 2015

vorgelegt von

Sahar al Khasswneh

aus Irbid- Jordanien

Hiermit versichere ich, Sahar al Khasswneh, dass die vorliegende Arbeit mit dem Title, Testing the New Applications of Luminescence dating in Archaeology, selbstständig und ohne Benutzung anderer als der von mir angegebenen Hilfsmittel verfasst habe. Alle Stellen, die wortgenau oder sinngemäß aus anderen Veröffentlichungen entnommen sind, sind als solche kenntlich gemacht. Vorliegende Studie hat noch keiner an andern Stellen als akademische Abschlussarbeit vorgelegen.

Sahar al Khassawneh
Berlin, den 01.10.2015

1. Gutachter: Prof. Dr. Dominik Bonatz

2. Gutachter: Prof. Dr. Andrew S. Murray

Eingereicht am: 01.10.2015
Tag der Disputation: 16.12.2015

"No man is poor who has a Godly mother."

to my mother

Acknowledgment

First of all, I would like to express a profound gratitude to Prof. Domonik Bonatz for his supervision, encouragement and advice throughout all the stages of my work. His continuous support and motivation were prime factors to achieve my PhD thesis.

My deepest gratitude to Prof. Andrew Murray for giving me a full access to the laboratory and research facilities in Nordic Laboratory for the last two years. During that time, I had the chance to wok closely with Prof. Murray; he showed me all the encouragement and patience by responding to all my questions and queries so promptly. He motivates, updates and supports the new ideas in OSL, opening a door to creativity and ingenuity by inspiring students and young researchers, then presenting them to the scientific community. I am lucky to have the chance to wok with him.

The major part of this work took place in Nordic Laboratory for Luminescence Dating and DTU Nutech department at Risø campus; gratitude and thanks to every member of the laboratory and Neutech department with no exception. Special thanks go to Kristina Thomsen for her huge effort in single grain measurements.

This Phd project is an awarded grant from the faculty of Archaeology- Yarmouk University, Jordan; therefore, I would like to thank prof. Ziad al Sa'ad, Prof. Zeidan Kafafi and Mrs Sana'a al Khasawneh.

My thanks also go to Prof. Stephen Bourke, Dr. Hans Gebel, Michel Vinter, Mohamad Tarawneh and Wael Abu Azizeh, for providing me with the samples that are used in this study and for the useful discussions I had with every one of them.

Abstract

With recent major improvements in luminescence dating resulting from new developments in methodology and instrumentation, luminescence dating has become a much more powerful chronometric tool. These new developments have been widely used in geological applications, but there are very few publications testing their applicability in archaeology. This study aims to test the applicability of two major new techniques in luminescence dating to archaeological problems. In the first part, we report the first application of using the stable infrared stimulated luminescence signal measured at elevated temperature (290^{o}C) to pottery samples from Pella, Jordan. The average Optically Stimulated Luminescence (OSL) age is 2850±220 (n=35) years, with the overall uncertainty dominated by systematic uncertainties; this agrees well with the range of ^{14}C ages of 2970 to 3270 cal. years BP for the same destruction horizon.

The method is also applied to the dating of young heated artefacts from three different archaeological sites in Denmark, one from the early Pre-Roman Iron Age 200 BC to AD 100, and two from the Viking period between AD 800 and 1200. No previous radiometric dating has been reported for these sites. Quartz OSL ages were derived to support the archaeological associations, and compared to the new feldspar ages. On average, there may be a small overestimation of feldspar ages compared to those from quartz, but if so it is only of significance for the heated stone samples.

The second part of the research investigated of the application of OSL dating to sediment deposition in the arid zone directly resulting from human activities (well digging and construction of irrigation channels). Quartz and feldspar luminescence signals were both measured to provide two estimates of luminescence ages, and both ages are in agreement with each other, and with the archaeological assumption of the site age.

In the last part, a very recently developed technique, rock-surface dating, was applied to a three rocks sampled from the Jibal al-Gadiwiyt kite structure in

southern Jordan. By examining the resetting of OSL with depth and time, this approach was able to provide detailed information about the burial and light-exposure history of the rock. The derived construction and burial ages (based on rock-surface dating but confirmed by sediment dating) are ~10,000 years; considerably older than the archaeologically assumed age of 6000 years.

By using a variety of archaeological sites, this study demonstrates the immediate usefulness and future potential of recent developments in OSL dating. The accuracy of these and other luminescence dating methods, and the ability of luminescence to date otherwise undateable material, opens up many new and exciting opportunities in archaeology for the future.

Kurzfassung

Neueste Verbesserungen der Lumineszenzdatierung. Dank neuer Entwicklungen der Methodik und Instrumentierung ist die Lumineszenzdatierung zu einem noch weit leistungsfähigeren Werkzeug der Chronometrie geworden. Die neuen Entwicklungen wurden weithin für geologische Materialien verwendet, jedoch befassen sich nur wenige Studien mit der Frage der Anwendbarkeit dieser letzten Entwicklungen in der Archäologie. Die vorliegende Untersuchung hat zum Ziel, Anwendbarkeit der neuen Techniken der Lumineszenzdatierung in der Archäologie zu testen. Im ersten Teil berichten wird über die erste Anwendung des bei hoher Temperatur (290°C) gemessenen stabilen infrarot-stimulierten Lumineszenzsignals auf Keramikproben. Das mittlere OSL-Alter (mittels Optisch Stimulierter Lumineszenz ermitteltes Alter) wurde mit 2850 $\pm$ 220 bestimmt, wobei die allgemeine Unsicherheit von systematischen Unsicherheiten dominiert wird; dies steht in Einklang mit dem Bereich der ^{14}C-Alter zwischen 2970 und 3270 kalib. Jahre (cal years) für denselben Zerstörungshorizont.

Die Methode wurde auch für die Datierung junger, erhitzter Artefakte aus Dänemark verwendet. Es wurden Proben aus drei verschiedenen Ausgrabungsstätten in Dänemark genommen: eine aus der frühen vorrömischen Eisenzeit (200 v. Chr. bis 100 n. Chr.) und zwei aus der Wikingerzeit (zwischen 800 und 1200 n. Chr.). Berichte über frühere Strahlungsmessungen an diesen Stätten liegen nicht vor. Es wurden Quarz-OSL-Alter ermittelt und mit Feldspat-Altersbestimmungen verglichen. Es gibt Hinweise darauf, dass die mögliche Überbewertung der Feldspat-Alter verglichen mit Quarz nur für die erhitzten Gesteinsproben von Bedeutung ist.

Im zweiten Teil wurde die Anwendung der OSL-Datierung auf durch menschliche Aktivitäten verursachte aride Sedimentablagerungen untersucht. Quarz und Feldspate wurden mit Standardmethoden der Lumineszenzdatierung gemessen. Beide Altersbestimmungen stehen im Einklang mit der archäologischen Altersannahme für die Ausgrabungsstätte.

Schließlich befasste sich die Studie mit der Technik zur Datierung von Gesteinsoberflächen anhand einer Desert Kite Structure (Trockenmauerbauwerk in der Wüste)im Südosten Jordaniens. Das Wissen über die Geschichte dieser Bauwerke ist bruchstückhaft und die Anwendung einer Datierungsmethode fällt schwer, weil die ^{14}C-Datierung wegen des Fehlens von organischem Material nicht verfügbar ist; ebenso fehlen Artefakte, die für eine entsprechende Datierung verwendet werden könnten.

Table of Contents

List of Figures

List of Tables

Abbreviations

a	annus (Latin word for year).
ka	kilo annus (=1000 years).
Gy	Gray, unit of radiation dose.
s	Second, time unit.
D_e	The equivalent dose in unit Gray.
SAR	Singe Aliquot Regeneration.
SAAD	Single Aliquot Additive Dose.
L_i	OSL signal from the natural and the regenerative dose in SAR protocol.
T_i	OSL signal from the tests dose in SAR protocol.
^oC	Celsius or centigrade, unit of measurement for temperature.
IR	Infrared light
IRSL	Infrared Stimulating Light.
IR_{50}	First detected signal after stimulation by Infrared light at 50 ^oC
$pIRIR_{290}$	Second detected signal after stimulation by Infrared light at 290 ^oC
K-feldspar	Potassium feldspar.
CAM	Central Age Model. (*Statistical model for D_e distribution in single grain measurement*)
MAM	Minimum Age Model. (*Statistical model for D_e distribution in single grain measurement*)
IEU	Internal- External Uncertainty. (*Statistical model for D_e distribution in single grain measurement*)
L(x)	The luminescence intensity at depth x for rock surface
x	Depth into the rock, mm
t_e	Time exposure of the rock, ka
t_b	Time of burial for rock surface, ka
μ	The light attenuation coefficient (cm^{-1}) in the rock
$\overline{\sigma\varphi o}$	Trap-emptying rate at the surface of a rock

D_o	Rate of fillings for luminescence traps, Gy
^{232}Th	Thorium-232, one of Thorium isotope
^{238}U	Uranium-238, one of Uranium isotope
^{40}K	Potassium-40, a radioactive isotope of potassium
^{60}Co	Cobalt-60, is a synthetic radioactive isotope of cobalt.
HCL	Hydrochloric acid
H_2O_2	Hydrogen peroxide
HF	Hydrofluoric acid

1. Chapter 1: Introduction and study outline

Chronometry is an essential part of archaeology. It provides a meaningful understanding of human evaluation by relating events and objects within a timescale. Archaeologists are able to define the space dimension of any archaeological object by associating it to its location. But to derive the time dimension of the same object is almost always a challenging task, because it is an indirect process. Errors in chronology lead directly to misinterpretations in narrating the past. Thus the accuracy and uncertainty of any given date are of direct concern to every archaeologist.

Several methods have been developed in this field, falling into two groups: *relative dating* and *absolute dating* methods.

Before the 20th century, relative dating methods were the only available means for dating used by archaeologists and geologists. These were largely based on the ordering events and locations of prehistory sites in sequential order without defining any specific ages. *Stratigraphic dating (the Law of Superposition, attributed to Steno in 'Dissertationis prodromus' from 1669)* relies on interpreting the significance of geological or archaeological strata. Stratigraphic dating assumes that because of natural depositional processes, sediments and other materials found deeply buried will have been laid down earlier—and therefore are older—than superimposed materials. Detailed drawings and stratigraphic descriptions (section profile) from one location can then be compared with other profiles from surrounding sites to establish lateral chronological connections. Geological stratigraphy usually neat and not disturbed, but this doesn't apply to archaeological stratigraphy. Human activities may disturb the early layers such digging for the foundation of new constructions, reuse of the soil or agriculture activity, this may cause bring objects from older layers like ceramics shards to earlier layers.

Seriation is an archaeological technique based on the description of stylistic changes in artefacts and of changes in the popularity of distinct styles in order to

accurately describe the sequence of variation over time. The seriation of stratified deposits permits archaeologists to assess the relative age of particular styles. This information may then be used to assume the relative age of unstratified deposits (e.g. surface sites or tombs). Flinders Petri is the first to establish *Seriation* in his work on the Egyptian tombs (Petrie, 1899), (Kendall, 1969).

Ceramic typology is another widely used technique for relative dating; ceramics are classified based on physical characteristics and so different assemblages can be compared. This system also provides a basis of identifying locally produced and imported ceramics and their approximate source area.

Petri notified in the late of the nineteenth century to the importance of pottery typological change with stratigraphic changes; he tested his theory on Tell el-Hesi in Palestine (Petrie W., 1891) and on other sites such as Tell Jemmeh (1926–1927), Tell el-Farah (1928–1930). Albright had established standard pottery typology mostly based on his work on Tell Beit Mirsim in 1920's for the Levant (Albright, 1931, 1932). Kenyon excavation in Jericho had developed the basis of stratigraphic divisions in excavations with its links to pottery typology (Kenyon, 1957 and 1971) (Lapp, 1961) (Herr, 2002).

There are many other less widely used relative dating methods, e.g. *obsidian hydration* for glassy materials and *fluoride measurements* for bones. Absolute dating, on the other hand, allows accurate historical reconstruction and provides direct insight into culturally significant periods by providing ages measured in calendar years. The earliest methods of absolute dating were based on analysis of historical records (e.g. inscriptions, manuscripts, and coins). But such information is not always available, even in the historical period, and in the twentieth century other methods began to be developed to measure ages directly from the material of interest. These new techniques use a variety of physical and chemical measurements to establish the time when materials and objects were made, used or changed. *Dendrochronology* was one of the first absolute chronometric techniques to be developed. This uses variations in the thickness of tree

rings to determine age by comparison with known age tree ring records; the ages range varies according to the region and knowledge of climate history. It is one of the most accurate methods in dating (in principal it can date to within 1 year, independent of the length of the record), but its main drawback is the scarcity of suitable material in archaeological deposits, and its dependence on a continuous record going back to the period of interest based on relatively long-lived vegetation with annual growth rings. In addition, annual rainfall is a regional climatic event, and so tree ring records are strongly affected by the region. Nevertheless, the International Tree Ring Database has contributions from 21 different countries and this is main source for calibration of the ^{14}C dating method (see below).

The decay of radioactive elements can also be used to keep track of time, methods developed on this basis are known as radiometric dating methods. The nature of material usually defines the method of dating, and the age range that can be measured. Glassy minerals, such as mica and obsidian, can be dated by the *fission track* method which measured the trail of damages caused by ^{238}U atoms fission within the material (Naeser, 1979), the age range can be back between 20,000 and two billion years ago. The *Potassium–Argon* method relies on the buildup of the Ar isotope ^{40}Ar, following the radioactive decay of ^{40}K, and this method is used to date igneous and volcanic rock and ash; the method requires the complete loss of argon during the heating-recrystallization process (McDougall & Harrison, 1990). It has been widely used to date older materials from a few tens of thousands of years back to as much as 4 billion years old. However recent developments in the method have allowed it to be applied too much younger events; the Pliny eruption of Vesuvius (AD 79) has been dated using a variant of the method ($^{40}Argon/^{39}Argon$) (Renne *et al.*, 1997). The *uranium series* method makes use of the build-up of an isotope of thorium (^{230}Th) following the radioactive decay of the parent ^{238}U. This requires the absence of any thorium isotopes in the solution from which the carbonate is formed, and it is used to date such materials as travertine, marl, coral, mollusc shells, bone, and teeth, which are formed through precipitation processes; its upper age limit is ~500,000 (Ivanovich & Harmon., 1992). All these techniques are suitable for

dating a variety of natural events (mineral heating, precipitation etc.). But from an archaeological perspective these techniques rarely date material directly associated with human activity. Using these methods in archaeology relies on the association of the dated materials and the strata containing human evidence. Nevertheless, they are very important in prehistoric archaeology, and in studies of human evolution and migration.

The most widely used dating method in archaeology is undoubtedly ^{14}C (radiocarbon) dating. The method can be used to determine the age of organic matter that is between a few hundred years to approximately 50,000 years old (about 10 half-lives). The potential of ^{14}C was recognised in the 1940s by Willard Libby and his team (Libby *et al.*, 1949; Ramsey, 1995). The method is based on the radioactive decay of ^{14}C to ^{14}N. The ^{14}C, along with nonradioactive ^{13}C and ^{12}C are converted to carbon dioxide and assimilated by plants and organisms. After death of the organism, the uptake ceases, and the isotope decays with a half life of ~5600 years. A major technological leap in development occurred in the 1980s with the direct counting of ^{14}C atoms on an accelerator mass spectrometer. This has the advantage of very much smaller sample sizes of up to 1,000 times smaller than those used by conventional radiocarbon dating (down to 1-2 milligrams of carbon). As well as reducing the sample size, the new technique also reduces the statistical error involved in the measurement of the concentration of ^{14}C atoms; it is also easier to minimise the effects of contamination using smaller samples. As a result modern ^{14}C ages have smaller counting errors than older results. However, it is important to realise that these errors are only part of the uncertainty if a ^{14}C age is to be expressed in calendar years. This is because the production rate of ^{14}C in the atmosphere has varied through time. This effect must be compensated for by calibration using known age organic material (e.g. tree rings, U-series dated coral). Calibration introduces further uncertainty into a ^{14}C age, and indeed in some periods it is possible for a single ^{14}C count rate to give two possible ^{14}C ages. Nevertheless, archaeologists have largely relied on ^{14}C dates to build the chronology of the prehistory time.

We now move on to so-called trapped electron methods. The first of these is *Thermoluminescence (TL)* dating, developed originally for dating pottery, tiles, bricks and other heated artefacts. TL dating is based on the accumulation of energy as trapped electric charge in crystalline structures. The accumulation of energy arises from the decay of radioactive elements (^{238}U and ^{232}Th and their radioactive daughter products, and ^{40}K); these radionuclides are ubiquitous, and are thus present in all sediments. As a result, they are incorporated into any artefact based on such sedimentary minerals. The emission of alpha and beta particles and gamma radiation creates defects in the crystalline structure of some minerals (e.g. quartz and feldspar), and these defects trap charge carriers (electrons) depending on the size of the absorbed dose of radiation. The charge carriers can be released by heating or exposure to light, and this process is accompanied by the release of the stored energy (some in the form of luminescence) (Aitken, 1985). By combining the measurement of the total amount of stored energy together with a knowledge of the rate of absorption of energy from the natural radiation background, one can derive the time elapsed since last heating.

The accuracy of thermoluminescence dating is generally about 5-10%, if the material was completely reset. The applicable time range overlaps with that of radiocarbon dating, spanning from a few decades back to more than 300,000 years ago, but it is not widely used because of the difficulty of resetting the signal other than by heating. *Optically stimulated luminescence (OSL)* dating is also based on the same dosimetric principles as TL dating, but the advantage of OSL dating lies in the much wider range of material that can be dated - it can be applied both to materials heated to high temperature (e.g. ceramics) and to materials exposed to daylight (e.g. sandy sediments transported by water or wind). For materials which have exposed to light, OSL dating measures the time elapsed since the last exposure to light, prior to burial. As with TL, it overlaps the age range of ^{14}C and has been used to date sediments >500 ka. In younger periods (<20 ka), it is particularly useful when the absence of organic matter

precludes the use of radiocarbon. This study will focus on the use of OSL dating in various archaeological applications.

OSL is now widely used in the geosciences and recent developments in understanding, instrumentation and measurement techniques have improved the accuracy and precision of the method; as a result, it is now considered a very useful chronometric tool in geology and geomorphology for establishing the time of sediment deposition. Despite the fact that the beginning of luminescence dating was developed in the archaeology frame to serve as dating method, and the standard routine methods of luminescence dating had proved its reliability in archaeology, however recently there are few studies in archaeology conducted in which luminescence dating is the focal technique ((Aitken, 1985; Roberts, 1997; Feather, 2003; Wintle, 2008; Bailiff, 2008). In near eastern archaeology, relative dating and ^{14}C are the dominant methods adapted to build the region chronology. The use of luminescence dating has been limited to a few studies that used few ceramics in analysis (al Khasawneh *et al.,* 2011; Bakraji et al., 2011; Bakraji et al., 2013 and Porat *et al.*, 2013).

There are also few luminescence labs that are established as part of archaeological and anthropological institutions to be part of their research works. The most notable of which are The Luminesce Dating Laboratory in the department of Archaeology at the University of Durham (UK) and the Luminescence Dating Laboratory at University of Washington (US).

Based on that, it is proposed that the best approach to advocate the use of new luminescence dating applications in archaeology is to carry an intensive detailed investigation of these techniques in different archaeological contexts.

This study aims to test the application of methods developed recently in luminescence dating to archaeological materials, and to use the methods to resolve some chronological problems for representative archaeological sites that are difficult to date by other radiometric methods, or in situations where luminescence ages can be used to support existing chronological information.

Different luminescence techniques will be applied to achieve the highest efficiency and accuracy of the derived age as significant chronological tools in archaeology in general and in the near eastern archaeological sites particularly. The recent application of using the more stable feldspar signal measured at elevated temperature (denoted as pIR IRSL) will be tested for the first time to feldspar from heated materials. The test should illustrate the usefulness and the accurate ages of the method that can provide. The study will also investigate the application of OSL dating to arid sediment deposits resulting from human activity; it will discuss the availability of well-bleached signal in sediments with no geological depositional history but is valuable for luminescence dating. Finally, the study will test the very recently developed luminescence technique, rock-surface dating, which determines the last time rock surfaces were exposed to light. The new method will be tested to a kite structure in the southern eastern Jordan. This study will be the first radiometric of its kind for dating these structures in the Levant.

The current study will be divided into five parts as follow,

Chapter 2- OSL dating: this chapter will go through the principle of OSL dating; mechanism and age equation. It will present a review and description of the techniques that will be used in this study.

Chapter 3- Investigating SAR OSL Dating technique for young archaeological heated materials using potshards from the Pella (tell Tabqat Fahl) in the Jordan valley: the first case of this study. We will report here on the first application to pottery samples of the stable infrared stimulated luminescence signal measured at elevated temperature (in this case 290°C, $pIRIR_{290}$) after stimulation at 50°C (IR_{50}). The study will use a potsherds collected from three superimposed Iron age units at Pella (Jordan); based on ^{14}C dating, typology and seriation these units were deposited between 2700 and 2900 years ago. Polymineral fine grains were chosen for dating. Analysis and interpretation of the derived ages and comparison to the established archaeological age of the site will be discussed at the end of the chapter.

Chapter 4- Testing the application of post IR IRSL dating to Iron- and Viking-age ceramics and heated stones from Denmark: the second case of our study and we will test the same technique of using the post-IR IRSL signal at elevated temperature ($pIRIR_{290}$) SAR protocol for the dating of young heated artefacts (ceramics and stones). In this case the samples lack for any previous radiometric dates. Seven heated stones and seven potshards were collected from three different archaeological sites in Denmark: one site from the early Pre-Roman Iron Age 200 BC to AD 100, and two from the Viking period between AD 800 and 1200. The assumed dates are based on associating founds and building construction techniques to the Pre-Roman Iron Age and Viking period.

Chapter 5- Application of OSL dating to a Chalcolithic well in Qulbān Banī Murra, Jordan: this chapter will present the first OSL dates for an arid environment from the southeast Jordan using luminescence dating (quartz OSL and feldspar post IR-IRSL). The study is applied for two sediment samples taken from Qulbān Banī Murra site. The site represents one of the major pastoral well culture sites exist that extends of the central parts of the "Mid-Holocene Green Saharo- Arabian Pastoral Belt stretching from Yemen to the western Maghreb (Gebel, 2013). The archaeological age of the site expected to belong to the Chalcolithic culture (5^{th} millennium BC). The site includes partly megalithic burial fields connected to a water management system. The nature of these sites is known to lack for organic matter for ^{14}C dating, and few artefacts founds.

Chapter 6- Dating a Near Eastern desert-hunting trap (kite) using rock surface dating: will be the last application that will be used and presented in the current study. In this chapter we will date directly, for the first time, a desert kite structure in the southeast of Jordan using the recent application in Luminescence; rock surface dating. Very little is known about the age or use of these widespread structures; any chronology is usually based on the assumption that they are in some way associated and contemporaneous with some nearby occupation site, and a wide range of ages has been proposed from ~6000 BC until the last century. Here we use the quartz OSL signal from rock surfaces to

date the Jibal al-Gadiwiyt kite located in the south east of Jordan. This is believed to be the first time luminescence has been used to date one of these enigmatic structures, and certainly the first application of rock-surface dating.

Chapter 7- Conclusions: The final chapter will summarize the results for the applications of the selected luminescence techniques to different archaeological sites and materials. We will evaluate the usefulness of the applications according to the achieved accuracy and certainty. It will discuss the applicability of luminescence dating in supporting other radiometric dates or the potential of being as standing alone radiometric technique. The evaluation will also include the significance of additional information about the history of materials that can be obtained using luminescence signal and how can be employed in archaeology.

"Light, the visible reminder of Invisible Light"
T.S. Elliot

2. Chapter 2: OSL dating

2.1 The beginning of Luminescence Dating

Luminescence is the emission of light by some minerals when are subjected to stimulators like heat or light. It is a phenomenon exhibited by crystals in minerals such as Quartz, alkali Halides and Feldspars. The phenomenon was first described by Sir Robert Boyle, where he conducted several experiments on diamond stone, he put his observations as a result of his experiments before the Royal society in October 1863; as he described ''a glimmering light'' from a diamond when he kept it close to his warm body. To verify that warmth produced light in the diamond he held the diamond stone near a candle flame that caused the diamond to shine in the dark (Boyle, 1664). More knowledge about the mechanism and causes of creating luminescence has been widened with the progress in Quantum Physics and the development of sensitive photomultiplier had also enabled scientist to detect luminescence signals and relate it with crystal structure and electrons delocalization. The first apparatus designed for measuring the signals was by Urbach and developed By Daniels and Boyed, but being applied in archaeology as a method of Dating for heated artifacts was first suggested by Danial in the University of Wisconsin 1953. The study based in examining the ability of crystal to produce Thermoluminescence as a result of suffering high energy radiation exposure such as gamma rays, Beta particles, alpha particles and X- rays, defining the proportional relation between light emitted from crystals and the amount of energy absorbed by radiation, had gave a notion of using it in dating (Daniels, Boyd, & Saunders, 1953).

2.2 Luminescence; principle and mechanism

Luminescence is the emission of light from minerals like quartz when it is subjected to light or heat. The origin of light is explained on bases of energy levels model. The

energy level model in solids is visualized as two level of energy known as bands; the valence band where electrons are normally present at room temperature and a higher energy level known as the conduction band (Figure 2.1), the energy level between the two bands is called gab or forbidden band. Ionizing radiation excites electrons from the valence band, or ground state, across the energy gap to the conduction band where they are free to move about. Usually the activated electrons will dissipate their energies instantaneously and leave the conduction band to transit again to the valence band. Energy levels within the gap cannot normally allow for electrons to stay, but crystalline lattice in solid may contain defects resulting in localized charge deficiencies allow occupation for electrons in metastable energy levels within the gap. Excited electrons can thus become trapped at these defects. Release electrons from the traps requires energy stimulation; heat and light can stimulates these electrons from their traps. Upon release the electrons recombine and return to the ground state, in the process emitting light, or luminescence, and thus these traps are called luminescence traps. If the stimulus caused by heat then the emitted light is called thermoluminescence (TL). If the stimulus is light, it is called optically stimulated luminescence (OSL).

For dating purposes, materials that contain minerals suitable for dating like quartz and feldspars must be subjected to light or heat in the past to reset the luminescence signal (zeroing event, setting the o'clock to zero). Subsequent to signal resetting; exposing minerals to continuous ionizing radiation from the decay of natural radionuclides (^{232}Th, ^{238}U and ^{40}K), will evict electrons from the valence band within the crystal structure; and some of this electrons will be trapped again in the luminescence traps and a latent luminescence signal will gradually accumulates (Figure 2.2). This signal can be measured in the lab by emptying the traps again using heat or light. The intensity of the signal is an indication to the amount of absorbed radiation.

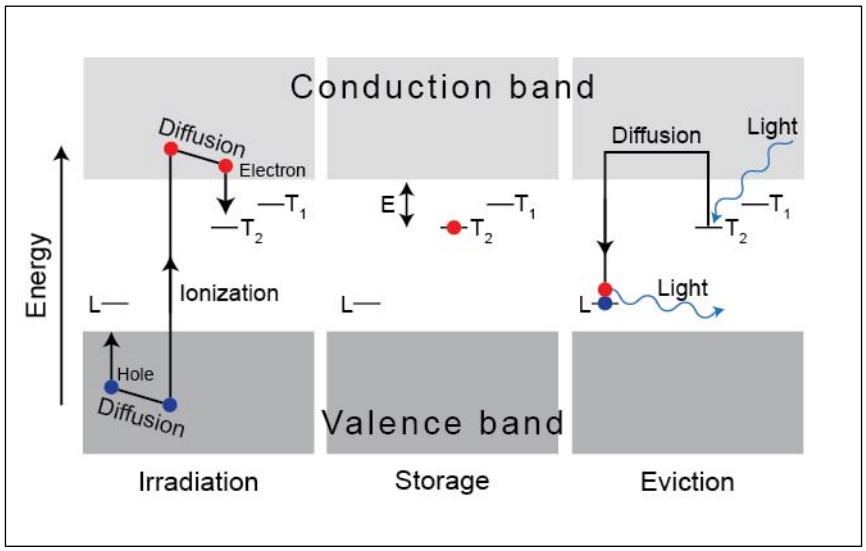

Figure 2.1: Energy level representation for the process of luminescence. (Aitken M. J., 1998) (p. 14)

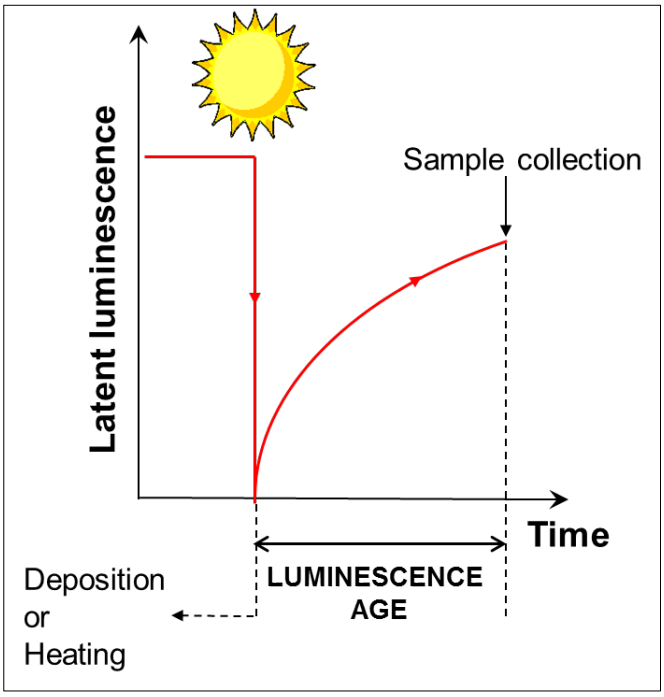

Figure 2.2: A simplified schematic of the physical process behind luminescence dating

Optical Stimulation Luminescence (OSL) is a description when light is used for stimulating luminescence signal in the laboratory. The method first introduced by Huntley in 1985 as a new method for sediment dating. A green light from Argon ion laser light used for stimulating light for quartz and feldspars (Huntley

et al., 1985). Infra red light (IR) was used for feldspars (Hütt & Jaek, 1989). Other light sources for photon stimulation like Blue LED are used later, and all described under the general name of optical stimulation light (*OSL*).

OSL also applied for heated archaeological materials. The first experiment in 1992 for quartz extracted from heated stone from Sweden dated to Viking Age and the results were compared with TL ages from the same site (Bøtter-Jensen & Duller, 1992).

2.3 Equivalent dose (D_e) and Age equation

In the lab, and under reduced red light, quartz and feldspars minerals are extracted from the samples (sediments, ceramics or rocks) by means of mechanical and chemical procedures, different size of minerals usually used for measurements. Lose grains of minerals are fixed on disks (aliquots) and loaded to TL/OSL apparatus to measure the stored natural luminescence signal by exposing them to external stimulus (blue light or Infrared) (Figure 2.3). The intensity of the natural luminescence signal is then measured by sensitive photomultiplier with different light filters for specific spectral regions. The intensity of the recorded signal decrease by time in an exponential decay function called the decay curve (Figure 2.4) (Aitken, 1998). This natural luminescence signal and knowledge of the back ground radiation; the sample age can be estimated using equation 2-1

Equation 2-1

$$\boldsymbol{Age\ (ka)} = \frac{\boldsymbol{Equivalent\ dose; D_e\ (Gy)}}{\boldsymbol{Annual\ dose\ rate; D_r\ \left(\frac{Gy}{ka}\right)}}$$

D_e- Equivalent dose is the total amount of radiation dose absorbed by the mineral throughout its time span that is responsible for creating the natural luminescence signal; it is measured by calibrating the natural signal against laboratory- administered radiation. The D_e value is measured in unit of Gy. The

annual dose rate D_r is the average amount of radiation per year that the sample receives during life span; it is in the unit of Gray per time and so the resultant ratio (Age) is in time unit.

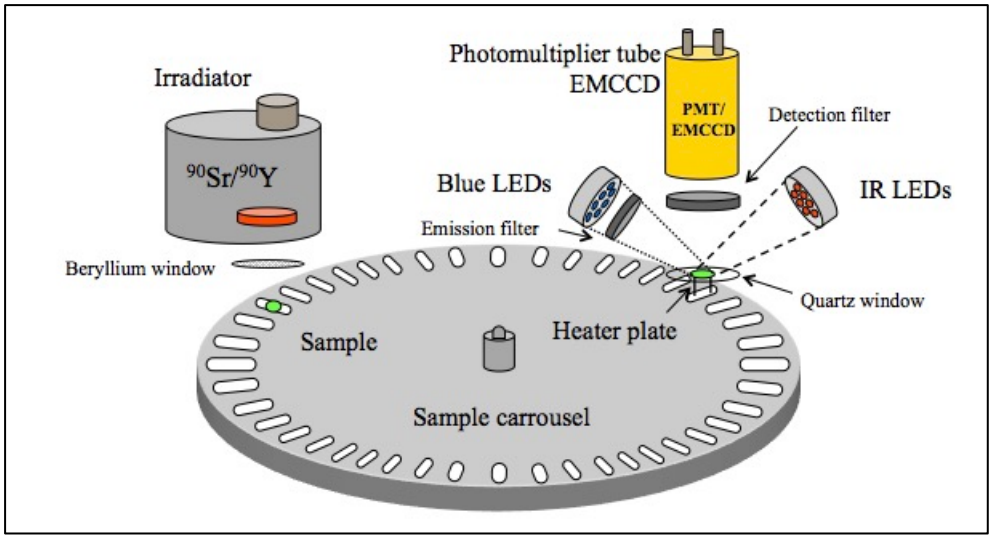

Figure 2.3: Risø TL/OSL reader designed Automated 48-position sample changer system. The reader is equipped with blue LED and IR LEDs for light stimulation and Filter holder to allow fitting of different optical detection filters to the photomultiplier.

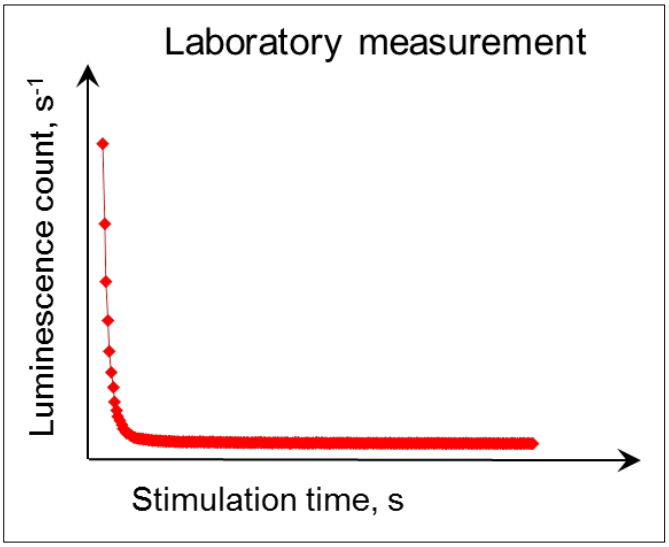

Figure 2.4: Decay curve, recorded luminescence signal plot as a function of time of stimulation.

Recently there is an increased precision of estimating D_e due to the advanced and sophisticated laboratory Instrumentations and procedures for measuring OSL

signal and hence D_e. As a consequence, several methods and protocols have presented and tested for the best accurate equivalent doses can be measured. In the following sections, we will discuss the recent methods that are widely tested in geology and had proved their reliable dose estimates; we will use those methods to test them for archaeological materials.

2.4 Review of the employed techniques in this study

2.4.1 Single-aliquot regeneration SAR

The concept of single aliquot is to define the equivalent D_e by using only one aliquot (small portion of grains mounted on one disk). Huntley *et al*. (1985) suggested the possibility to make measurements on a single aliquot. Duller (1991) suggested a single aliquot method by giving additive doses to potassium feldspar extracts and using IRSL signal. The method is known as single aliquot additive dose (SAAD). It is a sequence of preheats, stimulations for short time (0.1s) and then giving a dose before repeating the sequence. The measured natural and added dose signal during stimulation is used to build up a growth curve where D_e is determined by extrapolation. Duller used a second aliquot to measure the natural signal after repeated preheats and stimulation for short time (0.1s) to correct any signal loss caused by repeating preheats and stimulation of the first aliquot. This correction is also used to correct the measured data from possible accumulation of signal by the added doses (Duller, 1994 and 1995).

Several methods were suggested later for the single aliquot (Galloway, (1996), Murray et al. (1997), Liritzis et al. (1997) and Murray and Roberts (1997)). The breakthrough of the single aliquot was by introducing the *Single Aliquot Regenerative dose (SAR)* protocol by Murray and Wintle (2000). The protocol use the comparison of the natural luminescence signal with different laboratory-induced signal for the same aliquot in different cycles of irradiation and measurement. The advantage of SAR-protocol is that it corrects for sensitivity changes that may occur during the measurement cycles by a giving test dose in

each step. The growth curve is constructed by the ratio of the OSL response from the natural and the regenerative dose (L_i) to its corresponding OSL signal from the test dose (T_i). The D_e is then obtained through interpolation (Figure 2.5 and 2.6).

Table 2-1 describes the measurements steps for SAR protocol. In each cycle the luminescence signal is measured after preheat at 260°C (step 2 and 3 in Table 2-1), a test dose is given after the OSL stimulation to monitor sensitivity change (step 4), the luminescence signal is measured again after preheat of 220°C (step 5 and 6). The preheat steps is to remove signal from any shallow traps. Before continue with the next cycle a washout step is carried on by stimulating the aliquot at high temperature 280°C to ensure no charge transfer to the next cycle (step 7 in Table 2-1).

Table 2-1: SAR protocol; i indicate to the step index (1..n). D_1 is for natural signal=0 Gy, $D_{2,3,4..n}$ are given generating doses to build the growth curve, D_5=0 Gy for recuperation test and D_6=D_2 for recycling ratio test.

Step	Treatment	Observed
1	Give dose, D_i	
2	Heat (preheat, 200-260 °C for 10s)	
3	Stimulate (blue LED light) for 40s at 125 °C	L_i
4	Give test dose, D_i	
5	Heat (cut heat, 160-220 °C)	
6	Stimulate (blue LED light) for 40s at 125 °C	T_i
7	Stimulate (blue LED light) for 100 s at 280 °C (or > Preheat in step 2)	
8	Return to 1	

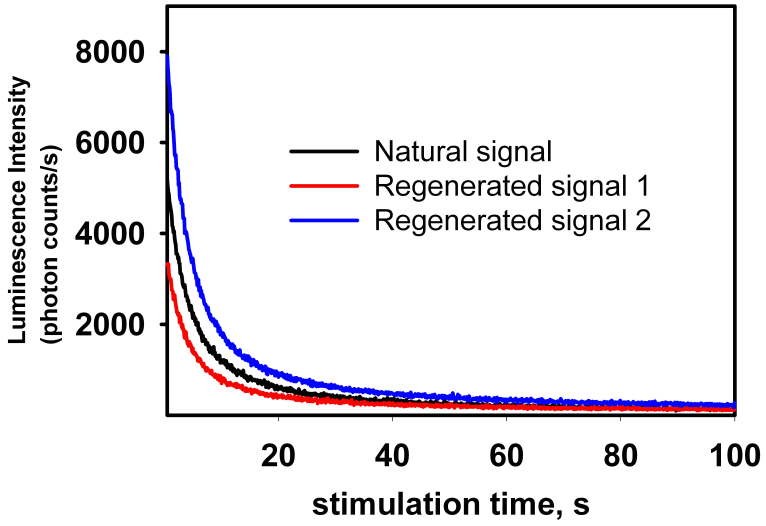

Figure 2.5: Decay curves for natural and regenerated doses for one aliquot. Black line is decay curve for the natural signal, red line for regenerated dose that is less than the natural dose and the blue line is from generated dose bigger than the natural dose

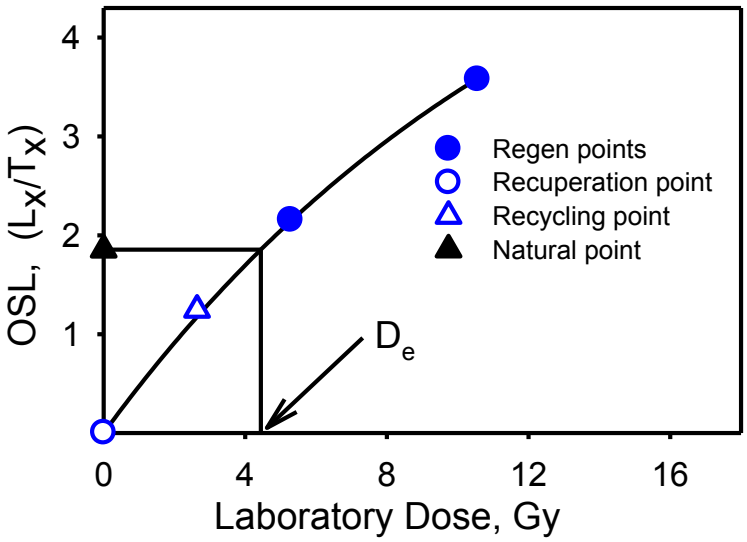

Figure 2.6: Growth curve for SAR protocol obtained by plotting the ratio of the OSL signal from the natural and regenerative doe (L_i) and the OSL signal from the test dose (T_i) against the given regenerative doses.

Estimating D_e from one single aliquot allows a large number of D_e to be measured for one sample, this helped to improve the precision of the measured equivalent doses by increasing the number of measurements. SAR protocol also allows for several checks for the reliability of the estimated D_e value, such checks are the following,

Recuperation ratio: Measuring the signal response to one cycle with zero regenerated dose (D_5 in Table 2-1, following the largest regeneration dose) allows to monitor any build up of dose due to thermal transfer of charge. In ideal conditions it should measures zero signal, but the observed measurement shows a recuperated signal. It is explained to arise from thermal transfer of charge inserted, by the test dose (step 4), into thermally- shallow but light-insensitive traps (Murray and Wintel, 2000). For quartz a ratio less than 5% of the natural is accepted as not effecting the estimation of D_e.

Recycling ratio: is comparing two recycling steps with the same regenerative dose to check the sensitivity change after several irradiations, preheats and stimulations (D_2 and D_6 in Table 2-1, D_6 is chosen to be after the largest and the recuperation dose). A ratio within 10% of the first regenerated dose indicates that SAR protocol is able to correct for any sensitivity changes in the laboratory-regenerated SAR cycles and that the quartz signals are unlikely to be significantly contaminated by those from feldspar.

Dose Recovery: is a test for overall performance for the chosen protocol, it test the protocol ability to measure a known laboratory dose. The test is applied to several aliquots after their natural OSL signal is bleached using blue light stimulation at room temperature, then the aliquots will receive known dose either by beta source or gamma source. The given dose then is measured using the chosen SAR protocol. The ratio of the measured dose to the given dose should be close to unity for the best SAR performance (Murray & Wintle, 2003).

Preheat Plateau: is used for testing the dependence of the equivalent dose to the preheat temperatures. Because luminescence traps have different energy depths,

some traps are not very stable at ambient temperatures and lose their electrons over the time period relevant to archaeology. Other traps are sufficiently deep that they are not easily emptied during the exposure to heat or light. Obviously, neither very shallow nor very deep traps are useful for dating, and an important task in dating is to isolate those traps which were emptied at the time of interest and which have been stable since then. Because the natural signal is the product of only stable traps and because signals induced by artificial irradiation include unstable components, the task involves making these two signals comparable, using various thermal ("preheat") treatments to simulate long periods of time, "plateau" tests to measure comparability, and normalized dosing to equalize sensitivity. It applied by measuring number of aliquots at different preheats, the estimated D_e is plotted against temperature and the stable value for the estimated D_e represent the best temperature to be used. A detection of changes of the derived D_e when the preheat temperature is changed is an indication for the possibility of thermal transfer of charge. Therefore preheat plateau should be undertaken before estimating D_e. The preheat plateau test can be applied for the natural D_e, or as dose recovery preheat test, where the natural signal is bleached followed by irradiation and then measuring the given dose at different preheats (Murray & Wintle, 2000 and 2003).

SAR protocol became a fundamental protocol for estimating D_e for feldspar and in other techniques on luminescence technique. It will be the base of the next luminescence dating methods that we will discuss on the next sections (sections 2.4.2, 2.4.3 and 2.4.4).

2.4.2 K-rich feldspar and post IRIRSL (pIRIR$_{290}$) method

Hütt *et al.* (1988) had reported for a luminescence signal from feldspar by stimulation near infrared at room temperature known as IRSL signal. IRSL signal is found to be exclusive to feldspar since quartz is not stimulated within the infrared region wavelength. Hütt results allowed for further development on dating feldspar (Hütt *et al*. (1989), Duller & Wintel (1991), Bøtter-Jensen &

Duller (1992), Barnett & Bailiff (1997), Bailiff & Barnett (1994)). IRSL SAR was used also for feldspar dating (Wallinga *et al.,* 2000, Blair *et al.,* 2005). Using IRSL signal for dating feldspar has several advantages over quartz OSL. IRSL is exclusive for feldspar since quartz does not affected by infrared stimulation, this had allowed to use IRSL signal from polymineral fine-grains extraction (Rees-Jones (1995), Banerjee *et al.,* (2001), Roberts & Wintle (2003) and Buylaert *et al.* (2007)).

Feldspar has higher age limit (~500,000 years) compared to quartz (~300,000 years) because of its higher luminescence sensitivity and saturation dose, which count another advantage for dating feldspar.

However, an underestimation feldspar age is very likely due to athermal loss of luminescence signal with storage time (known as *anomalous fading*) (Wintle (1973) and (1978), Aitken (1985), Spooner (1992) and (1994)). Anomalous fading is a phenomenon explained as quantum mechanical tunnelling of charge from deep traps to nearby recombination centres. It is also observed in the lab as signal decay laboratory irradiation without administrating any thermal or optical stimulation (Visocekas, (1982), Templer (1986)). To overcome the fading problem it is suggested to use more stable luminescence signal and to avoid age underestimation of feldspar caused by the anomalous fading (Jain & Singhvi (2001), Thomsen et al. (2008)). Other methods suggested corrections models to measure the fading rate at the laboratory and apply to correct the feldspar ages (Huntley and Lamothe (2001), Auclair et al. (2003)).

A major development in dating feldspar was using the IRSL signal at elevated temperature, which means stimulate with IR at low temperature (50 ^{o}C, denoted as IR_{50}) followed by second IR stimulation at elevated temperature (e.g. 290 ^{o}C, denoted as $pIRIR_{290}$) (Buylaert J. *et al.,* 2009). The method is called post IR IRSL and the principle is to empty charge carriers in unstable traps before measuring the signal from the more stable traps without any contribution of those unstable traps. The strength of the post IR IRSL method is it has smaller fading rate compared to the signal measured only at 50 ^{o}C.

The method protocol is based on SAR protocol (Table 2-2), and uses same tests to monitor the performance of the measurement.

Table 2-2: The post-IR IR SAR measurement protocol. To define D_e growth curve is built by using the ratio of L_{i290} and T_{i290} against regenerating doses.

Step	Treatment	Observed
1	Give a dose, D_i	
2	Preheat (320 °C for 60 s)	
3	IRSL, 100 s at 50 °C	L_{i50}
4	IRSL, 100 s at 290 °C	L_{i290}
5	Give test dose, T_i	
6	Preheat (320 °C for 60 s)	
7	IRSL, 100 s at 50 °C	T_{i50}
8	IRSL, 100 s at 290 °C	T_{i290}
9	IRSL, 100 s at 325 °C	
10	Return to step 1	

2.4.3 Single grain and poor bleached samples

Using single aliquot SAR had enabled to derive many of independent estimates of D_e for the same sample and hence the distribution of D_e can be evaluated. A good distribution will emerge from an ideal or fully resetting of the natural signal in grains (e.g. heated samples or Aeolian and windblown sediments). After resetting in such cases the signal will rebuild homogenously in all grains, and so we would expect close measurement of D_e within the same sample. But in other cases such as water wash sediments or insufficient heating, this would lead to incomplete bleaching or resetting for the natural signal in some grains and so the rebuild of the signal will be in different levels. This means high distribution of the calculated D_e (Thomsen *et al.* (2005) and (2007), Duller (2008), Cunningham *et al.* (2011)). To overcome this problem of poorly bleached samples, luminescence from single grains was used to calculate D_e after discarding the poorly or partially bleached ones that might over estimate the age (Figure 2.7 , 2.8).

Using single grain is governed by different statistical approaches for the single grain dose distributions. The widely used is Central Age Model (CAM), the Minimum Age Model (MAM) (Galbraith *et al.* (1999), Arnold *et al.* (2007), Zenobia *et al.* (2006), Guerin, *et al.* (2015)), other methods suggested like the Internal-External Consistency Criterion (IEU) and lowest 5% method (Thomsen *et al.* (2003) and (2007), Olley *et al.* (1998), Bailey & Arnold (2006)).

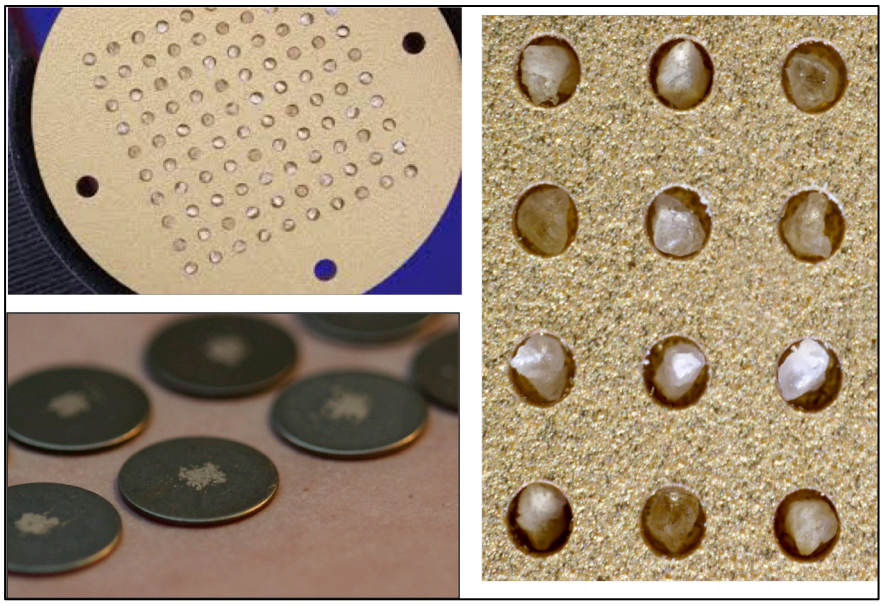

Figure 2.7: Risø single grain disk with 100 holes in size of 180-300µm compared to multi grain disks (left down).

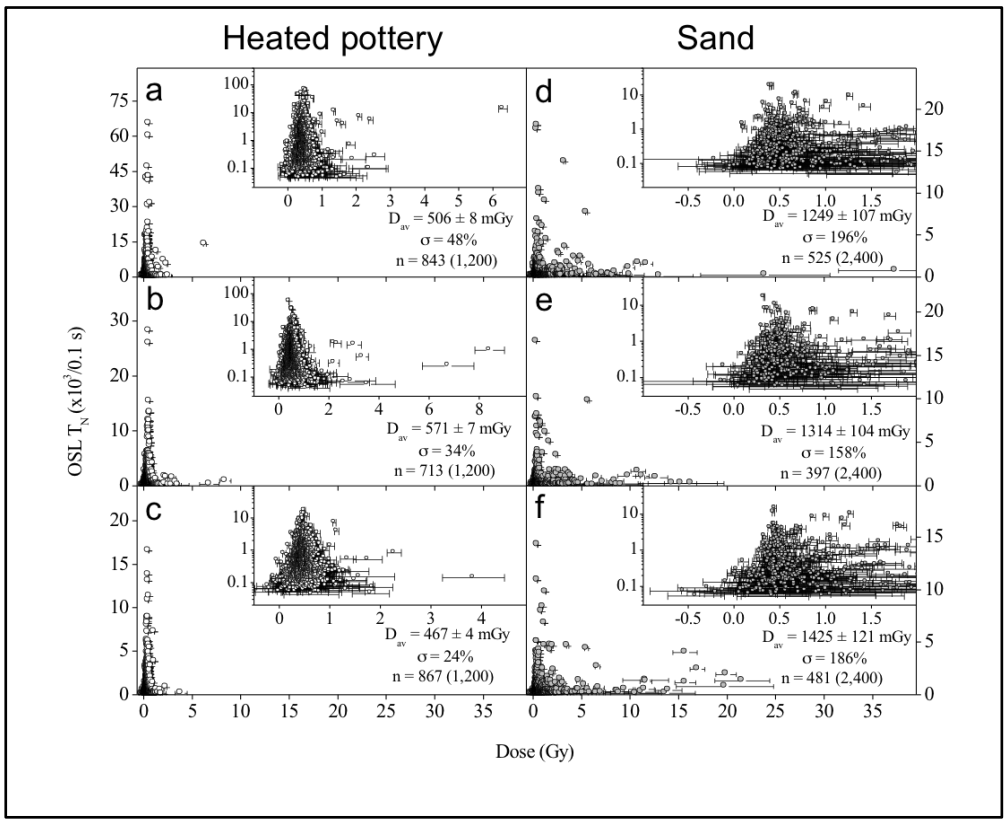

Figure 2.8: Single grain dose distributions from pottery and sand samples. The figure demonstrates how heated samples give more symmetric distribution for D_e about the mean dose compared to sand sample (after Thomsen *et al.*, 2007).

2.4.4 Rock surface dating

The principle of rock surface dating is based on resetting of luminescence signal on rock surface down to the depth due to light penetration in the rock surfaces during daylight exposure, followed by build up for the signal after being covered and shielded from light (e.g. burial or construction of rocks).

The method was first developed using thermoluminescence (TL) signal from calcitic rocks (e.g. Liritzis (1994), Liritzis *et al.* (1997), Liritzis and Galloway (1999), Theocaris *et al.* (1997)). Other works aimed to use the OSL signal for rock surfaces to avoid the residual TL signal in rocks and enable of dating young samples (Habermann *et al.* (2000), Greilich *et al.* (2005), Vafiadou *et al.* (2007), Liritzis *et al.*, (2008)). Many applications were focused on archaeological stone

structures such as monolithic, buildings and walls (Liritzis et al. 2013). Sohbati *et al*. (2011) tried to establish a routine rock surface dating by employing a mathematical model describing the resetting of the luminescence with depth in rocks during one daylight exposure. The model was later expanded to describe sequence of signal resetting and build-up as a result of sequence of daylight exposures and burials events (Freisleben *et al.*, 2015).

The rock surface dating assumes that during light exposure, the stored luminescence will decrease because of light penetration into the rock causing charge release from their OSL traps. The charge release happens in different rates at different depths described on mathematical equation as

Equation 2-2

$$E(x) = \overline{\sigma\varphi_o} e^{-\mu x}$$

The parameter $\overline{\sigma\varphi_o}$ is the trap-emptying rate at the surface. μ is the light attenuation coefficient (cm^{-1}) in the rock and *x* is the depth into the rock (cm). Assuming L(x) is the luminescence intensity at depth x and for time exposure t_e, then L(x) can be expressed as

Equation 2-3

$$L(x) = L_0\, e^{-E(x)t_e} = L_0\, e^{-\overline{\sigma\varphi o}t_e\, e^{-\mu x}}$$

L_o is the initial trapped charge, for the first time exposure, L_0=1 and represent the saturation level.

When the rock is buried and light covered again, the traps are being refilled with charge due to the background radiation from the rock and the surrounding sediments.

Table (2-3) summarise a set of equation that combine the burial and exposure time with de-trapping and re-trapping of charge that describe the cycle of exposure and burial events for the rocks.

Table 2-3: Model expressions for multiple burial and daylight exposure events. The model profiles are normalized to 1 (Freisleben *et al.*, 2015).

Event order	L(x)
Saturation	$L_0=1$
First daylight exposure t_{e1}	$L_1(x)= e^{-\overline{\sigma\varphi o}te1\, e^{-\mu x}}$
First burial t_{b1}	$L_2(x)= (L_1(x)-1)\, e^{-F(x)tb1}+1$
Second daylight exposure t_{e2}	$L_3(x)= L_2(x)\, e^{-\overline{\sigma\varphi o}te2\, e^{-\mu x}}$
Second burial t_{b2}	$L_4(x)= (L_3(x)-1)\, e^{-F(x)tb2}+1$
etc.	…….

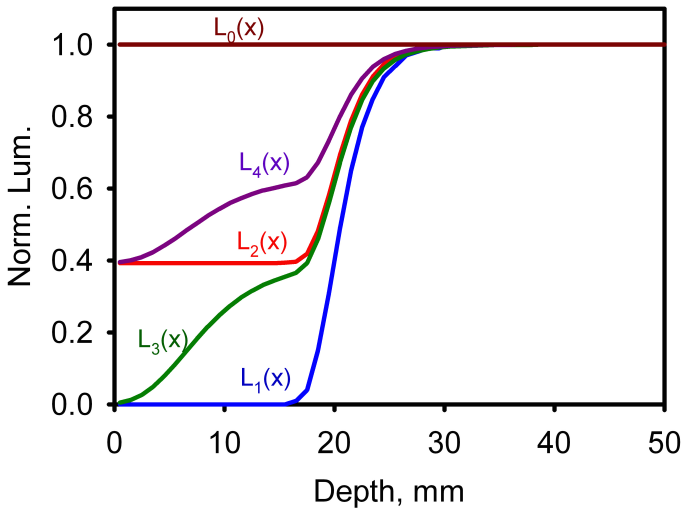

Figure 2.9: remodelling for normalised luminescence- depth profiles for multiple sequential events of burial and daylight exposure (reproduced after Freisleben, 2015). Same assumptions are taken into the modelling; exposure times t_{e1} and t_{e2} were chosen such that the inflection points occur at depths of 10 μ^{-1} and 2.5 μ^{-1}, respectively.

Figure 2.9 is shows a sequence of events through their luminescence- depth profiles. L_0 (brown) represent the saturation level for luminescence at all depth through the rock signal, it takes place before any light exposure. L_1 (blue) the first light exposure causes signal bleaching at certain depth. L_2 (red) subsequent burial-time for the rock enough to rebuild the signal to certain depth (internal and external). L_3 (green) a second exposure take place and rest the signal with depth. L_4 (violet) burial event and hence rebuilding the signal.

2.4.5 Radio Activity and Annual Dose rate

The second part of the age equation is the annual dose rate; the average amount of radiation per year that the sample receives during life span. The total dose rate is the sum of beta, alpha, gamma and cosmic rays. Cosmic ray dose depends on the location (latitude, longitude and altitude of the sample and can be computed using the work of Prescott and Hutton (1994).

The nuclear decay of the radioactive elements ^{232}Th, ^{238}U and ^{40}K is the main contributor for alpha, beta and gamma doses. The final dose delivered to the sample depends on the water content of the sample and the grain size. For ceramics and rock the effect of dose rate comes from within the sample itself (internal dose rate) and from the surrounding sediments (external dose rate), consideration for the range of radiation and sample geometry must be taken into account for evaluating the final sum of the dose rate (Aitken, 1985).

Several laboratory techniques can be used to define the concentration of the radionuclide. In the scope of this study, two techniques were used, high-resolution gamma spectrometry (Murray, 1987) and Risø Low-level beta GM multicounter.

3. Chapter 3: Investigating SAR OSL Dating technique for young archaeological heated materials using potshards from the Pella (tell Tabqat Fahl) in the Jordan valley

The first case of the study will test the usefulness of pIRIR dating method for heated materials. The method will be applied to pottery samples from well know age site, Pella in Jordan valley.

3.1 Introduction

This chapter investigates the usefulness of luminescence signals stimulated by infrared light at elevated temperatures from known-age archaeological ceramics gathered from Pella (Tabaqat Fahl) site in the Jordan Valley.

The stability of luminescence signals stimulated by IR at elevated temperature was first investigated by Thomsen *et al.* (2008); they found that such signals were significantly more stable than the conventional signal measured at or about room temperature, especially if the room-temperature stimulation preceded the elevated temperature stimulation. Buylaert *et al*. (2009) tested the application of this new signal to the dating of K-feldspars extracted from sediments; they used a 250 ^{o}C preheat for 60s, followed by a 100 s IR stimulation at 50 °C and finally a 100 s elevated temperature IR stimulation at 225 °C, with blue light detection (320–460 nm); they called this signal post-IR IRSL. Based on studies of the source of the IR stimulated luminescence signal by Murray *et al.* (2009); Thiel *et al*. (2011) increased the preheat temperature to 320 ^{o}C (60 s) and the elevated temperature of stimulation to 290 ^{o}C ($pIRIR_{290}$). They applied this revised protocol to samples of Japanese loess, one with age control, and were unable to detect significant signal instability. As a result of these early studies, the feldspar

pIRIR signal is now widely used in dating both sand-sized extracts of K-feldspars and polymineral fine-grains (Buylaert *et al.*, 2012).

Although IR dating of ceramics has been used almost since the first identification of the signal by Hütt *et al.* (1988), such studies either ignored the possibility of anomalous fading or corrected for it by determining fading rates, e.g. Auclair *et al.,*(2003) and Huntley & Lamothe (2001). Despite the identification of much more stable IR signals from feldspar, few if any studies have tested their application to ceramics. Even young heated materials should be well suited to pIRIR protocols, because the high temperature firing should completely empty any IR-sensitive trapped charge (Murr *et al.*, 2009) (Thomsen *et al*, 2011) and eliminate the possibility of thermal transferred signals (Ollerhead *et al.*, 1994); these often limit the applicability to young unheated materials because of the resulting apparent large residual dose, even in well-bleached sediments.

To test the usefulness of such signals, ceramics of broadly agreed age were collected from three superimposed strata from the archaeological site Pella (Tabqat Fahl) in Jordan. The ages of these layers are based on stratigraphy, typology and serration of related finds (see next section). Both IR signals measured at 50 ^{o}C (IR_{50}) and $pIRIR_{290}$ signals are used in our studies. Routine laboratory tests (recycling ratio, recuperation, and dose recovery), heating and stimulation plateaus are examined to test the reliability of our SAR protocol when applied to the heated fine-grains extracted from the Pella ceramics. The resulting equivalent doses are used to determine luminescence ages for comparison with the known ages, and the results are discussed in terms of the reliability of the IRSL ages.

3.2 Site description and independent age control.

Pella (modern name Tabaqt Fahl) lies in the northwest of Jordan, about 30 km south of Lake Tiberias, 130 km north of the capital Amman, and five km east of the Jordan river. The site lies around sea level, at latitude 32^{o}27', longitude

35°37'. The total settlement landscape is spread across 10 square kilometres, situated in the foothills of the east Jordan valley. A copious water source is located at the base of the southeast corner of the mound, and famed hot springs exist three km north, at Wadi el Hammeh (Figure 3.1). The annual average rainfall is about 400 mm (Edwards, 2013).

Pella is one of the longest occupied archaeological settlement landscapes in the Jordan Valley. Large-scale excavations on the mound commenced in 1979, as a joint project of the University of Sydney Australia, the College of Wooster Ohio, and the Jordanian Department of Antiquities. Excavations are on going with 27 field seasons completed (McNicoll *et al*. 1992; Bourke, 2007 and 2014). There are 38 designated excavation Areas, with many other localities explored in less detail across the ruin-field. The largely artificial central settled mound is about 400 × 250m in extent, and rises over 30m high. Settlement on the main mound goes back deep into Neolithic times (ca. 7000 BC), although the modern tell contours are shaped by 4m thick mud-brick fortification walls that first surrounded the site in the Middle Bronze Age (Bourke, 2007). Across the Wadi Jirm to the south of the main mound, a largely natural hill, Tell Husn, has a more restricted occupational range, stretching from the late Chalcolithic period (ca. 4000 BC) onwards. Many farmsteads, field-walls and burial grounds dot the landscape surrounding the main mound, for upwards of three km in all directions. (Figure 3.1)

Because of its long largely unbroken occupational sequence, Pella is considered a key site in determining the chronology of settled life in the north Jordan valley; the results of 35 years of excavations have shown that occupation has been continuous over the last 12000 years.

Excavations in more recent times have focussed on the south-central area of the main mound (Area XXXII), where the largest Bronze Age temple ever discovered in Jordan has been under excavation for the past 15 years (Bourke, 2012). In the recent years, work has shifted to the west of the temple, where a series of Bronze

and Iron Age (around 1650-750 BC) Civic Buildings contemporary with the nearby temple are being uncovered (Bourke, 2011, 2013, 2014).

Since the early 1990s, a program of intensive radiometric sampling has been carried out (Bourke 1994 and 2006), Bourke *et al.* (2009), Wild & Fischer (2013)), to complement traditional typological methods of establishing relative chronology (McNicoll *et al.* 1992, Bourke, 2000, Bourke *et al.* 2006).

Table 3.1 lists a selection of ^{14}C ages from the Iron Age destruction horizon from which the OSL samples were collected (Wild & Fischer, 2013).

In addition, one sample (VERA 5308: 5205 ± 35 cal. years B.P., not shown in the table) was taken from a fill layer no more than 30 cm below the horizon sampled for OSL; given the archaeological context (Late Bronze/Early Iron Age), the date was clearly anomalous. Further analysis of this fill deposit revealed a red pebbly clay matrix similar to deposits at the base of the occupational sequence. It contained exclusively sherds and botanical remains drawn from Chalcolithic period horizons. As part of the extensive levelling fills brought in to even up the topography preparatory to the construction of the Civic Building, this deposit had been drawn from Chalcolithic period horizons eroding out from the south side of the tell three metres below the Iron Age structure. The proximity of this clay matrix, with its associated Chalcolithic sherds, is important when discussing outliers in the OSL ages (see section 3.6), particularly given that the mid-body sherds collected for OSL had no typological significance.

3.3 Sampling and Sample Preparation

3.3.1 Sampling

The archaeological materials came from three deposits in Trench XXXIIFF, locus 10.6, locus 15.1 and locus 15.2, all excavated in January 2013 (Bourke S. J., Pella in Jordan (2013) and (2014)). Both were drawn from thick Iron Age destruction debris layers, which sealed all earlier construction and occupation within the

Iron Age Civic Complex. Based on typology, almost all the pottery from this horizon dates from the later Iron I and early Iron IIA periods (ca. 1050-900 BC).

From each of the loci, around 20 potsherds were collected for luminescence dating (Figure 3.2). Because of the destructive nature of this method, we were restricted to using samples of little or no use in any further archaeological study; as a result no meaningful diagnostic studies could be undertaken on these potsherds individually and the associated ages can only come from the ages assigned to the layers as a whole. The samples were taken in January 2013; within 4 days, and early in cloudy misty mornings, in such manner to avoid any direct sunlight exposure.

Any soil attached to the potsherds fragments was kept as a light-protection cover and later used for external dose rate measurement. In addition, ~30 g of soil from each layer was collected directly for dose rate measurement.

Table 3-1: relevant radiocarbon ages for samples from the destruction horizon

	VERA # (ABA)	**^{14}C age (BP)**		
Pella	VERA 5311	2940 ± 35	IA I-II	1270-1020 BCE (94%)
Pella	VERA 5301	2930 ± 35	IA I-II	1260-1010 BCE (91%)
Pella	VERA 5316	2925 ± 35	IA I-II	1260-1010 BCE (95%)
Pella	VERA 5310	2885 ± 35	IA I-II	1210-970 BCE (93%)

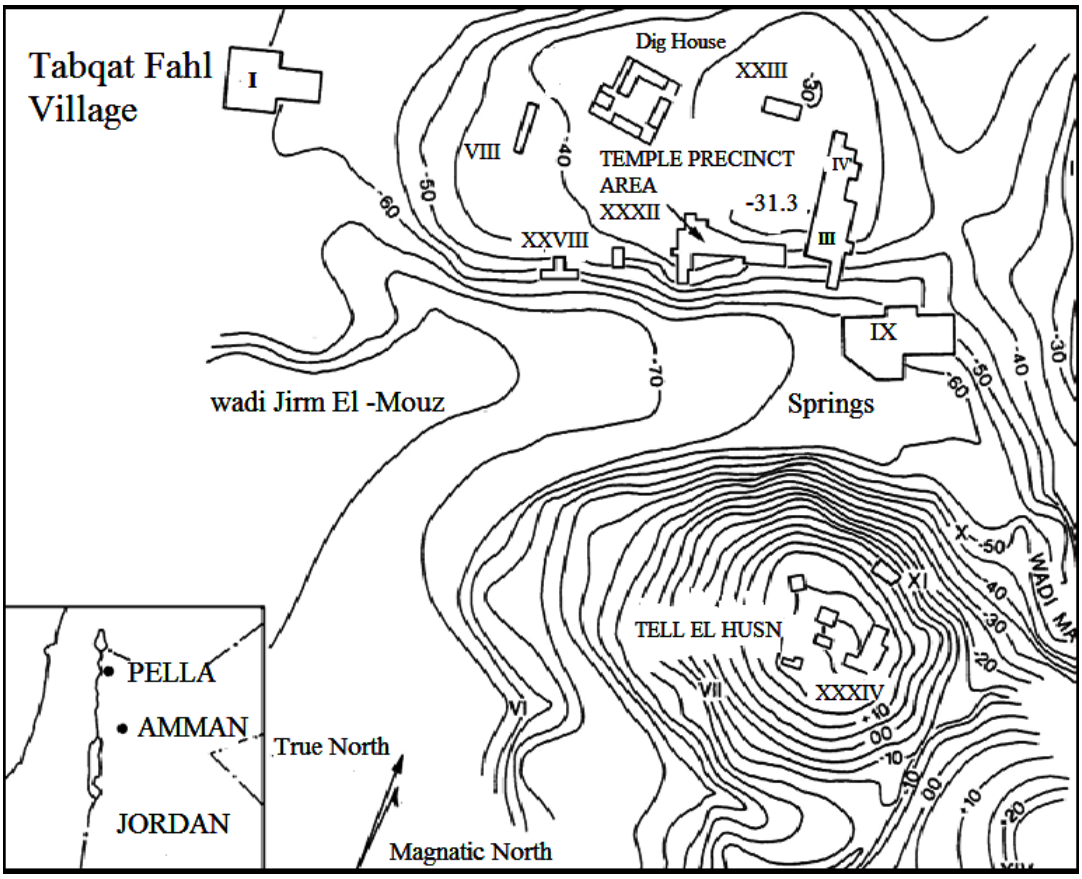

Figure 3.1: contour map of Pella with location map shown inset (adapted from Bourke, et al., 2009)

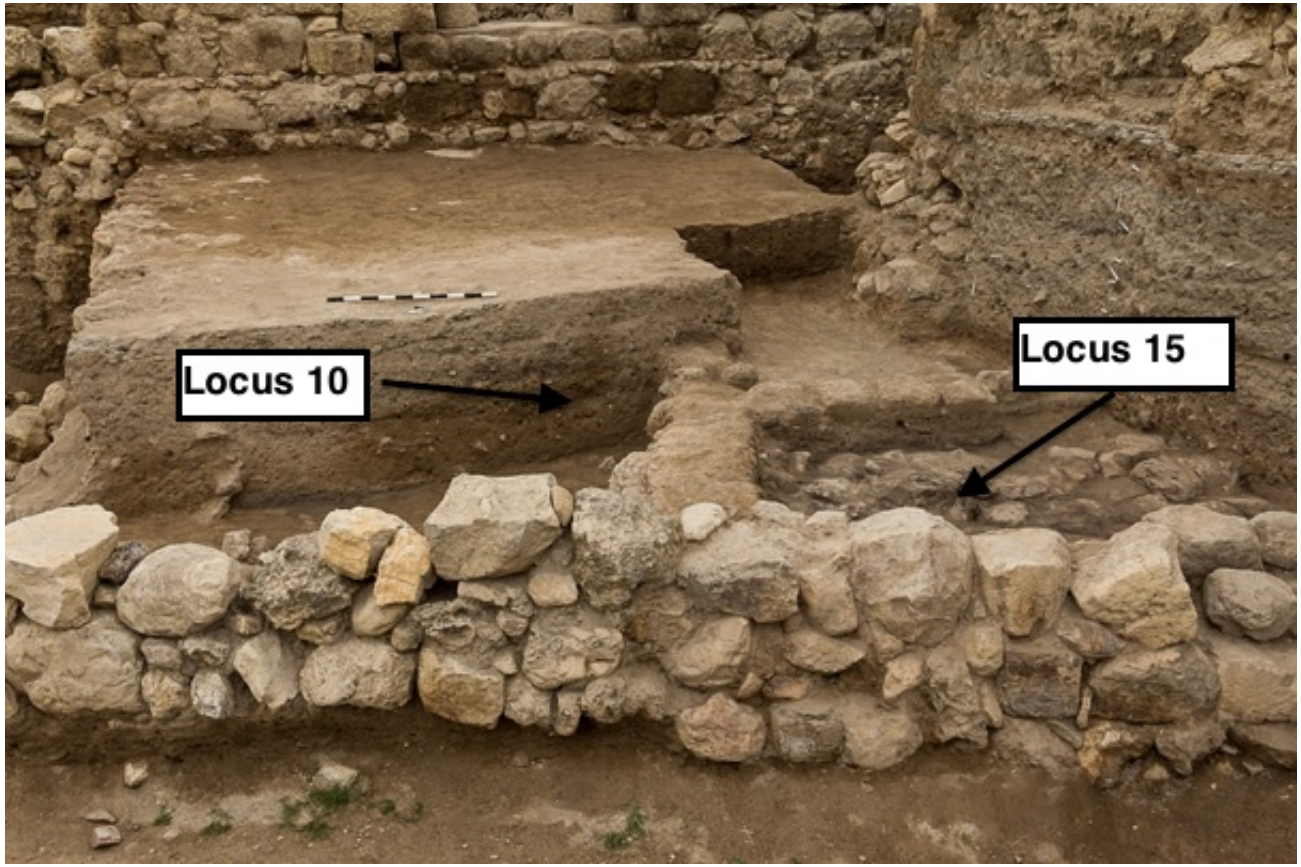

Figure 3.2: potshards were collected from layer 10‰6 and the stratigphicaly underlying layers 15.1 and 15.2 (bottom layer) (photograph by S. Bourke)

3.3.2 Sample preparation and measurement facilities

The potsherds were treated under subdued red lights; the procedure that was followed in preparing the samples is as described in (Aitken, 1985). Measurement for water content was undertaken for each of the fragments before applying any chemical treatment, after removing around 1 mm of the surface, a double face vice was used to break the fragments and ease the process of crushing with the agate mortar. Two fraction of sand size were extracted; 90-300 μm for coarse grains preparation and <90 μm for fine grains preparation.

For both grain size cleaning with 30% of HCl was applied for 3 hours, followed by a overnight rinsing in 10% of H_2O_2 to remove any organics matter, and a final step of chemical cleaning was rinsing in 0.01 N of sodium oxalate to dismiss clays materials, repeated washing was carried on after each step. For coarse grains, samples were treated with 10% HF before separating K-feldspar and quartz were using a heavy liquid solution ($\rho < 2.58$ g/cm^3), quartz later was etched for 40 min with diluted HF (40%) to remove the outer alpha-irradiated shell from the grains.

Fine grains in the size 4-11 μm were extracted by applying Stokes' settling (Frechen *et al.* 1996), around 1 mg to 3 mg of sample in acetone suspension was mounted over 0.97cm diameter aluminium disks and dried at 50 ^oC.

All Luminescence measurements were carried out using Risø TL DA 20 reader, equipped with IR diodes emitting at 875 nm, blue diodes emitting at 470 nm, and a calibrated $^{90}Sr/^{90}Y$ beta source. Poly-mineral fine grains OSL was measured through a blue BG-39/7-59 filter combination (Bøtter-Jensen *et al*. 2003).

3.3.3 Dosimetry

External dose rate: Sediment samples from each layer were collected for gamma dose rate measurement. Radionuclide concentrations were measured using high

resolution gamma spectrometry (Murray *et al.*, 1987) and these concentrations were converted into infinite-matrix dry dose rates using the factors given by Guérin *et al*. (2011), and an assumption that there was 20±10% escape of ^{222}Rn during burial (this is likely to cover all reasonable scenarios). Typical shards are 5 to 10mm thick; according to Aitken (1985) this will result in an external gamma dose rate to the shard of ~90% of the infinite matrix dose rate (with a further contribution of ~10% of the internal infinite matrix gamma dose rate). The radionuclide concentrations and derived external infinite-matrix dose rates are summarised in the end of Table 3.4.

Internal beta dose rate: about 3 g from each potsherd was ground and mixed with wax (to retain ^{222}Rn) before measuring the beta contribution to the annual dose rate by beta counting in a Risø low-level gas flow beta multi-counter system (Bøtter-Jensen & Mejdahl, 1985 and 1988). We adopted the counting geometry and sample preparation developed by (Ankjærgaard & Murray, 2007) by comparing the observed beta count rates with the predicted infinite-matrix beta dose rates derived from gamma spectrometry analysis of Uranium series, Thorium series and ^{40}K standards.

Two considerations were taken into account before using the conversion factors from Ankjærgaard and Murray (2007). First; they neglected the contribution of beta dose rate from other nuclides contamination in their ^{238}U and ^{232}Th standards. In order to define the beta count rate from each nuclide chain individually, we used the gamma spectrometry analysis of each standard to derive the beta dose rate contribution fraction of ^{238}U, ^{232}Th series and ^{40}K to the total beta dose rate. For the ^{40}K standard 100% of the dose rate was derived from ^{40}K, for ^{232}Th standard, 88.8% was derived from ^{232}Th series, and for the ^{238}U standard, 88.7% was derived from the ^{238}U series. The observed beta count rate from each standard was multiplied by these factors before deriving the conversion factor from beta count to beta dose rate.

In addition, Ankjærgaard and Murray also assumed 20% loss of radon when calculating the conversion factor in their U-series calibration; here we make the more correct assumption of full radon retention in these standards (mixed with wax). The revised conversion factors are summarised in Table 3-2 together with the original conversion factors of Ankjærgaard and Murray (2007).

In order to test the reliability of the new conversion factors, the beta count rate was measured for the soil samples from Pella site and several other samples that are not related to the current study, the average of the ratio of the predicted beta count rate derived from gamma spectrometry to the observed count rate was 1.02±0.03 (n=20); this average included ^{238}U and ^{232}Th standards, and the measurement of a composite of 14 potsherds of each layer.

Internal alpha dose rate: Ankjærgaard and Murray (2007) did not consider the possibility of deriving an alpha dose rate from beta counting. We have used the known activity concentrations in their U and Th-series radionuclide standards to derive infinite matrix alpha dose rates (allowing for ^{232}Th contamination in ^{238}U standard and vice versa). The observed beta count rates, after correcting for the real contribution (see above) to beta count rate from each decay series in the standard sample, were divided by these infinite matrix alpha dose rates to give the conversion factors given in Table 3-2. The observed beta count rate from a shard includes some contribution from ^{40}K, which does not contribute to the alpha dose rate. Rather than assume some global average fractional contribution to beta count rate from ^{238}U and ^{232}Th, we derive a more sample specific conversion factor, excluding the beta count rate contribution of ^{40}K, by estimating the average activity ratios from measurement of the average ^{238}U, ^{232}Th and ^{40}K activities in our shards; these were estimated by combining the beta counting samples of 14 potsherds from each layer into a single gamma spectrometry sample (Table 3-3). The resulting activities suggest that, in our samples, 45.1±1.6% of the beta counts are derived from the U-series, and 5.5±0.3% from the Thorium-series from Layer L10.6, 54.5±3% from the U-series and 4.5±0.5% from Thorium-series for the middle layer L15.1, and finally the

bottom layer L15.2, the fractional contribution from Uranium series was 45.4±1.9% and for Thorium series it was 5.4±0.5% (Table 3-3). On average, the likely beta count rate derived only from the U- and Th-series for each shard were then derived by multiplying the total beta count rates by these fractional contributions, and these predicted beta count rates from the ^{238}U and ^{232}Th -series were converted to alpha dose rates by multiplication by the conversion factors of Table 3-2, assuming an 'a' value 0.09±0.01 (see Aitken, (1985), appendix K).

A summary of the internal alpha and beta dose rates for the potsherds is given in Table 3-4.

Water content: to estimate the water attenuation factors, measurements of the field and saturated water contents were undertaken for all soil (for gamma dose rates) and shard (for alpha and beta dose rates) samples. Field water contents were chosen as most closely representing the long-term burial average. Water content corrections used the equations given by Aitken (1985)

The cosmic dose rate contribution was evaluated following (Prescott & Stephan, 1982) and (Prescott & Hutton, 1994) taking into account the depth of the samples, and combined with the total external dose for each layer to give the total dose rate.

Table 3-2: Activities derived from gamma spectrometry for the standards used in Ankjærgaard & Murray (2007) together with a comparison of their conversion factors and those derived here using the modifactions discussed in the text.

	^{238}U ($BqKg^{-1}$)	^{232}Th ($BqKg^{-1}$)	^{40}K ($BqKg^{-1}$)	Observed beta counts	Count rate/beta dose rate, $ks^{-1}/(Gy\ ka^{-1})$ (Ankjærgaard & Murray, 2007)	Modified Count rate/beta dose rate, $ks^{-1}/(Gy\ ka^{-1})$	Count rate/alpha dose rate, $ks^{-1}/(Gy\ ka^{-1})$
^{238}U standard	972±9	14.7±0.7	515 ± 10	739.4±1.6	66.7 ± 3.1	53.05±0.96	3.9±0.1
^{232}Th standard	9.36±1.23	1792 ± 30	571± 14	878.56±1.84	61.3 ± 0.8	56.7±1.9	2.4±0.1
^{40}K standard	-	-	13767±94		61.20 ± 1	61.20 ± 1	-

Table 3-3: gamma spectrometry analyses of mixtures of 14 potshards from each layer, and the fractional contribution from each nuclide to beta count rate factors.

	Beta dose rate (Gyka^{-1})			Alpha dose rate (Gyka^{-1})	
	^{238}U	^{232}Th	^{40}K	^{238}U	^{232}Th
L10.6	1.21 ±0.02	0.137 ±0.006	1.133±0.050	22.9 ±0.3	3.56±0.16
L15.1	2.32±0.04	0.182±0.008	1.51±0.12	44.1±0.6	4.87±0.34
L15.2	0.843±0.014	0.094±0.010	0.79±0.05	16.1±0.2	2.5±0.2
Fractional beta count rate contribution from each nuclide					
	^{238}U	^{232}Th	^{40}K	Observed average beta count rate	
L10.6	0.45±0.02	0.055±0.003	0.49±0.03	150±2	
L15.1	0.55±0.03	0.045±0.005	0.41±0.05	180±3	
L15.2	0.45±0.02	0.054±0.005	0.5±0.04	198±2	

Table 3-4: Derived beta and alpha dose rates using the observed beta count rate from each shard. The gamma dose derived from gamma spectrometry analyses of sediment samples from each layer is given at the end of the table.

Sample	Observed beta counts (cks^{-1})	Beta dose rate (Gy/ka)	Alpha dose rate (Gy/ka)
L10.6.1	169.8±2.4	2.98±0.1	28.83±0.04
L10.6.2	131.4±2	2.3±0.1	22.32±0.03
L10.6.3	170±2.3	2.98±0.10	28.9±0.04
L10.6.4	441±3.4	7.7±0.3	74.9±0.1
L10.6.5	167.5±2.2	2.94±0.10	28.5±0.04
L10.6.6	155.6±2.2	2.7±0.1	26.43±0.04
L10.6.7	153±2.1	2.7±0.1	25.98±0.03
L10.6.8	139±2	2.4±0.1	23.6±0.03

L10.6.9	142±2	2.5±0.1	24.12±0.03
L10.6.11	105.2±1.7	1.9±0.1	17.86±0.02
L10.6.12	183.4±2.1	3.22±0.11	31.15±0.04
L10.6.13	177±2	3.11±0.1	30.06±0.04
L10.6.14	123.1±2	2.2±0.1	20.9±0.03
L10.6.15	136.2±1.9	2.4±0.1	23.1±0.03
L10.6.16	167.9±2.1	2.9±0.1	28.5±0.04
L10.6.17	216.9±2.5	3.81±0.13	36.83±0.05
L10.6.18	156.3±2.4	2.74±0.10	26.6±0.04
L10.6.19	105.6±2	1.6±0.1	17.9±0.03
L10.6.20	131.6±2	2.3±0.1	22.3±0.03
L15.1.1	191.6±3.3	3.4±0.2	37.6±0.9
L15.1.2	164.6±3.02	2.9±0.2	32.3±0.1
L15.1.3	187.9±2.8	3.3±0.2	36.9±0.1
L15.1.4	172±2.8	3.1±0.2	33.8±0.1
L15.1.6	177.1±2.1	3.2±0.2	34.8±0.8
L15.1.7	143.5±1.8	2.55±0.14	28.2±0.1
L15.1.8	196.4±2.2	3.50±0.2	38.6±0.1
L15.1.9	171.5±2.1	3.1±0.2	33.7±0.1
L15.1.10	292.3±3	5.2±0.3	57.38±0.11
L15.1.11	219.2±2.5	3.9±0.2	43±0.9
L15.1.12	123.2±1.9	2.2±0.1	24.2±0.1
L15.1.13	144.2±2	2.56±0.14	28.3±0.1
L15.1.14	165.4±2.0	2.9±0.2	32.5±0.1
L15.1.15	177.3±2.2	3.2±0.2	34.8±0.1
L15.1.16	221.6±2.5	3.9±0.2	43.5±0.1
L15.1.17	171.8±2.1	3.1±0.2	33.7±0.1
L15.1.18	135.4±2.1	2.4±0.1	26.6±0.6
L15.1.19	248.4±2.6	4.4±0.2	48.8±0.1

L15.1.20	169.0±2.6	3±0.16	33.2±0.1
L15.2.1	157.3±2.0	2.76±0.11	26.8±0.04
L15.2.2	133.5±1.9	2.3±0.1	22.74±0.04
L15.2.3	280.7±2.7	4.9±0.2	47.8±0.1
L15.2.4	107.8±1.7	1.9±0.1	18.4±0.03
L15.2.5	178.5±2.5	3.1±0.1	30.4±0.05
L15.2.6	264±3.1	4.6±0.2	45±0.1
L15.2.7	282.8±2.5	5±0.2	48.2±0.1
L15.2.8	175.5±2.1	3.08±0.12	29.9±0.1
L15.2.9	133.1±1.9	2.3±0.1	22.7±0.04
L15.2.10	259.2±2.6	4.6±0.2	44.2±0.1
L15.2.12	221.3±2.4	3.9±0.2	37.7±0.1
L15.2.13	211.2±2.2	3.7±0.2	36±0.1
L15.2.14	199.6±2.2	3.5±0.1	34±0.1
L15.2.15	184.1±2	3.23±0.13	31.4±0.1
L15.2.17	171.7±2.1	3.01±0.12	29.3±0.1
L15.2.18	167.6±2.1	2.9±0.1	28.5±0.1
L15.2.19	161.8±2	2.84±0.11	27.6±0.04
L15.2.20	136.3±1.8	2.4±0.1	23.21±0.04

External dose rate				
Soil samples	Gamma dose rate (Gy/ka)	^{238}U (Bq/kg)	^{232}Th (Bq/kg)	^{40}K (Bq/kg)
L10.6	1.01 ± 0.1	132.2±32	13.8±1.6	502±25
L15.1	1.64 ± 0.15	180±24	12.9±1.3	341±21
L15.2	1.26 ± 0.11	130±23	11.4±1.8	325±24

3.4 Luminescence Characteristics

The majority of the samples provided few sand-sized grains of K-feldspar and quartz, some of the few potsherds that provided quartz; the quantity was insufficient to prepare enough aliquots for efficient equivalent dose measurement. And so all further studies were undertaken using poly-mineral fine grains.

In total, fifteen potsherds from deposit L10.6, nineteen from L15.1, and eighteen potsherds from L15.2 were used for estimation of equivalent dose (D_e). At least eight aliquots were prepared for each potshard.

A modified single aliquot regenerative dose SAR protocol for K-feldspars (Buylaert *et al.*; 2009) was used to estimate the D_e; the preheat temperature before any IR stimulation was fixed at 320 ^oC and held for 60 seconds before cooling and subsequent IR stimulation. Two stimulations were used: IR at 50 ^oC for 100s to remove any unstable signal followed by post IR- IRSL stimulation at 290 ^oC for 100s. The same parameters were used for measurement of signals induced by the test dose. An illumination step using the IR source for 100s at 325 ^oC was used at the end of each SAR cycle to reduce the charge transfer after repeated thermal and stimulation treatment (Murray & Wintle, 2003).

The observed $pIRIR_{290}$ luminescence signals were relatively weak for most of the samples (Figure 3.3) but still stronger than the corresponding IR_{50} signals. Dose response curves were constructed using integration of the first 20 seconds of the stimulation curves, after subtracting a background based on the final 80 seconds.

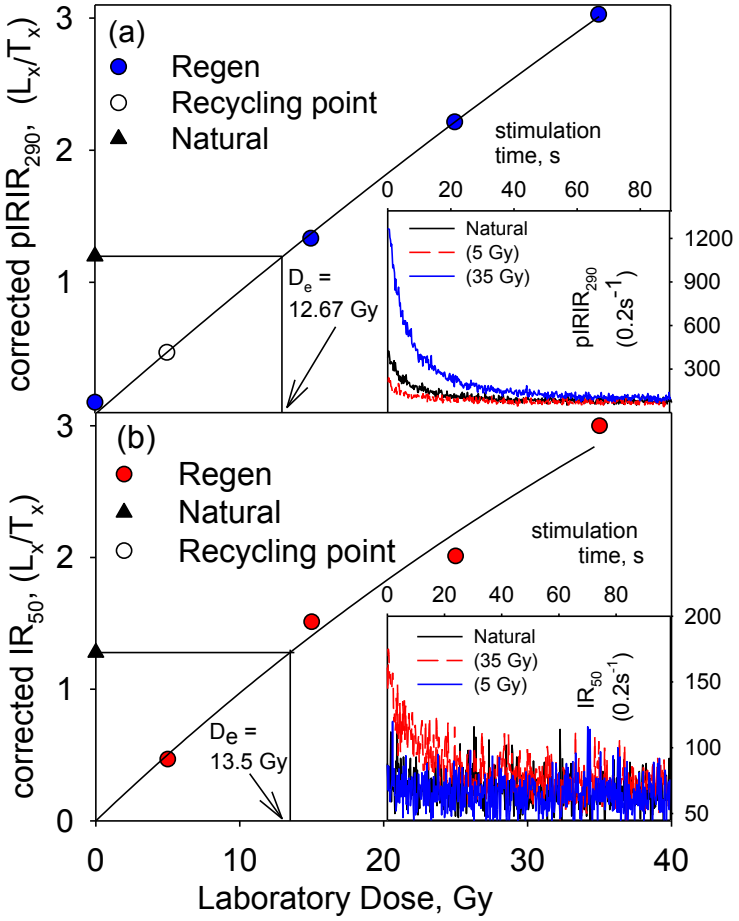

Figure 3.3: representative dose response curve and (inset) natural and regenerated stimulation curves (a) for post-IR IRSL signals at 290 °C and (b) for IR signal at 50 °C for shard L15.1.4, from layer L15.1.

The performance of the measured $pIRIR_{290}$ signal was tested by means of the recycling and recuperation ratios; the average of both values was taken only for aliquots which gave an error within 30% and for samples which used in age calculation (see section 3.5.1), 69% of the measured aliquots satisfied the criteria for the recycling ratio test, and the average is 1.07±0.02 (n= 240), which indistinguishable from, or within 10% of unity. For the average recuperation; 46% of the measured aliquots was used to estimate the average (6.95±0.31, n=161). All these values are considered acceptable, given the weak signals and the correspondingly large uncertainties.

3.4.1 D_e and the first stimulation temperature

The reliability of the dose estimates was investigated by comparing the $pIRIR_{290}$ D_e values integrated after first IR stimulation at various temperatures; samples L10.6.12, L15.1.4 and L15.2.10 were chosen for the measurements. Eighteen aliquots were prepared from each sample, and our SAR protocol applied to groups of 3 aliquots with the first IR stimulation temperature ranging from 50 ^oC to 250 ^oC in 40 ^oC steps. The results are summarised in Figure 3.4, and the equivalent dose is considered independent of first stimulation temperature in the temperature region 50 to 210 ^oC, for all three samples. The same variables were applied to the test dose which chosen to be 70% of the expected natural dose (Figure 3.4). The ratio between the equivalent doses from the IR signal and $pIRIR_{290}$ varied between the three samples. For sample L10.6.12 both equivalent doses were similar (mean ratio 0.995±0.042, n=18). On the other hand, for sample L15.1.4 the D_e ratio of first IR to $pIRIR_{290}$ was 0.89±0.04 (n=18), and the last sample L15.2.10 gave a ratio of only 0.68±0.04 (n=18).

3.4.2 D_e and the Preheat temperature

The estimation of equivalent doses was also tested for dependence on preheat temperature. Twenty one aliquots of each of the samples L10.6.12, L15.1.8 and L15.2.13 were prepared; for each sample aliquots were divided into 7 groups of 3 aliquots, and each group was measured using our SAR protocol but with different preheat temperature ranging between 100 and 310 ^oC, increasing by 35 ^oC in each step. The first IR stimulation was fixed at 50 ^oC and the pIRIR stimulation temperature was kept 30 ^oC less than the preheat temperature. The same conditions were fixed for the test dose signal measurement. (Figure 3.5)

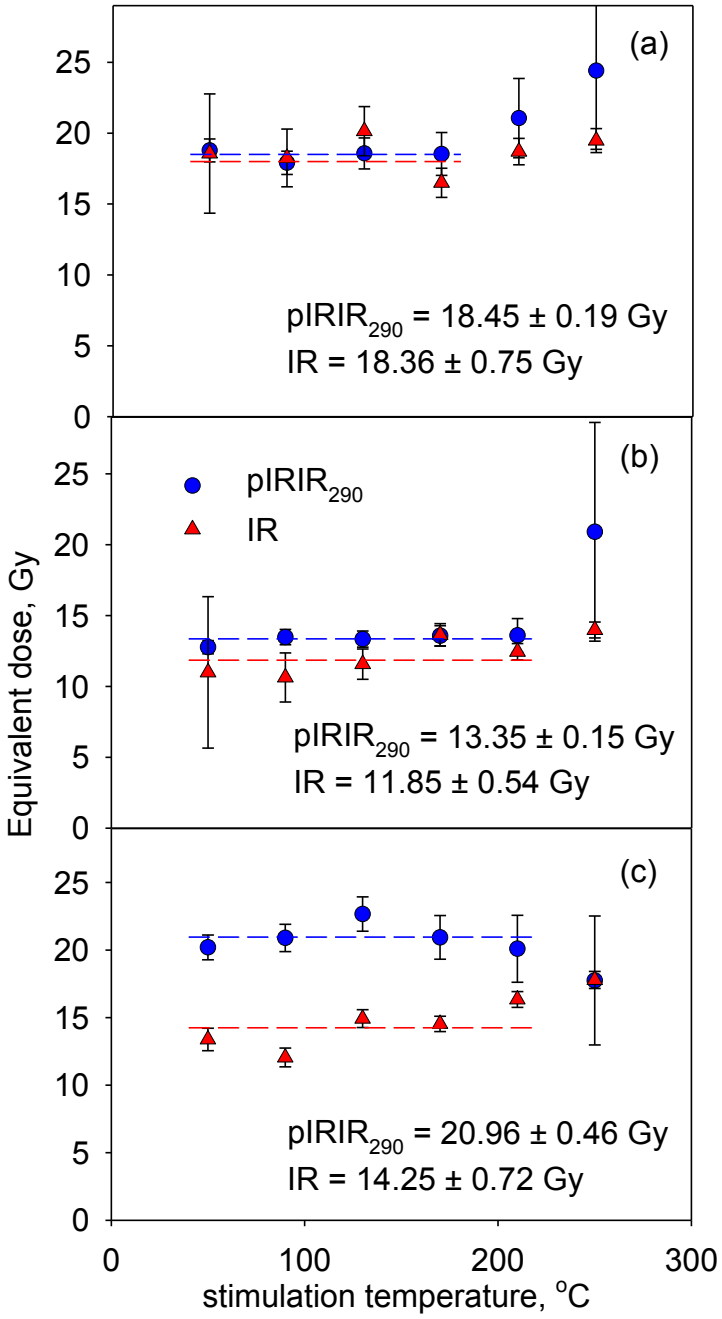

Figure 3.4: Dependence of D_e values on the first IR stimulation temperature for three representative samples (a) L10.6.12, (b) L15.1.4 and (c) L15.2.10. Red symbols- IR and blue symbols- $pIRIR_{290}$.

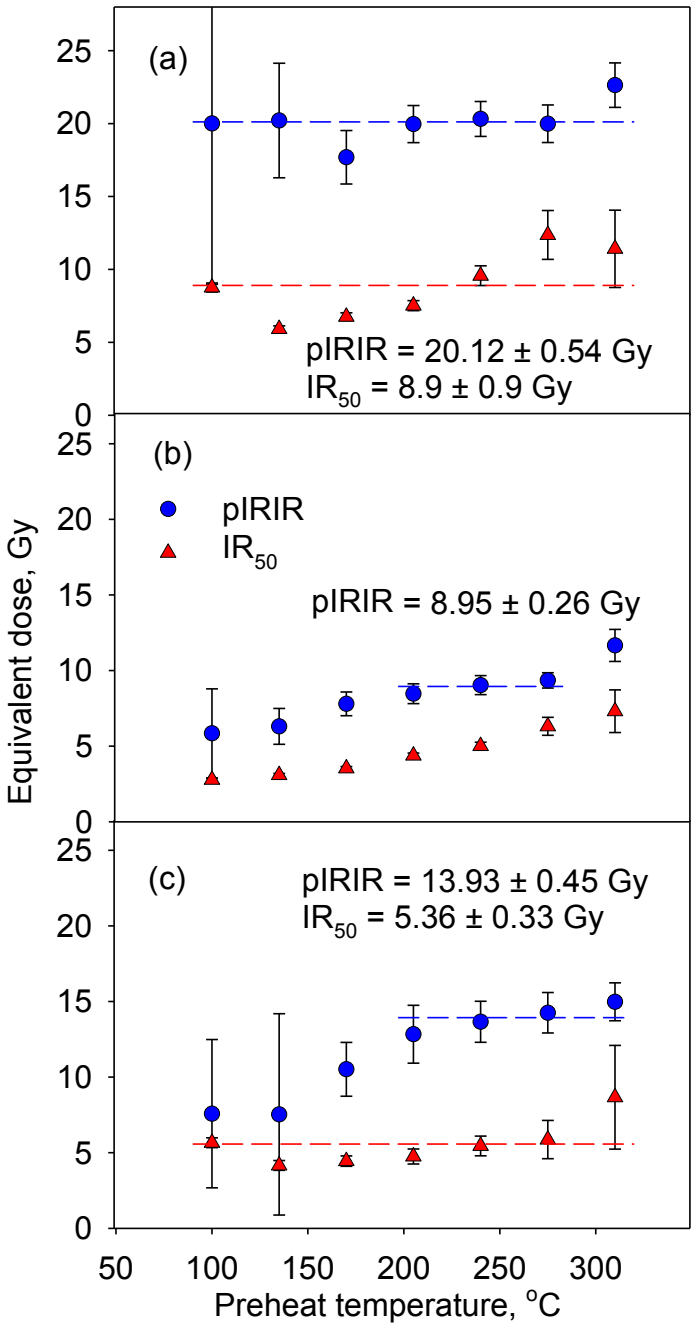

Figure 3.5: Dependence of D_e values on the preheat temperature for three representative samples (a) L10.6.12, (b) L15.1.8 and (c) L15.2.13. Red symbols - IR_{50}, blue symbols – pIRIR.

The equivalent dose does not vary significantly over the entire temperature range for sample L10.6.12, for both IR_{50} and pIRIR signals. For sample L15.2.13, the equivalent doses obtained from the IR_{50} signal appears not to change significantly over the entire range, but the pIRIR signals are only independent of temperature between 205 and 310 ^{o}C. On the other hand, sample L15.1.8 behave different for the IR_{50}, where the D_e increases steadily with temperature, although again the pIRIR signals are independent of temperature between 205 and 310 ^{o}C.

Based on the results of Figures 3.4 and 3.5, we chose to continue measurements using a 320 ^{o}C preheat and a pIRIR stimulation temperature of 290 ^{o}C.

3.4.3 Dose Recovery

Finally the overall performance of the chosen measurement protocol was tested using a dose recovery test. Murray (1996) first tested the ability of a regenerative protocol to measure a dose applied before any thermal treatment by giving doses in addition to the natural dose using ^{60}Co gamma irradiation to test his modified SARA protocol. Later Murray & Roberts (1997) exposed different aliquots to daylight prior to dosing. This was justified as an attempt to imitate the natural signal bleaching process for their samples; this approach was later adopted by others (Wallinga *et al.*, 2000). In this study we used two tests for dose recovery test.

In the first test, 3 different samples (L10.6.1, L15.1.3 and L15.2.2) were heated at 500 ^{o}C for 20 minutes. Aliquots were prepared and irradiated with about 21 Gy. The ratio of the measured dose to the given was 1.20±0.03.

In the second test, 18 aliquots were prepared from the same samples and were exposed to light using solar stimulator for 4 hours before giving laboratory dose equals 21.3 Gy, the ratio of the measured dose to the given using $pIRIR_{290}$ SAR protocol was 1.34±0.07 (n=10). For the same samples another 18 aliquots were prepared and exposed to light for 4 hours, measuring the residual signal and subtracting the average for each sample from the previous dose recovery

measurements had improved the ratio of the measured to the given markedly to 1.02±0.08 (n=18). Results are summarized in Figure 3.6.

The second test was by subjecting the samples to an additional large beta dose in addition to the natural dose to confirm the suitability of our protocol, 32 aliquots were prepared from different samples, the D_e had been estimated and an additional beta dose was given to all aliquots. Because of the weak signals for the natural dose; the chosen given dose was about 10 times greater of the natural dose and the test dose was 70% of the given dose, the ratio between the measured and the given dose (after subtracting the measured natural dose from the total measured dose) was in the range 0.75 to 1.35, with average ratio of 0.99±0.04 (n=32). For the same measurement; the ratio for the measured dose (by integrating the IR signal) to given dose was 1.04±0.03 (n=29), both ratios are indistinguishable from unity (Figure 3.6).

We conclude that optical bleaching is unable to rest the samples to their original, but nevertheless we are able to measure accurately a dose given in addition to the natural dose. This confirms the ability of our chosen protocol to measure a dose given to our samples before any optical or thermal treatment.

.

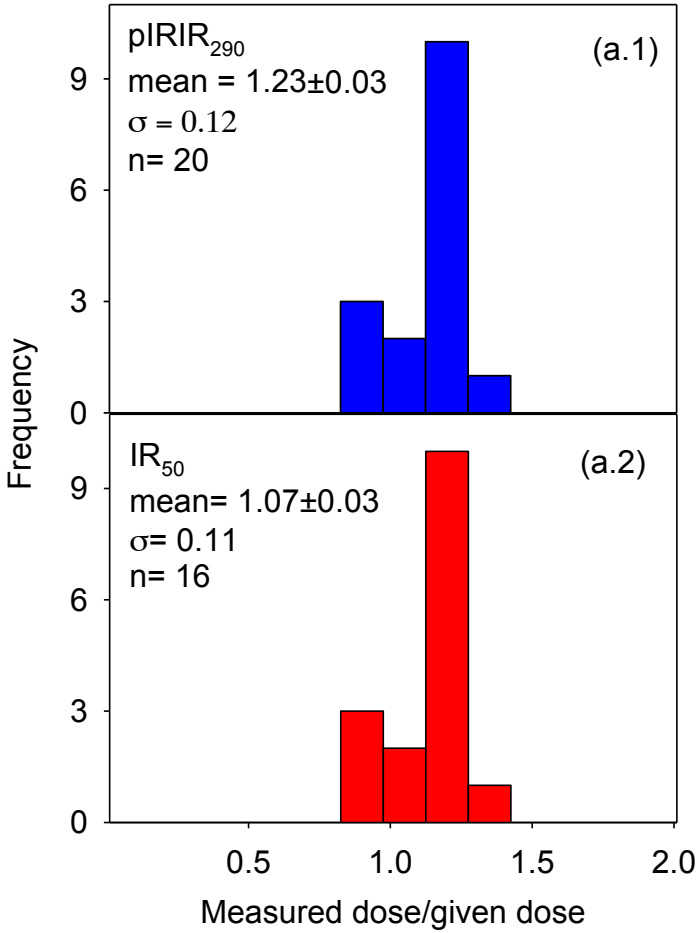
pIRIR290
mean = 1.23±0.03
σ = 0.12
n= 20
(a.1)
IR50
mean= 1.07±0.03
σ= 0.11
n= 16
(a.2)
Frequency
0
3
6
9
0.5
1.0
1.5
2.0
Measured dose/given dose

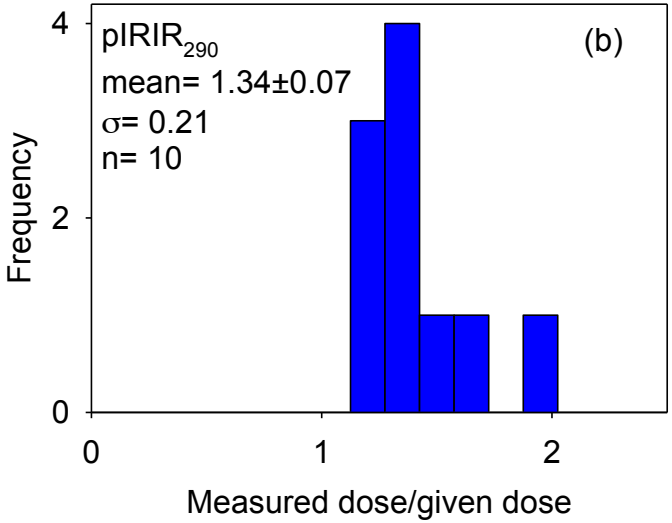
pIRIR290
mean= 1.34±0.07
σ= 0.21
n= 10
(b)
Frequency
0
2
4
0
1
2
Measured dose/given dose

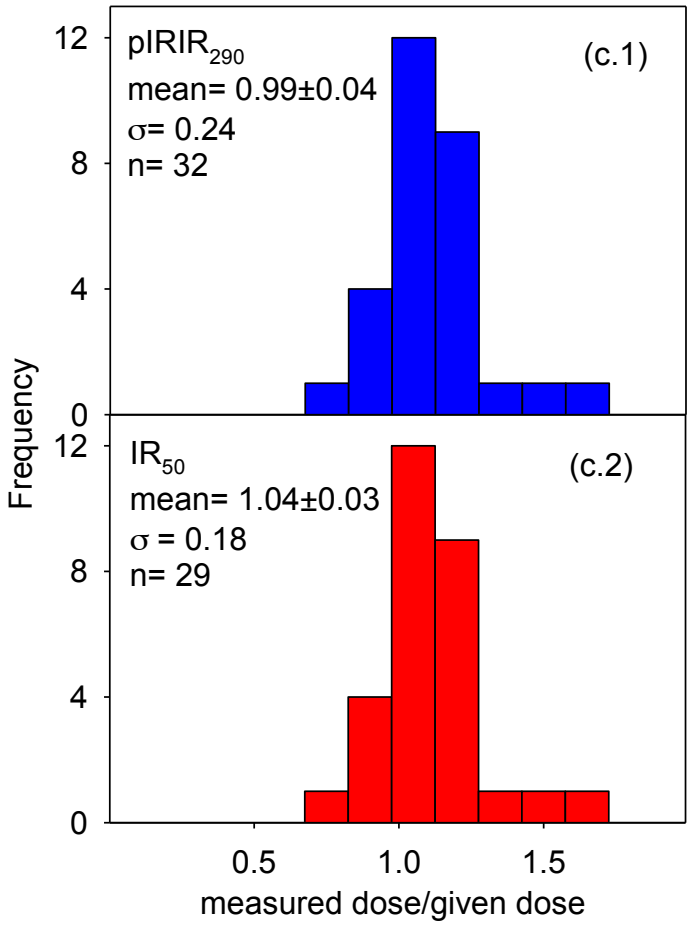

Figure 3.6: Ratios of measured equivalent dose to the given dose for both signals in dose recovery measurements: (a1 for $pIRIR_{290}$ signal and a2 for IR_{50} signal) samples heated to 500 ^{o}C in oven before giving laboratory dose; (b) samples exposed in solar stimulator for 4 hours before giving laboratory dose. Note that the IR_{50} were too weak to derive a meaningful dose recovery histogram; (c1 and c2 for $pIRIR_{290}$ and IR_{50} respectively) samples given laboratory dose in addition to their natural dose, the measured dose to the given dose ratio was calculated after subtracting the natural dose from the total measured dose.

3.5 Equivalent doses and ages

3.5.1 Equivalent Dose D_e

The integration of the signal was for the first 20 seconds of stimulation, and the background was integrated over the last 80 seconds for both IR_{50} and $pIRIR_{290}$ signals. One sample (L15.2.13) was rejected because of a poor recycling ratio. In addition the signals from many shards were very weak; we have chosen to reject all samples for which the average $pIRIR_{290}$ summed response to the natural test dose was <1000 counts. This resulted in the rejection of 14 shards out of a total of 52. Thomsen *et al.* (2011) have shown that the IR_{50} signal is significantly less thermally stable than the $pIRIR_{290}$ signals. Thus if a shard was not heated to a high enough temperature to fully reset the more stable $pIRIR_{290}$ signal, this should be revealed by an unusually low $IR_{50}/pIRIR_{290}$ ratio. However the IR_{50} signals were even weaker than the $pIRIR_{290}$ signals, and only 3 shards passed the intensity rejection criterion of 1000 counts when the IR_{50} signals were considered. Even relaxing this criterion to accept IR_{50} signals >500 counts only accepted 14 shards (out of 52). Figure 3.7 shows a plot of these few accepted IR_{50} equivalent doses against the corresponding $pIRIR_{290}$ equivalent doses and it can be seen that all are consistent with a straight line of slope 0.72 passing through the origin. There is no evidence here for inadequately heated outliers (these would plot significantly below the line) and so we assume that all shards were heated sufficiently to fully empty the IRSL signals.

Although it can be safely assumed that the $pIRIR_{290}$ signal does not fade significantly (Buylaert, *et al.*, 2011) (Thomsen, *et al.*, 2011), especially at such low doses, we have nevertheless measured fading rates for 3 aliquots each, of two samples, one from layer L15.1 and one from L15.2. The average g value measured over 12 hours storage was -1.6 ±0.4 % per decade (n=6; data not shown); there is no evidence here for any significant loss of signal confirming our expectations that no fading correction is necessary.

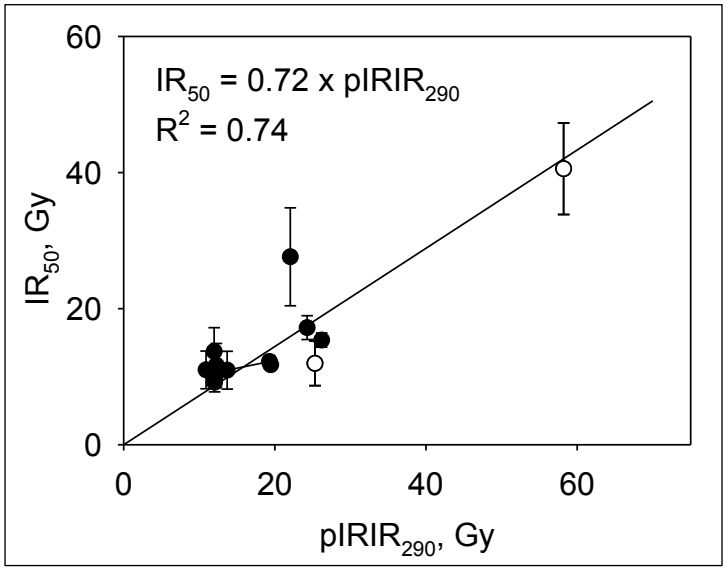

Figure 3.7: comparison of IR_{50} D_e and $pIRIR_{290}$ D_e; open circles represent age outliers (see text)

3.5.2 Ages

Age estimates have been derived from the equivalent doses (Table 3.5) and the dose rates (Table 3.4) for a total of 52 samples. In Table 3.5 we list ages with both random and total uncertainties in ages. The total uncertainties include those arising from external gamma dose rates (common to all shards from a given layer), beta source calibration (±2%) and water content (±25%).

We expect based on archaeological evidence; that the majority of the shards within a layer should be of the same broad age grouping. However it is clear from Table 3.5 that the random uncertainties in the individual shard ages do not explain the dispersion of the ages from each layer. There are three samples out of the 38 accepted results that are markedly older in age than the remainder (highlighted in Table 3.5). Two of these outliers have been 'accepted of the data set' of Figure 3.7; there is no evidence for insufficient heating as an explanation for the unusually large equivalent doses of these two samples. In any case, even if

these outliers are rejected, the ages within each layer remain over dispersed. We conclude that our calculated random uncertainties under estimate the true variability in our analyses.

The top half of Table 3.6 summarise the average age for each layer with the associated standard error, the over dispersion (the degree to which the random uncertainties underestimate the true dispersion) and the total error. The lower part of Table 3.6 repeats this information but excluding the three outliers discussed above and highlighted in Table 3.5. This information is repeated for the site average age of 2.85±0.12 ka at the bottom of Table 3.6.

Table 3-5: Summary of ages and related data for 52 potshards. The samples rejected because of low luminescence intensity (test dose response minus background, T-Bg, <1000) are identified by italics, and the single underlined sample was rejected because of poor recycling ratio. The 3 outliers discussed in the text are highlighted in grey.

	Sample No.	Age (ka)	Rand. Error (ka)	D_e (Gy)	Dose rate (Gy/ka)	(T-Bg)
1	L10.6.1	2.4±0.2	0.15	12.7±0.6	5.2±0.4	2802
2	L10.6.2	2.4±0.2	0.17	10.5±0.6	4.3±0.3	2058
3	L10.6.3	2.9±0.3	0.2	15.2±1.1	5.2±0.4	1334
4	L10.6.4	2.8±0.3	0.2	37.4±2.4	13.5±0.9	1852
5	L10.6.5	2.7±0.3	0.2	13.9±0.9	5.2±0.4	3256
6	L10.6.6	2.4±0.2	0.11	12.0±0.2	5.0±0.4	11175
7	L10.6.7	2.4±0.2	0.1	12.04±0.2	5.1±0.4	11127
8	L10.6.8	3.0±0.2	0.13	14.2±0.2	4.6±0.3	2870
9	L10.6.9	5.0±0.7	0.6	22.2±2.7	4.5±0.4	547
10	L10.6.11	10.7±3.5	3.4	38.7±12.3	3.6±0.3	549
11	L10.6.12	3.8±0.5	0.4	22.1±1.9	5.8±0.4	2995
12	L10.6.13	3.2±0.6	0.6	17.5±3.1	5.5±0.5	670
13	L10.6.15	6.6±2.3	2.3	29.1±9.9	4.4±0.3	448
14	L10.6.16	2.6±0.2	0.11	13.7±0.3	5.2±0.4	3210
15	L10.6.17	3.1±0.3	0.2	19.3±0.7	6.3±0.5	4630
16	L15.1.1	3.7±0.6	0.5	25.2±2.8	6.8±0.6	1275
17	L15.1.2	2.9±0.3	0.2	16.89±1.0	5.8±0.5	1126

18	L15.1.3	2.4±0.3	0.2	15.5±0.8	6.6±0.6	2601
19	L15.1.4	2.3±0.2	0.14	14.2±0.3	6.2±0.6	8952
20	L15.1.6	2.5±0.2	0.15	15.6±0.3	6.3±0.6	5894
21	L15.1.7	3.4±0.6	0.5	18.3±2.6	5.5±0.5	659
22	L15.1.8	3.0±0.4	0.3	20.8±1.8	6.9±0.6	3714
23	L15.1.9	3.5±0.4	0.3	22.1±1.3	6.3±0.5	1257
24	L15.1.10	3.7±0.4	0.2	32.7±0.7	8.9±0.9	3879
25	L15.1.11	4.1±0.5	0.3	29.3±1.5	7.2±0.7	3146
26	L15.1.12	8.7±1.3	1.1	38.8±4.4	4.5±0.4	3631
27	L15.1.13	3.2±0.4	0.3	16.1±1.2	5.04±0.5	4649
28	L15.1.14	5.9±3.0	2.9	35.7±17.6	6.1±0.5	381
29	L15.1.15	1.7±0.8	0.8	10.3±4.9	6.1±0.6	353
30	L15.1.16	2.5±0.3	0.3	18.6±1.8	7.4±0.7	1164
31	L15.1.17	4.1±0.5	0.4	25.2±1.7	6.2±0.6	782
32	L15.1.18	2.7±0.9	0.9	13.9±4.3	5.1±0.5	616
33	L15.1.19	1.5±0.2	0.2	11.86±1.2	8±0.8	1221
34	L15.1.20	4.0±0.4	0.3	24.3±0.9	6.1±0.5	3073
35	L15.2.1	2.6±0.3	0.2	13.3±0.9	5.2±0.4	1498
36	L15.2.2	2.7±0.2	0.12	12.3±0.3	4.6±0.3	3561
37	L15.2.3	2.3±0.2	0.14	18.9±0.9	8.4±0.7	1617
38	L15.2.4	6.5±0.6	0.4	25.3±1.4	3.9±0.3	1284
39	L15.2.5	2.9±0.3	0.2	16.1±0.8	5.6±0.4	1322
40	L15.2.6	1.69±0.14	0.1	13.6±0.5	8.1±0.6	5259
41	L15.2.7	6.7±0.7	0.6	58.2±4.7	8.7±0.6	3657
42	L15.2.8	2.5±0.4	0.4	14±2	5.6±0.4	1245
43	L15.2.9	2.8±0.6	0.6	12.8±2.8	4.6±0.3	756
44	L15.2.10	2.5±0.2	0.1	19.5±0.3	7.7±0.6	10969
45	L15.2.12	4.2±1.0	1.0	28.5±6.6	6.8±0.5	903
46	L15.2.13	1.8±0.2	0.13	12.1±0.8	6.8±0.5	2987
47	L15.2.14	4.8±0. 6	0.5	31.5±2.9	6.5±0.5	523
48	L15.2.15	4.4±0.3	0.2	26.2±0.6	6.0±0.4	12303
49	L15.2.17	4.5±0.5	0.4	23.9±1.8	5.3±0.4	1065
50	L15.2.18	1.95±0.2	0.2	10.9±0.8	5.6±0.4	4011
51	L15.2.19	2.0±0.2	0.1	10.9±0.3	5.4±0.4	2620
52	L15.2.20	3.0±0.6	0.6	14.0±2.6	4.7±0.3	956

Table 3-6: Summary of average ages of each layer and the site average age.

Layer	Number of accepted samples	Age average (ka)	Random uncertainty (ka)	Total uncertainty (ka)	Over-dispersion (ka)	Over-dispersion (%)
With outliers						
L10.6	11	2.79	0.13	0.24	0.29	10.5 %
L15.1	14	3.45	0.45	0.54	1.14	36.1 %
L15.2	13	3.32	0.49	0.51	1.27	42.2%
Without outliers						
L10.6	11	2.79	0.13	0.24	0.29	10.5 %
L15.1	13	3.02	0.21	0.30	0.74	25.1 %
L15.2	11	2.72	0.28	0.34	0.75	28.6 %
Site Average Age						
Including outliers	38	3.20	0.20	0.30	1.0	33.8 %
Excluding outliers	35	2.85	0.12	0.22	0.66	24.1 %

3.6 Discussion and conclusion

Very few of these samples contained sufficient sand-sized quartz for measurement, and in no cases were there sufficient grains of both quartz and feldspar to allow precise D_e estimation; as a result all work reported here used polymineral fine grains. Even so, more than 25% of the samples were rejected because of insufficient $pIRIR_{290}$ signal, leaving only 38 samples with signals strong enough to be useful. Within each occupation layer, it was anticipated that the majority of the sherds should be from the same period; nevertheless 3 (out of 38) gave ages markedly older than the remainder. However, it is an archaeological commonplace that older materials are often churned up in multi-period 'tell' sites such as Pella, which has superpositional occupation layers stretching back into the Seventh Millennium BCE.

In the particular case of the Civic Building, the deep foundations of this major structure would certainly have disturbed earlier horizons during the construction process. As well, the making of the large mudbricks used in the construction of the building complex often contained sherds of pottery from much earlier horizons, which were mixed in with the clay when the bricks were made. This resulted in materials from the Bronze Age (3400 BP) and the Chalcolithic period (5200 BP) being found together with Iron Age materials (2900 BP) contemporary with the building itself.

This observation is supported by such readings as ^{14}C sample VERA 5308 (5205 ± 35 cal. years BP), drawn from the same Iron Age horizons (as discussed above). We conclude that OSL has successfully identified that three of the sherds expected at the time of excavation to be Iron Age (ca. 1050- 900 BC) are in fact redeposited from earlier occupation potentially as old as the Chalcolithic period (5200 cal. years BP), probably during the construction of the Civic Building; such limited contamination being completely consistent with archaeological expectations, and does not affect the dating of the occupational horizon, which in all cases is pegged to the latest material in any given deposit..

The typical calculated random uncertainty on each OSL age is ~250 years. From an archaeological perspective, the expected age range per layer is of the order of 50 to 100 years. Thus we would expect analytical uncertainties to dominate the spread in the ages from each layer. However, the age range represented by sherds from the uppermost (yougest) layer is ~1000 years, >2500 years for the middle layer, and ~3000 years in the oldest bottom layer. We deduce that this considerable over- dispersion in our data is most likely to arise from unaccounted laboratory uncertainties; this over-dispersion is between 10 and 30% of the average age of each layer (Table 3.6). Because of this we cannot meaningfully discuss individual ages of each shard, but only the average ages for each layer.

If the three outliers discussed above are ignored, then the three layers have similar average ages, all of which are consistent with the average site age of 2850 years (±120 years random uncertainty, ±220 years total uncertainty; (Table 3.6). This average site luminescence age is completely consistent with the expected archaeological age range of between 2700 and 2900 cal. BP years (Bourke 2014, 18, which is in good agreement with the relevant ^{14}C ages (Wild & Fischer 2013, 461-464), summarised in Table 3.1, ranging between 2800 and 3200 cal B.P.

In conclusion this study was made more difficult than expected by the absence of sand-sized quartz and feldspars; that, together with the relatively weak signal from poly-mineral fine-grains, gave age uncertainties higher than expected. Nevertheless it has proved possible to identify three samples out of 38 as reworked material. This would have been difficult to demonstrate on typological grounds because these samples did not have marked typological characteristics.

Despite the difficulties in dating these potsherds, we have been able to determine a site age completely consistent with expectation, and this demonstrates the usefulness of pIRIR dating of heated materials from the Jordan Valley. This in turn shows that pIRIR dating can probably be used with confidence on heated materials of unknown age from this region.

4. Chapter 4: Testing the application of post IR IRSL dating to Iron- and Viking-age ceramics and heated stones from Denmark

This chapter will use the $pIRIR_{290}$ to ceramic and heated stones with no typological structure or previous radio metric dates. The test will use quartz OSL ages to support the age control.

5. Chapter 5: Application of OSL dating to a Chalcolithic well in Qulbān Banī Murra, Jordan.

This chapter will investigate the accuracy of ages derived by means of standard OSL dating to sediment deposition in the arid zone directly resulting from human activities.

5.1 Introduction

Pastoral well-culture occupations make up much of the central parts of the "Mid-Holocene Green Saharo- Arabian Pastoral Belt" (Gebel, 2013), stretching from Yemen to the western Maghreb. The sites are either characterised by extensive megalithic standing-stone burial fields with additional structural features such as ritual structures, well-troughs structures, dams, or by large pens associated with domestic structures (Gebel & Mahasneh 2013). Taken together, these features give evidence that more humid climate conditions sustained steppe environments used by large mobile shepherd communities, vanishing from 4000 BC when drier periods started. In south-eastern Jordan, Qulban Beni Murra represents a major pastoral burial centre, most probable the focal point of a tribal community commemorating its ancestors and meeting for social transactions. But as in most sites from these cultures, research has always hindered by the difficulty in establishing a robust absolute chronology. The sites are mostly deflated and heavily disturbed by later use or looting. Wells often were re-excavated in all periods, and the 5th millennium BC well bottoms were lost in drier periods as the diggings followed the aquifers at deeper levels. The relative-chronological dating of the site is mainly based on one *fossil directeur*, the "fan scraper"; together with the nature of its structures Qulban Beni Murra can be attributed to the Chalcolithic (Late Chalcolithic/Early Bronze) by comparison with other such evidence from the al-Naqab and Sinai as well as from Rajajil and Rasif in northern Saudi Arabia (Gebel, in press). In addition to this contextual dating, there is one radiocarbon date on dispersed organics

available; this associates the structure with the 2nd half of the 5th millennium BC; (see below). (Gebel & Mahasneh 2009; 2012, Gebel, 2010, Gebel *et al.* 2011).

Here we use the OSL signals from quartz and post IR-IRSL signals from K-rich feldspar to determine the last time of exposure to daylight of two sediment samples from Qulban Beni Murra site.

5.2 Archaeological setting, age control and sampling

Qulban Beni Murra is located on the shallow and dissected banks of Wadi Sahab al-Abyad between 30°03'50"/30°05'04"N and 37°14'35"/37°15'35"E. some 13 km N of the Saudi border (Figure 5.1). The immediate site extends for about 1.5 km along both sides of Wadi Sahab al-Abyad, and covers an area of more than one square kilometre - not including outlying grave structures. The wadi banks are shallow *hammada* slopes some 12-14 m above the wadi bottom. The remains of ca. 9 wells/ watering places rest in the wadi floor. The well complex from which the samples were taken (Structure D15) is located in a small mound formed by a mixture of a reddish silty sediment of unknown origin, the structures of the troughs, and the gravels from the well- diggings; the mound is built on the presumed mid-Holocene Wadi floor. The ground plan of the watering place (Figure 5.2) includes a "well room" with a staircase leading to the mouth of the well. The "well room" is joined by stone-paved curvilinear troughs (Spaces 3a-b and 4a-b), as well as two tongue-shaped structures with end rooms (Spaces 7-9 and 10-11, up to 10 m long); the latter apparently are trough lines with descending compartments leading away from the "well room". The paved spaces or troughs were lined and "chambered" by upright (0.5m) standing stone slabs (Figure 5.3), and the centre line of the base of these paved spaces reached their highest points close to the mouth of the well. The eroded reddish silty and very compact sediment in which the structural elements of the well/watering complexes are embedded appears to have been the lining material of the troughs; when mixed with water, this sediment hardens to an almost ceramic-like material, The upper part of the well shaft (1.2m in diameter) is made of

corbelled masonry; this rests on well compacted wadi deposits into which small cavities have been set to serve as steps supports. (Gebel & Mahasneh 2012, 2013, Gebel, 2013).

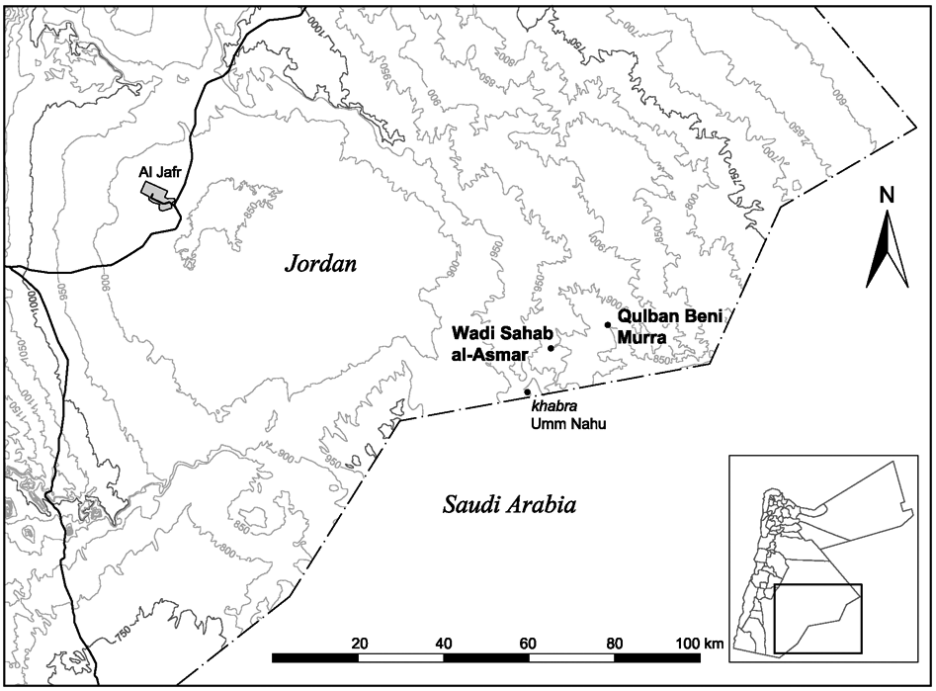

Figure 5.1: Location of Qulban Beni Murra in the south-eastern deserts of Jordan. (P. Keilholz).

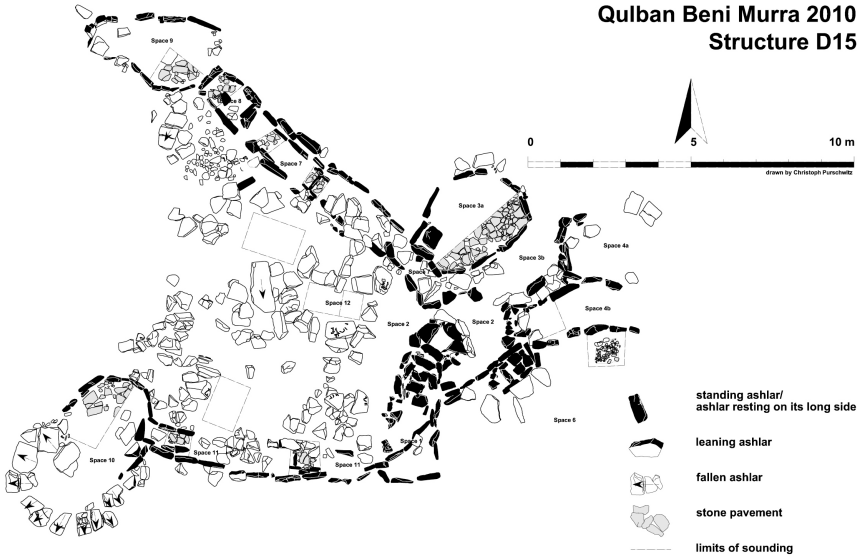

Figure 5.2: Qulban Beni Murra, Structure D15: Well/watering complex, dated to the 2nd half of the 5th millennium BC. (Field records: Pokrandt/Keilholz, graph: Purschwitz

Figure 5.3: Qulban Beni Murra- Area D, Structure D15- and sample location

Figure 5.4: Sampling process. (Photo and sampling taken by Dr. H. Gebel, 2010).

This hardened lining/embedding sediment has provided the only independent age control for this site. From a sounding in Space 12 in D15 (Figure 5.3), sample KIA43373 was taken in 2010 from the lining material, and the disseminated organics within this hardened sediment gave a calibrated ^{14}C age of 4459-4346 cal. BC (2σ range). This date associates the structure with the 2nd half of the 5th millennium BC. (A. Dreves, Leibniz Labor für Altersbestimmung und Isotopenforschung, Kiel University, in letter to J. Pokrandt, Kiel University, pers. comm.).

For our study, two OSL sediment samples were taken from the same context of 2010 (sounding in Space 12 in D15) ca. 50 cm below the surface (samples QBM3 and QBM6; laboratory codes BB644 and BB645, respectively). It remained unclear if this sounding (Figure 5.4), located about 4m WNW from the well mouth, was placed in a room or in an open space between to major trough lines. The section did not show any significant stratification, and there were no significant heterogeneities (stones, gravel beds etc.) within 50 cm of the sampling locations. Steel tubes about 1.5cm internal diameter and 30cm long were driven into the cleaned face of the section and sealed for transport. The radiocarbon samples were taken from similar neighbouring contexts.

5.3 Sample preparation and analytical facilities

In the laboratory, the sediment was removed from the tubes under low-level orange lighting. The inner part of the sample was prepared using standard laboratory procedures with dry sieving to separate the fractions 90-180 and 180-250 µm. Both fractions were treated with 10% HCL to remove carbonates, 30% H_2O_2 to remove organic matter and 10% HF for 20 minutes to remove grain coatings and residual fine material. Aqueous heavy liquid solution (LST Fast float, sodium heteropolytungstate) of density 2.58 $g.cm^{-3}$ was used to separate a quartz-rich fraction from K-rich feldspar grains. Both samples contained only a small amount of feldspar in the grain size range 90- 180 µm and the larger grain size range 180- 250 µm was almost pure quartz. The quartz-rich fractions were

then treated with 40% HF for 40 minutes to remove any remaining feldspar and to etch away the alpha-irradiated outer layer of quartz grains.

Grains were mounted on 10mm diameter stainless steel discs using silicon oil for luminescence measurements. Luminescence measurements employed an automated Risø TL/OSL-DA20 luminescence reader equipped with a calibrated $^{90}Sr/^{90}Y$ beta source delivering ~0.1 $Gy.s^{-1}$, blue LEDs (470 nm, ~80mW/cm^2) and infrared (IR) LEDs (870 nm,~135mW/cm^2) (Thompson *et al.*, 2006). Blue light stimulated signals were detected through 7.5 mm of UV Hoya U-340 filter, and signals were calculated by integrating over the first 0.4 s of the quartz stimulation curve less a background derived from the immediately following 0.4s. IRSL signals were detected through a blue BG-39/7-59 filter combination, and signals were calculated by integrating over the first 20s of the feldspar stimulation curve less a background derived from the final 10s.

5.4 Dose rate determination

Sediments from the ends of the tube samples were used to estimate gamma and beta dose rate. Water content were first measured and the sediments ignited at 450 ^oC for 24 hours; they were then homogenised by grinding and mixed with wax before casting in a standard counting geometry (Murray *et al.,* 1987). Radionuclides concentrations (^{238}U, ^{226}Ra, ^{232}Th and ^{40}K) were determined using gamma spectrometry, and converted into dose rates following Guérin *et al.*, (2011). The contribution from cosmic radiation was estimated following Prescott & Hutton (1994), and the burial depths measured in the field (see Table 5-1).

5.4.1 Quartz

Quartz grains were stimulated for 40s at 125 ^oC following the conventional SAR OSL protocol presented by Murray & Wintle (2000, 2003). Preheat was fixed at 260 ^oC for 10 seconds and cut heat to 220 ^oC for the natural/regenerative dose. OSL signals were measured at 125 ^oC for 40 seconds. To minimise any possible thermal transfer of charge; blue LED stimulation was given at 280 ^oC at the end

of each cycle. The purity of the quartz grains were tested by IR stimulation at 50 ^{o}C for 40 seconds followed by blue LED stimulation at 125 ^{o}C for 40 seconds (Duller, 2003).

From a comparison with the OSL curve from calibration quartz (Hansen *et al.*, 2015) it can be seen that the natural stimulation curves of the both samples are clearly dominated by the quartz OSL fast component (inset to Figure 5.5a; Singarayer & Bailey, 2003; Jain *et al.*, 2003). The resulting response of luminescence to dose is shown in Figure 5.5a; the data have been fitted with a saturating exponential function with characteristic exponential constant D_o=30.08 Gy.

Average recycling ratios and recuperation for sample QBM3 were 0.96±0.04 (n=18) and 10±6% of natural (n=18), respectively. The recycling ratio for sample QBM6 was 1.04±0.04 (n=18) and recuperation 10±3% (n=18). These data demonstrate the reproducibility of measurements made using our SAR protocol when measuring laboratory-induced signals.

We have also tested the dependency of the measured quartz D_e on preheat temperature, by determining equivalent doses using different preheat temperatures between 180 ^{o}C and 300 ^{o}C (the cut heat was set to be 40 degree less than the relevant preheat). The results are presented for sample QBM3 in Figure 5.5b, where it can be seen that there is no significant dependence of the D_e on the preheat temperature.

Finally a dose recovery test was undertaken to examine the overall performance of SAR protocol. Six aliquots of each sample were illuminated twice using blue light for 100 s at room temperature, the two illuminations separated by storage for 10 ks (also at room temperature) to allow for the thermal decay of the 110 ^{o}C trap. The aliquots were then given a dose of ~6 Gy using the beta source and measured in the usual manner. The mean ratio of the measured to the given dose is 1.05 ±0.02 (n=12). This demonstrates that our SAR protocol is able to measure

accurately a known dose given to these quartz samples before any thermal treatment.

The calculated D_e and the derived ages are summarized in Table 5-2. The two samples both give ages consistent with the second half of the 5th millennium BC.

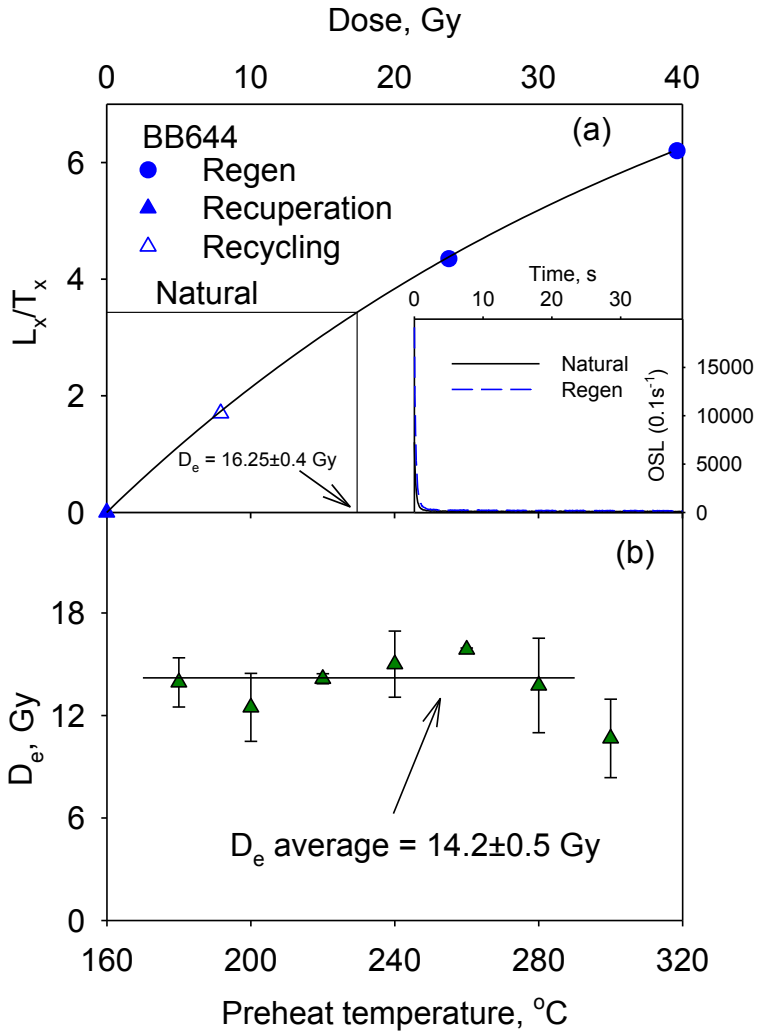

Figure 5.5: quartz dose-response curve and (inset) a typical decay curve from sample QBM3(BB644). (b) preheat plateau for quartz OSL for the same sample.

5.4.2 K- feldspar

5.4.2.1 $pIRIR_{290}$ luminescence characteristic and SAR performance

Feldspar measurements used the post-IR IRSL single-aliquot regenerative (SAR) protocol as described by Thiel *et al.* (2011). IR stimulation was applied twice, the first stimulation for 100 seconds while the sample was held at 50 ^{o}C (IR_{50}), followed by a second stimulation for 100 second while the sample was held at 290 ^{o}C ($pIRIR_{290}$). The test dose was chosen to be ~60% of the expected natural dose. Preheat was fixed at 320 ^{o}C for both the natural/regenerative and the test dose (Murray, 2009). A final IR illumination at 325 ^{o}C was applied at the end of each SAR cycle to minimise the thermal transfer of charge to the next cycle (Figure 5.6).

The reproducibility of the protocol was tested by means of examining the recycling ratio; both samples had ratios close to unity (QBM3= 0.98±0.01 (n=21) and QBM6=1.005±0.036 (n=21)). The average recuperation, expressed as a fraction of the equivalent dose was: QBM3 $pIRIR_{290}$– 4.01 ±0.19% (n=21); IR_{50}– 1.99±0.07% (n=21) and for sample QBM6 $pIRIR_{290}$–3.6±0.11% (n=21); IR_{50}– 1.74±0.07 (n=21).

We next tested the dependence of D_e on the first stimulation temperature for sample QBM3; 18 aliquots were measured in 6 sets of 3 aliquots, with the preheat temperature and the post IRIR stimulation temperature fixed at 320 ^{o}C and 290 ^{o}C, respectively. The temperature of the first IR stimulation started at 50 ^{o}C with an increase of 40 ^{o}C for each set of 3 aliquots. The same parameter values were used after the test dose in each set. Figure 5.7 presents the result of this experiment; there is no evident dependence of the D_e derived from either the $pIRIR_{290}$ signal or from the first IR signal on the first stimulation temperature.

The dependence on preheat was also investigated using sample QBM6. Seven sets, each of three aliquots, were used with a pIRIR protocol in which the preheat temperature was increased from 140 ^{o}C to 320 ^{o}C in steps of 30 degrees with each set. The first IR stimulation temperature was fixed at 50 ^{o}C, and the post

IRIR stimulation temperature was chosen to be 30° less than the preheat temperature. Figure 5.8 shows that the D_e derived from both signals is independent of preheat/pIRIR stimulation temperature over this temperature range.

Finally the overall performance of the post IRIR protocol was investigated using a dose recovery test (Murray, 1996). We chose to apply two different approaches to testing the ability of our protocol to measure a known given dose; the first method was by giving a laboratory dose in addition to the natural dose before any thermal treatment (Murray, 1996). In this approach, an ~65 Gy dose was given to each of ten aliquots of each sample before any other treatment (i.e. in addition to their natural dose) before measuring the total dose using the $pIRIR_{290}$ SAR protocol. In the same measurement sequence, the natural dose was measured using a further three aliquots of each sample, to provide a reference for the irradiated aliquots. The ratio of the measured dose (after subtracting the average of the natural dose) to the given dose for $pIRIR_{290}$ was 0.97±0.02 (n=20) and 0.80±0.03 (n=20) for IR_{50} (Figure 5.9a and b).

The second method involved; aliquots were reset using light prior to dosing. Twelve aliquots were exposed under a Hönle SOL2 solar simulator for 5 hours at a distance of 80 cm. An ~22 Gy dose was then given to each aliquot before measuring using the $pIRIR_{290}$ protocol. The average ratio for the measured to the given dose ($pIRIR_{290}$) was 1.01±0.09 (n=24) and 0.69±0.02 for IR_{50} (Figure 5.9c,d).

The results from both methods indicate that our SAR protocol is able to measure accurately a known dose given before any thermal or radiation treatment.

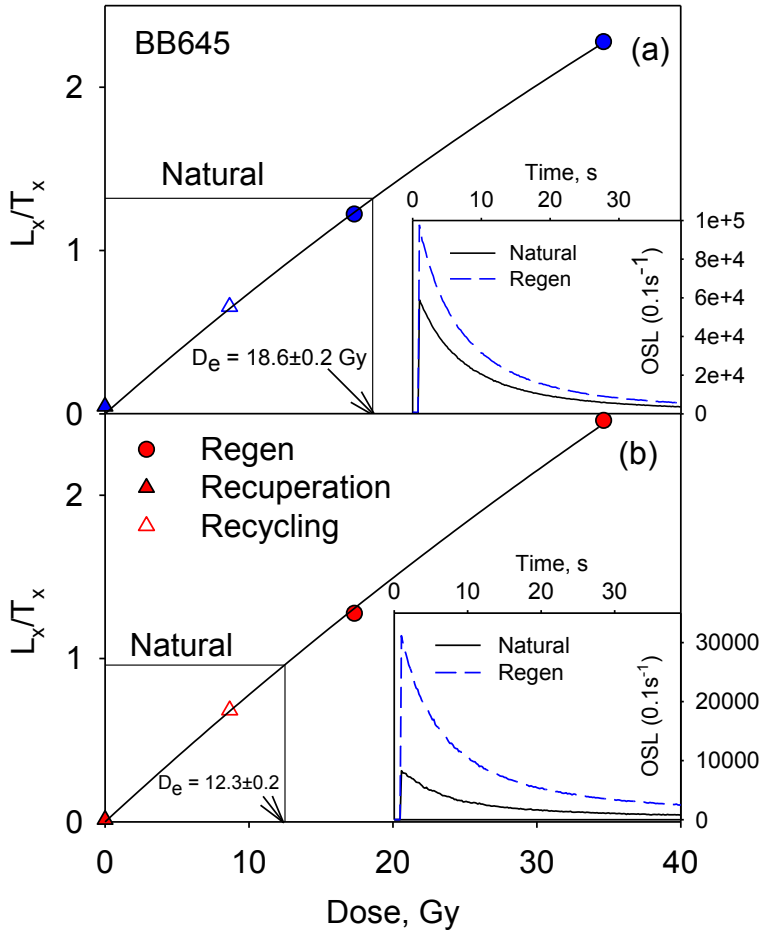

Figure 5.6: representative dose response curves and (inset) natural and regenerated stimulation curves for sample QBM6 (BB645) (a) for post-IR IRSL signals stimulated at 290 ^{o}C and (b) for IR signals stimulated at 50 ^{o}C.

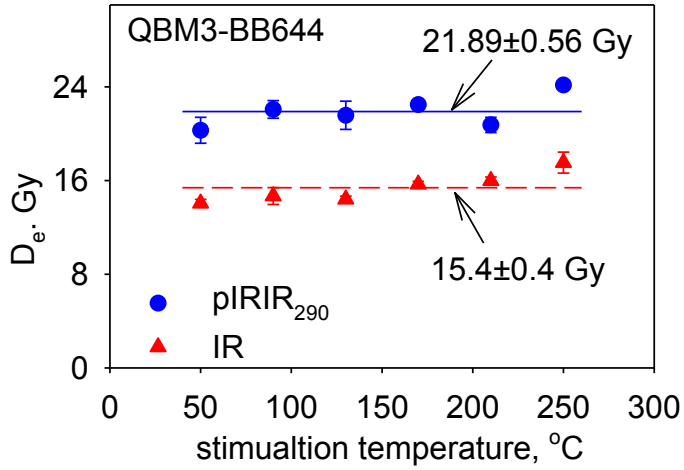

Figure 5.7: Dependence of D_e values on the first IR stimulation temperature for sample QBM3 (BB644)

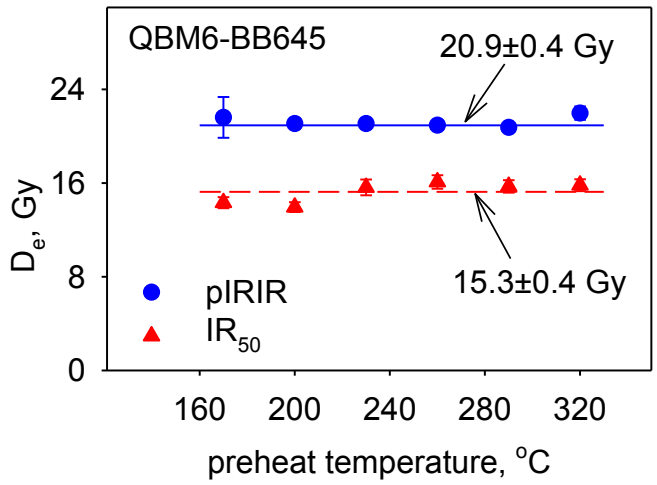

Figure 5.8: The relationship between the apparent equivalent dose and preheat temperature for sample QBM6 (BB645).

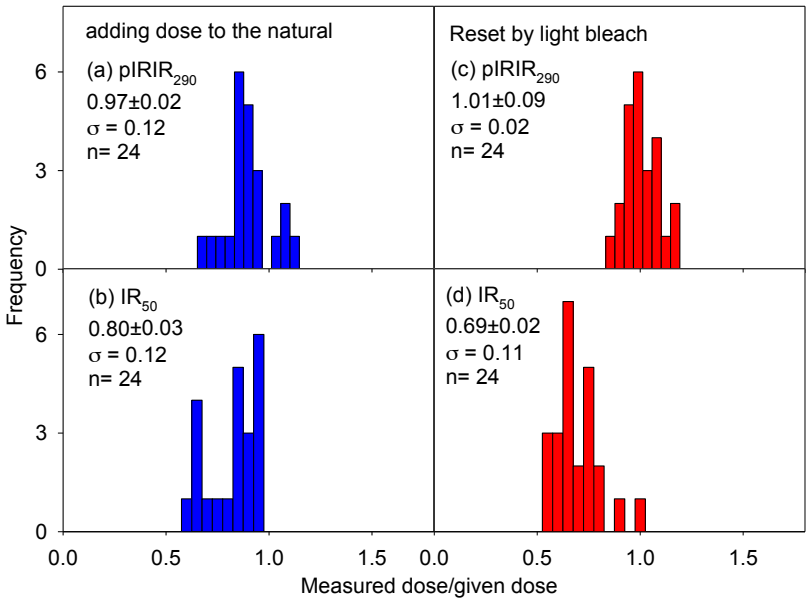

Figure 5.9: Dose recovery measurements. Ratios of measured dose to given dose for both $pIRIR_{290}$ and IR_{50} signals in dose recovery measurements for feldspar: (a,b). Samples measured after adding external dose to their natural dose (c,d) samples exposed in solar stimulator for 4 hours before giving laboratory dose.

5.4.2.2 Fading rate measurement.

Anomalous fading is the loss of luminescence with time exhibited by certain minerals for which kinetic studies have shown that the signal should remain stable (see Aitken, 1985, Appendix F). The most widely accepted explanation for anomalous fading is that electrons tunnel from traps to nearby recombination centres without passing through the conduction band. It is been shown by several studies that the signal loss can be approximated by a logarithmic decay (Huntley & Lamothe, 2001, Auclair *et al.*, 2003). It is thus convenient to express the fading rate as the percentage of signal lost during a storage period of one decade of time (the g-value) where the storage periods are expressed as decades relative to the laboratory irradiation period.

We have measured the laboratory fading for both samples; g-values were derived using the sensitivity-corrected IRSL signal after various periods of storage (Lamothe *et al.* 2003) (Table 5-2). The average g-value for the $pIRIR_{290}$ signal is 0.87±0.17%/decade (n=12), and the average g-value for the IR_{50} signal

is 5.2±2.2%/decade (n=12); this difference is expected since the IR_{50} signal is known to be less stable than the $pIRIR_{290}$ signal (e.g. Thompson *et al*. 2011)

5.4.2.3 D_e and IR ages

The D_e values for the IR_{50} and $pIRIR_{290}$ signals are shown in Table 5-2, together with the derived ages. Those based on the $pIRIR_{290}$ signal do not involve a fading correction (see e.g. Buylaert et al., 2012), whereas those based on the IR_{50} signal are corrected using the 'g' values shown and the equation of Huntley and Lamothe (2003).

5.5 Discussion and conclusions

Table 5-2 summarise the derived luminescence ages for the two samples from OSL quartz, $pIRIR_{290}$ and the corrected ages for the IR_{50} from feldspars. The two samples give the same ages within one sigma of error. The ratio of the corrected IR_{50} ages to the $pIRIR_{290}$ ages confirm that measuring at elevated temperature had minimised the loss of the signal due to anomalous fading.

OSL dating from quartz and $pIRIR_{290}$ from feldspar strongly support the archaeological age for the site. And the available ^{14}C date supports the OSL ages.

Table 5-1: Radionuclide concentrations and resulting dose rates

Sample	Risø code	w.c (%)	^{238}U (Bq/kg)	^{232}Th (Bq/kg)	^{40}K (Bq/kg)	γ-dose rate, (Gy/ka)	β-dose rate, (Gy/ka)	KF- Total dose rate	Qz- Total dose rate
QBM3	BB644	0.2	106±24	23.1±1.7	149±19	0.98±0.07	1.37±0.11	3.07±0.17	2.61±0.12
QBM6	BB645	3.1	102±15	19.1±0.9	165±13	0.92±0.07	1.34±0.08	2.99±0.14	2.42±0.12

Table 5-2: Quartz and feldspars ages.

Sample	Risø code	D_e, (Gy)			g- value (%/decade)		Age (ka)		
		Qz	$pIRIR_{290}$	IR_{50}	$pIRIR_{290}$	IR_{50}	Qz	$pIRIR_{290}$	Corrected IR_{50}
QBM3	BB644	16.4±0.8	20.0±0.4	12.5±0.3	1.0±0.3	4.8±0.9	6.4±0.5	6.5±0.4	6.2±0.8
QBM6	BB645	16.4±0.8	21.0±0.4	12.5±0.2	0.7±0.2	5.7±1.0	6.8±0.5	7.0±0.4	7.09±1.06

6. Chapter 6: Dating a Near Eastern desert hunting trap (kite) using rock surface dating

This chapter will report the first radiometric dating applied to kite stone structure in Jordan. We use the recent method developed in luminescence dating define the kite structure, the method will be applied to three rock samples collected from the Jibal al-Gadiwiyt kite structure in the south east of Jordan.

6.1 Desert kites

Desert kites are stone structures found throughout the Middle East and central Asia; they were first described in 1927 by Royal Air Force pilots flying over the eastern Jordanian desert and the name is derived from their resemblance to the child's toy when viewed from the air (Rees, 1929) (Figure 6.1a). Although recent studies have identified various forms and structures, in general they consist of two long low stone-walls, known as guiding walls, in a funnel-like shape converging into some sort of enclosure where the walls meet. At the corners of the enclosure, smaller cells or compartments called “blinds” were often erected in the form of 3 to 5m wide stone circles (Figure 6.1b). Some kites have well over a dozen of such smaller circles (Kempe & Al- Malabeh, 2010).

Many functions have been proposed for these structures but the most widely accepted hypothesis is that they were used to hunt wild animals, particularly gazelles - *G. subgutturosa or goitered gazelle* - (Maitland, 1927; Fowden, 1999; Holzer *et al.*, 2010; Bar-Oz *et al.*, 2011; Bar-Oz & Nadel, 2013; Zeder *et al.*, 2013). It is suggested that wild gazelle herds were chased into the funnel created by the outer walls and then herded into the end enclosures for capture or slaughter. The small cells or compartments have been interpreted as “hides” from which hunters could shoot the gazelle, and there are some of prehistoric rock art from the region that seem to support this Kites (Harding, 1954; Hoyland, 2001; MacDonald, 2005; Betts & Helms, 1986) (Figure 6.2). Nevertheless, this explanation should not be accepted too uncritically. The tops of the funnel walls are often no more than 30 cm above the

uncritically. The tops of the funnel walls are often no more than 30 cm above the desert floor, and in many cases there is no evidence that the walls were ever more than a single layer of stones high (Figure 6.1b).

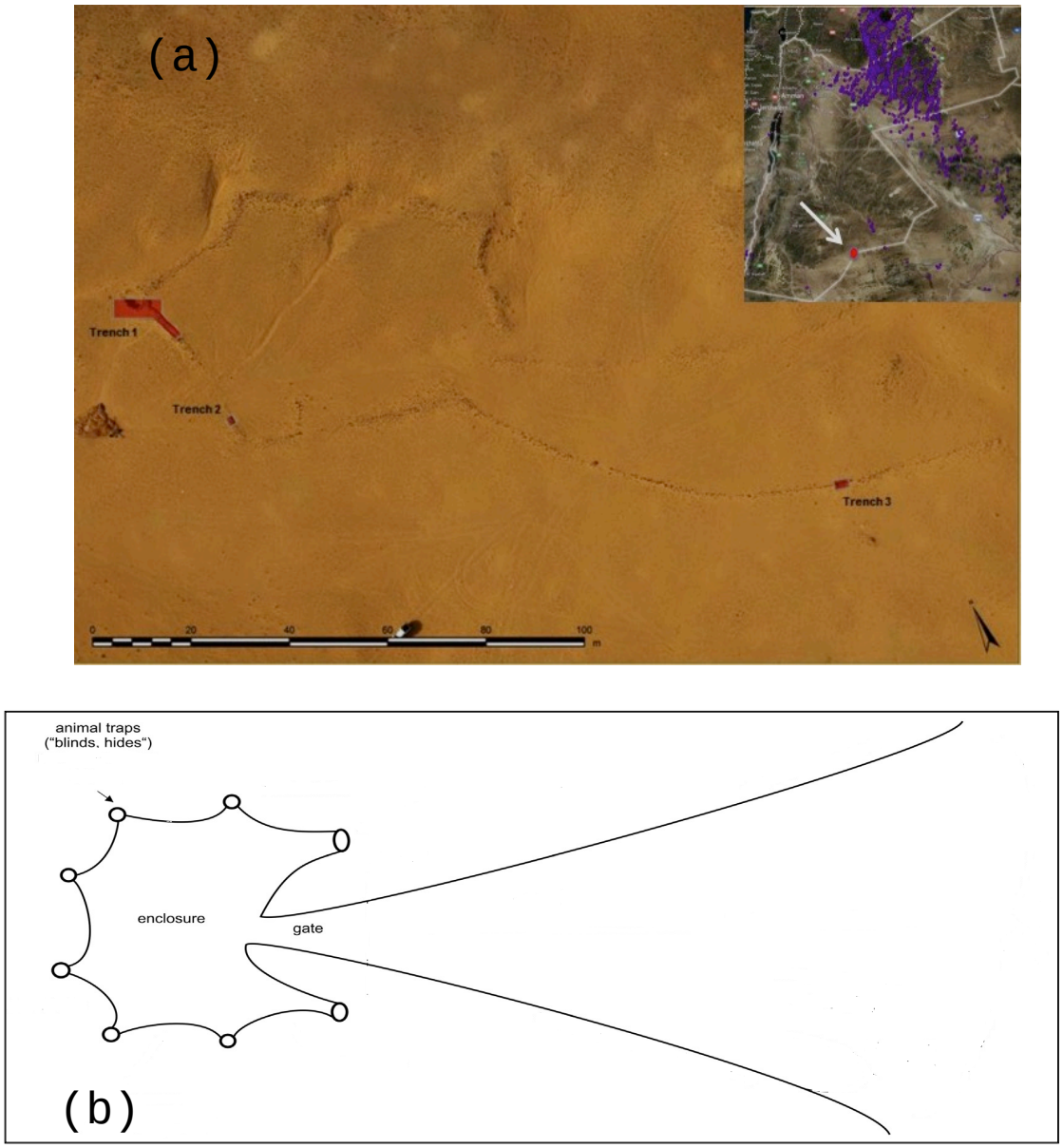

Figure 6.1: Kite structures, (a) Jibal al-Gadiwiyt kite in the southeast Jordan (provided by Tarawneh and Abu-Azezih, personal communication). (b) Scheme of the features of desert kite (after Kempe & Al-Malahbeh, 2012)

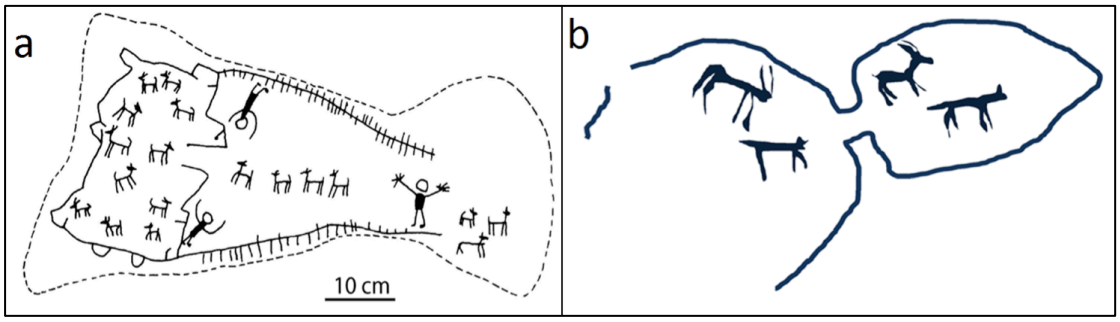

Figure 6.2: Rock art describe the kite function(a) drawing of Cairn of Hani rock arts, Jordan (after Harding 1954); (b) rock drawing from Wadi Hashad, northeast Jordan (after Hoyland 2001)

Recent investigations have significantly increased the number of known kite structures in the Near East, Egypt and Iraq, and high resolution satellite images have been used to identify kites in Yemen and throughout Central Asia (e.g. Kazakhstan and Ozbakistan; Barge & Brochier, 2011); of the 4616 structures so far identified, the largest group (1123) is found in Jordan (globalkite.fr) (Kempe & Al-Malabeh, 2013, Kennedy & Bishop, M. 2011) (Figure 6.3). But despite the ubiquity of these sites, and the considerable investment of labour that must have been involved in their construction, almost nothing is known about the period(s) in which they were constructed and/or used. Some (Betts 1998; Helms & Betts, 987) speculate that they were constructed in the Levant's Neolithic period (seventh millennium BC), others hypothesize that they were built early but kept in use for centuries; based on descriptions in travellers journals some may even have been in use up until the late nineteenth century (Burckhardt, 1831; Wright, 1895, Musil, 1928). However, these hypotheses depend on only a very few chronological studies (Hozler et al. 2011; Betts, 1998; van Berg *et al.,* 2004) and on comparative archaeological studies of kites and nearby sites. Unfortunately there is an almost complete absence of the organic matter needed for radiocarbon dating and there are very few archaeological finds associated with locally- known relative chronologies. As a result, there is no robust chronological framework for the construction or period of use of any of these numerous, widespread, and presumably important, structures.

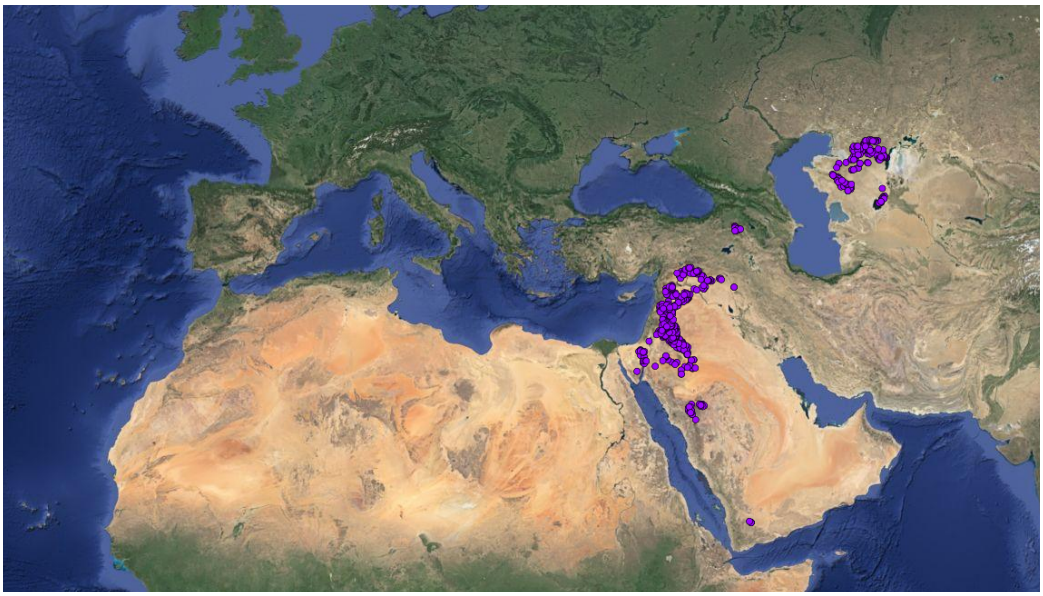

Figure 6.3: Kites and stone structures distribution on Near East, Egypt and Iraq, Yemen and throughout Central Asia (globalkites.fr).

6.2 Rock surface dating

Luminescence dating, and rock surface dating in particular, offers a solution to this problem of dating kites. Rock surface dating is based on ability of the luminescence signal in solid rock matrices to be reset to varying degrees as a function of depth into the rock surface as a result of light penetration into the rock during daylight exposure. This resetting is followed by signal build-up after the rock is again shielded from light (e.g. by burial or megalith construction). The resetting of the signal occurs because charge is released at different rates at different depths, as described in Equation 1 (based on Sohbati et al., 2011):

Equation 6-1

$$E(x) = \overline{\sigma\varphi_o} e^{-\mu x}$$

where E(x) is the trap emptying rate at depth x into the rock (cm), $\overline{\sigma\varphi_o}$ is the trap-emptying rate at the surface (s^{-1}) and μ is the light attenuation coefficient (cm^{-1}). Assuming the latent luminescence L(x,t) is directly proportional to the trapped charge concentration n(x,t) at time, t (s); then at time exposure t_e the residual latent luminescence at depth x is given by (Sohbati et al., 2011):

Equation 6-2

$$L(x) = \mathrm{L}_0\, \mathrm{e}^{-\mathrm{E(x)t_e}} = \mathrm{L}_0\, \mathrm{e}^{-\overline{\sigma\varphi o}\mathrm{t_e}}\, e^{-\mu x}$$

where L_o is the initial latent luminescence. This model was later expanded by Freiesleben *et al.* (2015) to describe the cumulative effects of several events of signal resetting and build-up as result of a sequence of daylight exposures and burials. Table (2.3) summarise the set of equations that combine the burial and exposure time with de-trapping and re-trapping of charge that describe such a cycle of exposure and burial.

6.3 Site description

Our study is centred on the Jibal al-Gadiwiyt (JGHD02) kite located in the south east of Jordan, just over 3 km north of the border with Saudi Arabia and ~100km south east of the city of Ma'an (Figure 6.1a). It is composed of two long low stone structures, a northern wall ~113m in length and a southern wall ~144m. The two walls converge at the western end and open into an irregular star-shaped polygon enclosure with five corners; this enclosure covers ~2632m^2, and is formed by a 196 m long wall with an inner diameter (E/W) of ~80m (Figure 6.1a). From examination of aerial photographs, two of the apices of the enclosure have outward facing circular structures (the cells referred to above) - one at the west corner facing the end of the guiding walls and the second on the first corner of the enclosure to the north of the entrance (Figure 6.1a). In 2014 excavation for the site began to uncover the structure from the west side (Trench 1) (Abu-Azizeh & Tarawneh, in press). This excavation revealed that the circular structure represented the top of a filled pit of depth ~1.2m and diameter ~4m (Figure 6.4a). The pit is lined with long stones sitting on the inner ground surface of the pit, most of which reach to within ~30 cm of the surface. Small cobbles are then stacked in layers above this lining until they reach the ground surface (Figure 6.4b).

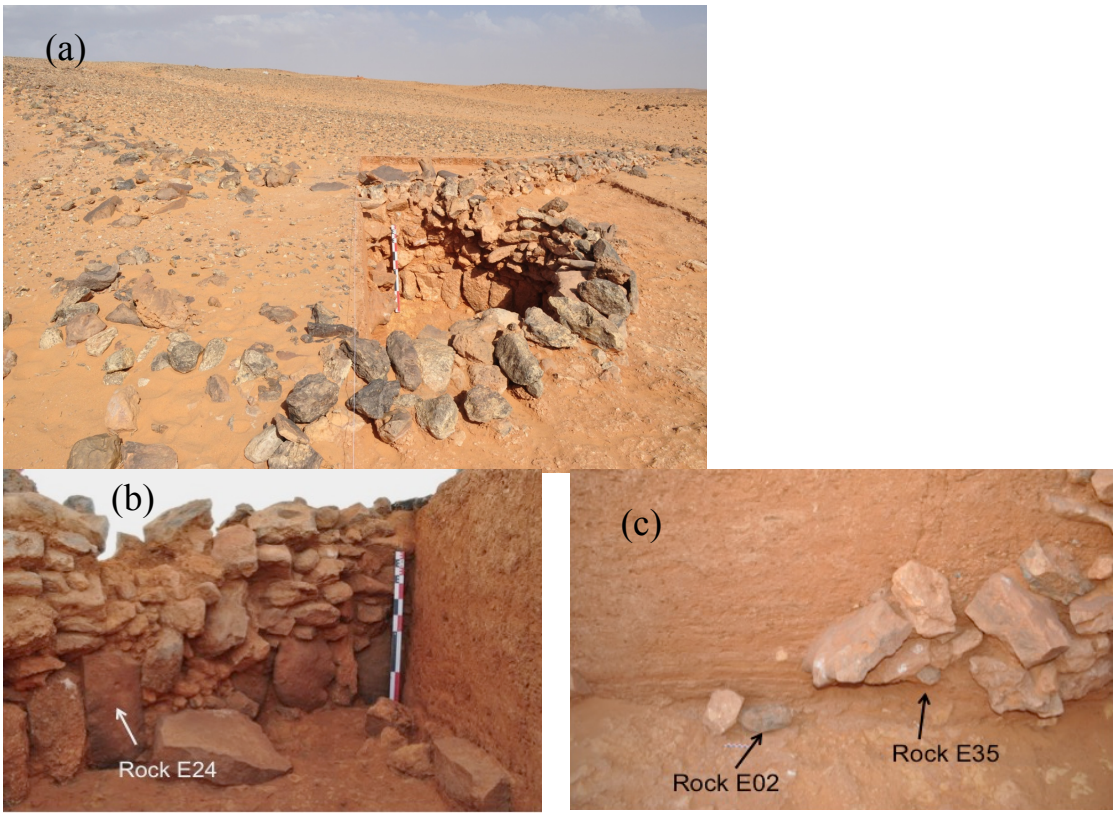

Figure 6.4: Trench 1 in Jibal al-Gadiwiyt (JGHD02) kite. (a) a top view for the open pit showing also the arm of the enclosure extending from pit. (b) Rock sample E24 from he wall construction. (c) Rock samples E02 and E35

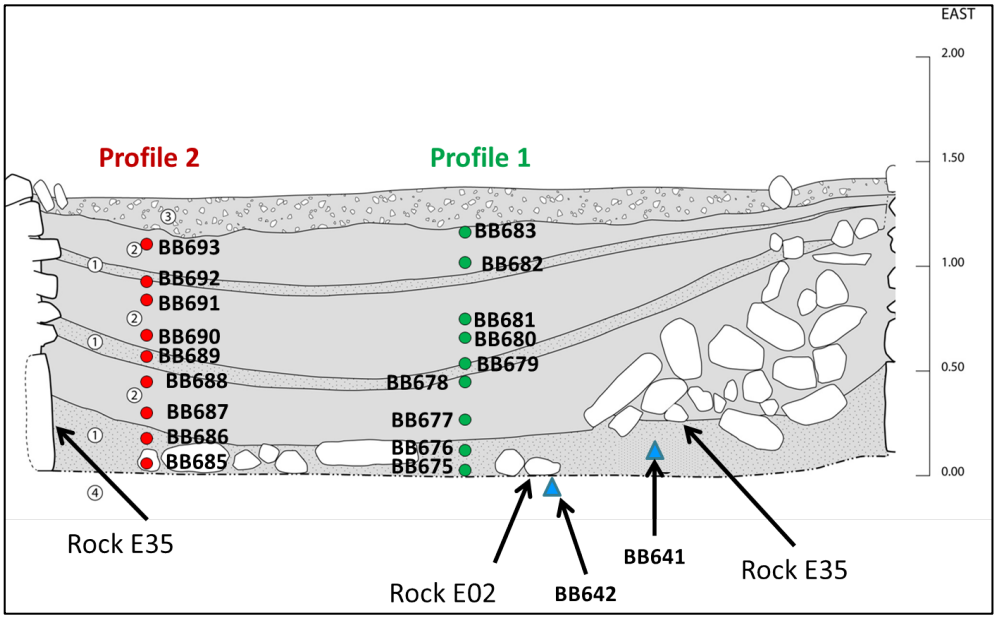

Figure 6.5: Sediment samples from two vertical profiles. The graph also shows the three rock samples and sediment samples associated with rocks E02 and E35.

The pit appears to have been back-filled over time with several sediment layers. The lowest layer appears to have been washed in, but this is overlain by thick blocky, presumably wind-blown, sandy layers (without any small stones) which curve upwards towards the walls of the pit (Figure 6.5c and Figure 6.6). Two thin, possibly water-lain, units containing gravels and pebbles are intercalated in the aeolian sediments. At the right side of the pit section a number of cobbles and rocks appear to have fallen or been pushed into the pit to form a ramp-shaped slope that reaches to the present surface (Figure 6.4c and Figure 6.5). These large clasts do not appear to originate from the wall of the pit, and they sit on top of the lowest (water-lain) sediment layer of the section. It is very unlikely that these large clasts could have been moved by water.

Finally, it appears that our kite is atypical, in that the buried pits are different to the cells or compartments described by Kemp and Al- Malabeh (2013); they suggest that the majority of kites have circles (interpreted as hides) constructed above surface. The excavation team suggest that the pits in the Jibal al-Gadiwiyt kite were intended as the final trap in the kite structure, into which the animals were driven for slaughter/capture (Abu-Azizeh & Tarawne, personal communication).

There is no evidence of when the kite JGHD02 was built, or for how long it was in use. However, the presence of nomadic camp site <600 m to the southeast has led to the suggestion that the two sites are related, and that kite was possibly used by the inhabitants of the camp site (Abu-Azizeh & Tarawneh, in press). Dating the campsite itself is only indirect; one radiocarbon date from a similar nearby site suggests that it could be attributed to the beginning of the 4th millennium BC (Late Chalcolithic/Early Bronze Age) (Abu-Azizeh, 2013).

6.4 Sample preparation and measurement facilities

6.4.1 Rock samples

The primary target sample (JGHD02/E24; Figure 6.4b and 6.5) was a single flat rock used to line the inner wall of the pit. This rock was ~50 cm high, ~25cm wide and ~10cm thick and was chosen because it was clearly part of the construction of the

pit. As a result of excavation, the surface, *I*, facing into the pit, had been exposed to daylight for 5 months prior to sampling. The surface, *O*, facing away from the pit, and presumably buried at the time of construction of the pit, remained buried at the time of sampling. The rock was sub-sampled in the field using hammer and chisel to give a piece of full thickness and width, but only ~20 cm high; this sub-sample was wrapped in black plastic sheet for return to the laboratory.

Two other rocks were sampled from within the back-fill (see Figures 6.4a and b, Figure 6.5). One rounded cobble (JGHD02/E02) lay directly on the pit floor; it is ~15cm on its longest axis, and ~10 cm on its shortest. A further cobble (~10 cm by ~6cm; JGHD02/E35) was collected from the bottom of the rock fall on the right side of the section; this cobble was recovered after half had been exposed by excavation, and the exposed/unexposed line was marked on the surface.

In the laboratory, solid cores (~10mm in diameter, ~20-50 mm long) were drilled from the surfaces of the rocks using a water-cooled diamond-tipped core drill. These cores were then sliced using a diamond wafering saw (blade thickness 300 µm) into disks of thickness ~1mm; the depths of the midpoint of each slice were tracked relative to the original surface (Figure 6.6)

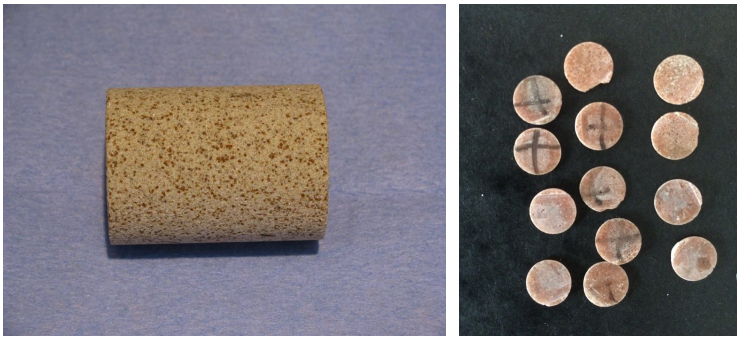

Figure 6.6: Rock core drilled into the rock of 10mm diameter and the slices of 1 mm thick.

Using a simplified XRF analysis (Kook *et al*., 2011) it became clear that these rocks are composed of quartz-rich sandstones– there was some carbonate, but any feldspar was below the detection limit. By treating the slices first with 10% HCl and then 40% HF full disaggregation of the quartz grains was possible, without any mechanical treatment. (Note that if HCl was not used, the discs were only slightly

attacked by the HF.) After disaggregation, the grain size fraction 180-250µm was separated for OSL measurement, and the quartz grains were mounted on 9.8 mm diameter stainless steel disks using silicone oil as an adhesive.

6.4.2 Sediment samples

Sediment samples were also taken, from two vertical profiles (at the centre and left of the section, see Figure 6.5) using tubes (~25 cm long, 1.5cm diameter) driven into a cleaned face. Further individual sediment samples were collected from the floor immediately beneath the cobble sample E02, and beneath the more elevated cobble E35 (Figure 6.5).

The sediment samples were prepared in the standard manner; the sieved sand-sized (180-250 µm) grains were cleaned using 10% HCL, 30% H_2O_2 and 10% HF. An aqueous heavy liquid solution (LST Fast Float, sodium heteropolytungstate) of density 2.58 $g.cm^{-3}$ was used to separate a quartz-rich fraction from potentially K-rich feldspar grains. However none of the sediment samples contained measureable feldspar. The quartz-rich fraction was further cleaned and etched using 40% HF for 40 minutes, and the samples were again wet sieved isolate a 180- 250 µm fraction.

6.4.3 Luminescence measurements

Luminescence measurements employed an automated Risø TL/OSL-DA20 luminescence reader (Bøtter-Jensen *et al.,* 2010) equipped with a calibrated $^{90}Sr/^{90}Y$ beta source delivering ~0.15 Gy/s, blue LEDs (470 nm, ~80 mW/cm^2) and infrared (IR) LEDs (870 nm, up to ~135mW/cm^2). OSL signals were detected through 7.5 mm of UV Hoya U-340 filter. Quartz dose estimates are based on a SAR protocol (Murray & Wintle, 2000; 2003), with signals derived from the first 0.4 s less a background from the following 0.4s.

Single grain luminescence measurements were carried out using a similar reader fitted with a single grain laser attachment (Bøtter-Jensen *et al.,* 2003). The stimulation light source is a 10mW Nd: YVO4 solid-state diode pumped laser emitting at 532 nm, which is focused sequentially on each of 100 grains mounted on a special aluminium sample disc. The diameter of each of the grain holes is 300 mm µm and

by visual inspection only one grain was loaded into each hole. Before loading the single grain discs they were screened for contamination by giving a beta dose and measuring in the usual manner; holes giving a measurable OSL signal were identified as contaminated, and if they could not be cleaned signals from these holes were ignored in further analysis. Only grains with an uncertainty on the test dose response of <20% and a sensitivity corrected natural signal below saturation on the laboratory dose response curve were included in further dose analysis. Applying additional rejection criteria (e.g. recycling ratio, IR depletion ration and recuperation) did not change either the estimated dose or the over-dispersion (Thomsen et al., in prep for further details).

6.4.4 Dose rate

Bulk samples of sediment and rocks were prepared for dose rate analysis by ashing at 50 oC to remove any organics, then crushing, homogenizing and casting in a fixed cup- shaped geometry for gamma spectrometry analysis (Murray *et al*., 1987). The resulting radionuclide concentrations were converted to dry dose rates using data provided by Guérin *et al*. (2011). The cosmic ray dose contributions (0.22±0.02 Gy/ka for the 3 rock samples) are based on the calculations suggested by Prescott and Hutton (1994). Water contents are based on measured field values. All water contents (expressed as % of dry weight) radionuclide concentrations and resulting dose rates are summarized in (Table 6-1), assuming a quartz internal dose rate of 0.06±0.03 Gy/ka. Total dose rates were calculated using the principle of superposition (Aitken 1985, Appendix H) taking into account the sediment water content; the external (sediment) gamma dose rate contributes, on average, about 3 times the internal (rock) contribution.

Table 6-1: Radionuclides concentrations and the resulting dose rates.

Code	Water Content (%)	^{238}U (Bq/kg)	^{226}Ra (Bq/kg)	^{232}Th (Bq/kg)	^{40}K (Bq/kg)	Beta (Gy/ka)	Gamma (Gy/ka)	Total dose rate (Gy/ka)
BB641	0.82	11.5±16.8	36.2±1.3	8.1±1.2	59±12	0.81±0.04	0.68±0.02	1.70±0.7
BB642	1.8	55.25±19.08	82.3±1.6	18.41±1.12	107±15	1.02±0.09	0.87±0.07	2.06±0.12
BB675	0.67	47.2±13.5	38±1	12.1±0.8	53±11	0.57±0.03	0.45±0.02	1.25±0.05
BB676	0.73	43.2±12.9	38.3±1.0	13.4±0.9	37±10	0.60±0.03	0.513±0.014	1.34±0.05
BB677	1.26	31.3±18.4	50. 8±1.5	14.1±1.0	54±14	0.57±0.02	0.520±0.014	1.31±0.05
BB678	0.67	55.60±18.13	58.6±1.4	18.7±1.3	89±14	0.75±0.03	0.65±0.02	1.25±0.27
BB679	1.80	100.1±21.7	62.9±1.7	23.3±1.2	129±17	0.94±0.03	0.80±0.02	1.94±0.06
BB680	1.97	88±20	57.4±1.5	19.7±1.4	128±15	1.11±0.04	0.92±0.02	2.15±0.07
BB681	0.64	53±15	53.0±1.2	19.4±0.9	150±13	1.02±0.04	0.83±0.02	2.01±0.07
BB682	1.73	23.07±15.07	46.1±1.2	14.89±1.10	171±13	1.03±0.03	0.80±0.02	1.99±0.06
BB683	1.21	64±17	68.2±1.4	21.20±0.99	125±14	0.98±0.03	0.71±0.02	1.87±0.06
BB684	4.62	122±16	54.7±1.2	18.70±1.12	62±12	1.14±0.03	0.94±0.02	2.11±0.06
BB685	2.37	51±13	49.66±1.07	16.3±0.7	67±10	0.84±0.03	0.74±0.02	1.71±0.05
BB686	0.58	124±15	54.5±1.2	19.21±1.13	75±12	0.78±0.02	0.673±0.013	1.62±0.05
BB687	1.58	43±13	51.92±1.08	18.0±0.8	80±10	0.87±0.03	0.76±0.02	1.77±0.06
BB688	1.63	41.97±11.13	39.6±0.9	11.0±0.8	33±8	0.85±0.03	0.723±0.014	1.72±0.05
BB689	1.24	95.5±16.7	65.6±1.4	23.01±0.95	125±14	0.56±0.02	0.498±0.012	1.26±0.04
BB690	2.81	40±15	52.9±1.2	19.17±1.09	137±12	1.13±0.03	0.94±0.02	2.16±0.06
BB691	1.71	71.31±16.11	62.0±1.3	22.3±0.9	139±14	1.00±0.03	0.79±0.02	1.94±0.06
BB692	1.45	77±13	76.95±1.09	22.2±0.7	152±10	1.12±0.03	0.91±0.02	2.25±0.07
BB693	2.25	64 ±17	53.3±1.3	14.4±1.2	70±13	1.31±0.02	1.045±0.014	2.57±0.07
BB694	1.74	53 ±16	56.3±1.3	18.4±0.9	36±12	0.82±0.03	0.69±0.02	1.70±0.06
BB695	0.45	92.5 ±17.2	99±2	18.2±0.9	55±12	0.79±0.03	0.73±0.02	1.74±0.06
Rock samples								
E02	0.4	16±15	20.89±1.09	3.66±1.09	0.0±12	0.23±0.03	0.22±0.02	
E24	0.001	7.5±3.3	15.4±0.3	2.8±0.3	8±2	0.197±0.005	0.17±0.004	
E35	0.01	19.1±0.4	19.13±0.37	7.3±0.3	2±2	0.251±0.006	0.252±0.005	

6.5 Luminescence characteristics

The inset to Figure (6.7) shows typical blue-light stimulated luminescence from quartz grains from slices taken at 3mm depth into the upper side of rock E24 and E35, following a preheat/cutheat to 260/220°C and 220/180°C for rock samples E24 and E35 respectively. The signal from calibration quartz (Hansen *et a*l., 2015) is shown for comparison, and it can be seen that the natural signal is dominated by the fast component. Fig (6.7) also shows the dose response curve for the same aliquots, with the sensitivity-corrected natural luminescence interpolated onto the response curve to give the D_e.

The performance of SAR protocol was first examined using recycling ratios and recuperation values. The overall average recycling ratios are 0.998±0.013 (n=140), 0.979±0.015 (n=264), and 0.994±0.008 (n=72) for grains from rock samples E02, E24 and E35, respectively. The average recuperation is ~2% (n=97) E02, 4% (n=264) E24 and 3% (n=72) E35, expressed as a fraction of the natural luminescence. These results confirm that our SAR protocol is able to correct accurately for any sensitivity changes in the laboratory-regenerated SAR cycles in our samples.

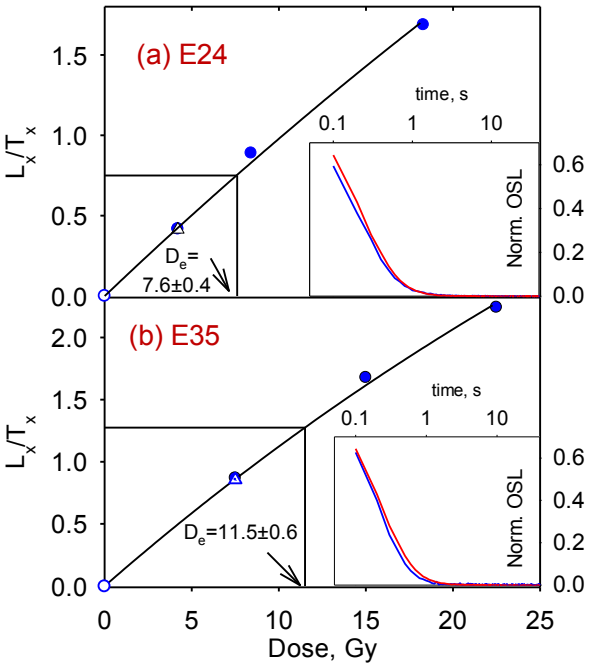

Figure 6.7: representative dose response curves and (inset) a typical stimulation curve compared to a normalized stimulation curve from calibration quartz for rock samples (a) E24 and (b) E35.

We then undertook dose recovery tests on fresh aliquots of grains from the 3 rocks; these gave measured to given dose ratios of 1.058±0.014 (n=24), 1.09±0.07 (n=6) and 1.05±0.03, (n=6) for E24, E02 and E35 respectively; results for rock E24 are shown in Figure (6.8a). As a result of dose recovery measurement at different preheats (Figure 6.8b) and thermal transfer tests (data not shown) it was decided to use preheat/cut heat of 200/160°C for sample E02, 260/220°C for E24 and 220/180°C for E35

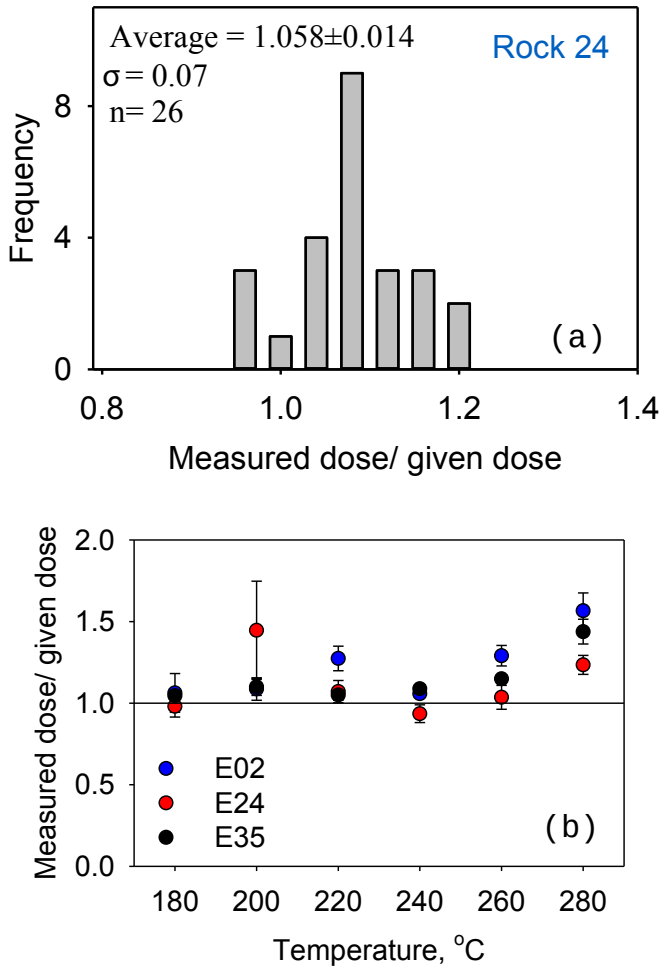

Figure 6.8: Dose Recovery test. (a) Ratios of measured to given dose after blue light stimulation at room temperature and storage for 10ks for rock sample E24. (b) Dose recovery results at different preheat temperatures for the three rock samples

6.6 Application of the rock surface model to the luminescence depth profile

Figure 6.9 (a, b and c) shows the normalised OSL profile (L_n/T_n) as a function of depth from the surface for samples E02, E24 and E35. It is clear from visual inspection that the surfaces of all samples had been exposed to sunlight prior the final burial event. The effect of the second daylight exposure (of about 5 months) of sample E24 after excavation is also obvious for surface (*I*); the effect of a very recent light exposure is not present in the profiles from samples E35 and E02 because cores were drilled into that part of the surface that had remained covered by sediment after excavation. The profile from the bottom surface of E02 does not penetrate as far into the rock as that from the top surface, or as far as the profiles from the other 2 samples, and it seems likely that this surface received significantly less light exposure than the other surfaces before burial. Presumably this was because it was exposed to daylight for a shorter time.

In order to quantify these qualitative observations, we now fit the data of Figure (6.9a-c) with the model initially developed by Sohbati et al (2011) and expanded by Freislaben et al. (2015).

Fitting the model

The equations described in chapter- Table 2-3(Freisleben *et al.*, 2015)- were fitted to the luminescence profiles from the three rocks samples. Equation $L_2(x)$ was used to fit the two surfaces of rocks E02 and E35 and Equation $L_3(x)$ used to fit rock E24. We assume that the light attenuation factor (μ) is constant throughout each rock, and so we fit the two profiles from opposite sides simultaneously, assuming both μ and $\overline{\sigma\varphi_0}$ (average excitation rate) are shared parameters in the two fits. The constant D_o was derived from relevant dose response curves determined using 12, 43 and 10 slices of samples E02, E24 and E35 respectively (Table 6-2), and the total dose rates as a function of depth are based on those given in Table 6-1.

The fitting results for the three rocks are shown as black solid lines in Figure 6.9a-c. The derived parameters are summarised in Table 6-2.

Table 6-2:the fitting parametres for the three rock after applying equation $L_2(x)$ for rock E02 and E35 and equation $L_3(x)$ for rock E24.

Surface	Parameter	Value from fitting		
		Rock E02	Rock E24	Rock E35
Top (Inward for Rock E24)	t_{e1}	9.3±2.5	37.2±7.5	99.6±40.8
	mu	0.49± 0.06	0.32± 0.02	0.97±0.09
	t_{b1}/D_o	0.22±0.02	0.132±0.008	0.20±0.01
	t_{e2}	--------	5.0	--------
Bottom (Outward for Rock E24)	t_{e1}	1.7±0.7	1236. 6±488.3	2571 ±1751
	mu	0.49± 0.06	37.2±7.5	0.97±0.09
	t_{b1}/D_o	9×10^{-18}±0.2	0.148± 0.004	0.24±0.01

Light intensity bleaching during daylight exposure t_{e1}

Rock E02 (on floor of pit): The profile shapes immediately prior to final burial can be calculated from the fitted parameter values – these are shown as a dashed line in figure 6.9a. These fits confirm the qualitative conclusion above, that the downwards facing side only received limited light exposure (during t_{b1}) before final positioning, insufficient to fully reset even the surface 1 mm of the sample and the fitting is unable to resolve the subsequent burial time. The upper surface, on the other hand, clearly received (during t_{e1}) a much longer exposure; according to the model fit this was sufficient to reset the signal to a depth of 1.7mm to <3% of the luminescence signal acquired during subsequent burial.

Rock E24 (standing rock in the wall of pit): The inward-facing surface (*I*) shows two exposures; an earlier daylight exposure (t_{e1} in Figure 6.9b) occurred during the use of the kite in antiquity, and the more recent exposure (t_{e2} in Figure 6.9b) known to have occurred after archaeological excavation. In contrast, the surface (*O*) facing away from the pit (buried at the time of sampling) shows only one exposure event t_{b1}, which must have taken place before or during construction of the wall.

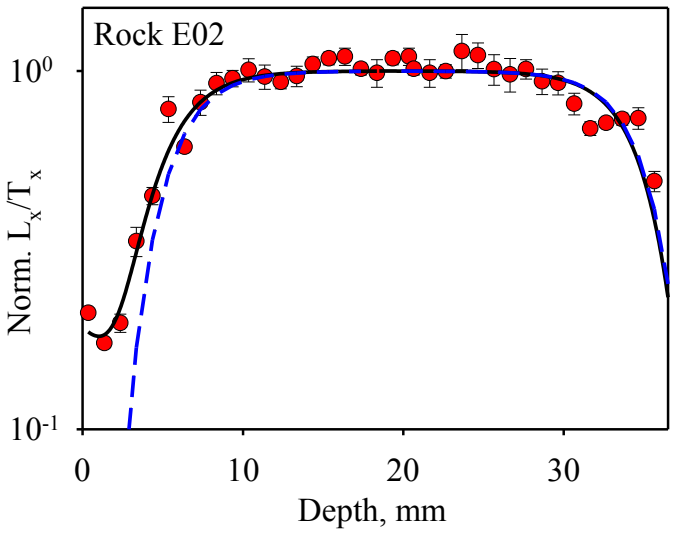

Figure 6.9: Measured luminescence-depth profiles for the three rocks.

(a) Rock E02; depth=0 mm is the top surface. black solid line is the result of fitting the data. Dashed blue line is the predict profile shapes for day light exposure.

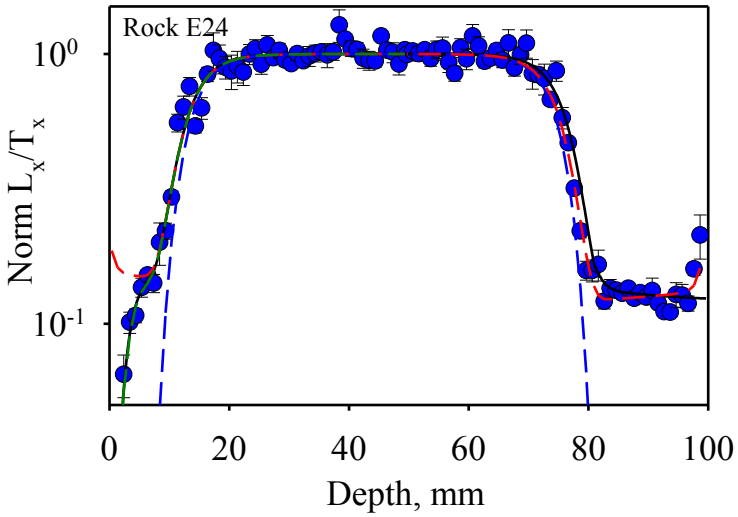

(b) Rock E24; depth=0 mm is the inward surface.black solid line is the result of fitting the data. Dashed lines (red, blue and green) are the predict profile shapes for sequence of daylight exposure and burial. Note that the predicted and the fitted data (green and black) lines are almost identical.

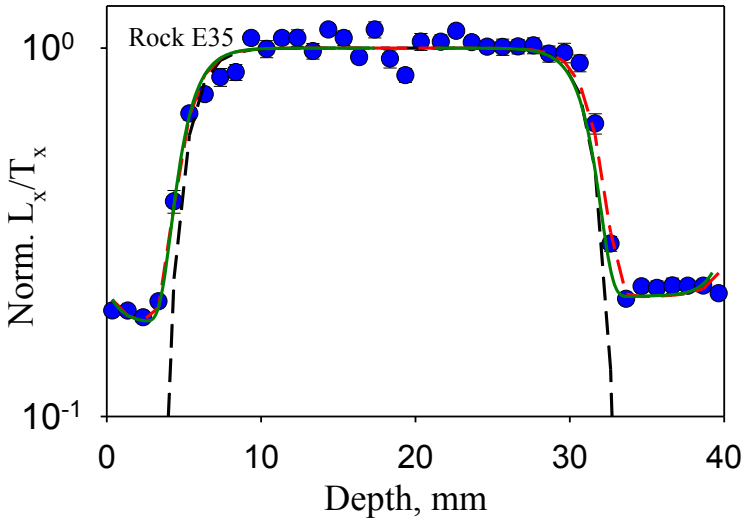

(c) Rock E35; depth=0 mm is the top surface. Green solid line is the result of fitting the data. Dashed lines (red and black) are the predict profile shapes.

As above, the parameter values have been used to predict the profile shapes that would have been present in antiquity, before burial. These curves are shown as dashed lines in Figure 6.9b and they can be compared to the total luminescence signals present after burial. On the outer-facing surface (*O*), it appears that the surface was bleached to <3% of the subsequent burial signal to a depth of 16 mm, and on the inward surface (*I*) to a depth of 8 mm.

The effect of modern exposure partially erased the burial signal on the inward facing surface (*I*). Using the fitted parameter values the effect of recent bleaching of the burial signal has been calculated; of the well- bleached slices (0 to 8 mm) only the two slices centred at depths 5.35 and 6.35 mm have lost < 10% of their burial signal.

Rock E35 (from pit back-fill): In this case, both surfaces each reflect only one exposure (Figure 6.9c); as discussed above it appears that at least the downward facing side received significant light exposure (during t_{b1}) before its final positioning in the pit. In the case of the upwards-facing side we cannot tell whether the light exposure occurred only before positioning, or whether there was further exposure after positioning, to give the total period of exposure of t_{e1}.

The parameter values were used to predict the profile shapes before burial in antiquity. These curves are shown as dashed lines in Figure 6.10c and they can be compared to the total luminescence signals present after burial. It appears that the upward facing side was sufficiently well bleached to a depth of 3 mm to reset the signal to <3% of the luminescence signal acquired during subsequent burial; in contrast, the downwards-facing side was reset to a depth of 7 mm.

Burial Ages

Burial ages were derived in two ways: (i) using the value of the parameter (t_{b1}/D_o) from the fitting model and D_o from the dose response curve for each side of the three rocks. (ii) Using the D_e estimates derived directly from the SAR growth curve of each slice identified above as well-bleached before burial. All these ages are summarised in Table 6-3.

Rock E02: only data from the top surface of the rock was used to estimate a burial age. Using the parameters from the fitting (t_{b1}/D_o) from the fitting and an average D_o from dose response curves, the estimate age is 9.9±1.1 ka. Using the SAR dose estimates from individual slices gives an age of 9.8±0.6 ka (n=3).

Rock E24: the outward-facing surface (*O*, covered at the time of sampling) was calculated above to have been well bleached to a depth of 16 mm, and the sensitivity corrected luminescence is approximately constant to that depth, except for the first 2 surface slices. These increase slightly because of the increased beta dose rate from the more active surrounding sediment, but this contribution is poorly known compared to the well-known internal beta dose rate of the rock (mainly because the directly relevant sediment sample was lost in transport, and the sediment beta dose rate on this side of the rock is based on a sample taken ~20 cm from the core locations). Fortunately we can avoid this problem by simply ignoring the two surface slices. The age resulting from fitting (i.e. using an average D_o) is 7.6±0.4 ka, compared to that based on direct SAR dose estimates from individual slices (3-16 mm) of 8.6±0.7 ka (n=14).

The profile from the inward surface is more complex because of the two exposures events (t_{e1} during the kite use and t_{e2} after archaeological excavation). Nevertheless, using the parameters from the fitting (t_{b1}/D_o) and D_o from the dose response curve gives a burial age of 9.0±0.9 ka. Only slices from depths 6 and 7 mm were both well bleached in antiquity, and unaffected by modern bleaching after excavation. Using direct SAR dose estimates only from these slices gives an age of 9.7±1.2 ka (n=2).

Rock E35: both surfaces of this rock seem to have a relatively simple history of exposure and burial; the upper surface was bleached to a depth of 3mm before burial, and the lower to 7mm. Using the fitted values of t_{b1}/D_o, and an average D_o from the dose response curves gives age of 8.8±0.5 ka for the top surface and 10.7±0.5 ka for the bottom surface. Using direct SAR dose estimates from the slices identified as well bleached gives ages of 10.8±1.1 ka (n=3; top surface) and 13.0±1.0 ka (n=6; bottom surface).

Table 6-3: Burial ages using the value of the fitting parameter (t_{b1}/D_o) and direct ages from D_e estimate derived from direct SAR measurements (given uncertainties are the total for random and systematic uncertainties).

Rock	D_o, Gy (Dose response curve)	Burial age, ka Using fitting parameter t_{b1}/D_o		Burial age, ka Using D_e estimates for well bleached slices	
		Top (inward for Rock E24)	Bottom (outward for Rock E24)	Top (inward for Rock E24)	Bottom (outward for Rock E24)
E02	45.9±1.8	9.9±1.1	---------	9.8±0.6	---------
E24	51.4± 2.4	8.9±0.9	7.6±0.6	9.7±1.2	8.6±0.7
E35	43.8± 1.6	8.8±0.5	10.7±0.5	10.8±1.1	13.0±1.0

6.7 Sediment age estimates

Since most of this sediment is presumed to be aeolian we expected that multi-grain measurements would provide reliable dose estimates. However, despite satisfactory dose recovery behaviour, multi-grain estimates of equivalent dose were unrealistically larger (~27 Gy) and highly scattered, and so single-grain analyses were undertaken.

For a preheat temperature of 200 °C, single-grain dose recovery ratios were satisfactory (0.98±0.01, n=6 samples). Figure 6.10 (sample BB694) presents a representative single-grain dose distribution for these sediment samples. The distribution has a leading edge at ~1 Gy and is clearly positively skewed, suggesting poor bleaching. We have used the IEU model (Thomsen et al., 2003; 2007) to analyse these data assuming an over-dispersion of ~30%; this corresponds to the over-dispersion observed for the apparently best- bleached sample (BB683). Reducing this over-dispersion by 5% only decrease the IEU dose estimates by 4% and still includes 96% of the individual dose estimates. These analyses are presented in detail in Thomsen et al. (in prep), and the resulting single-grain ages are summarised in Figure 6.11.

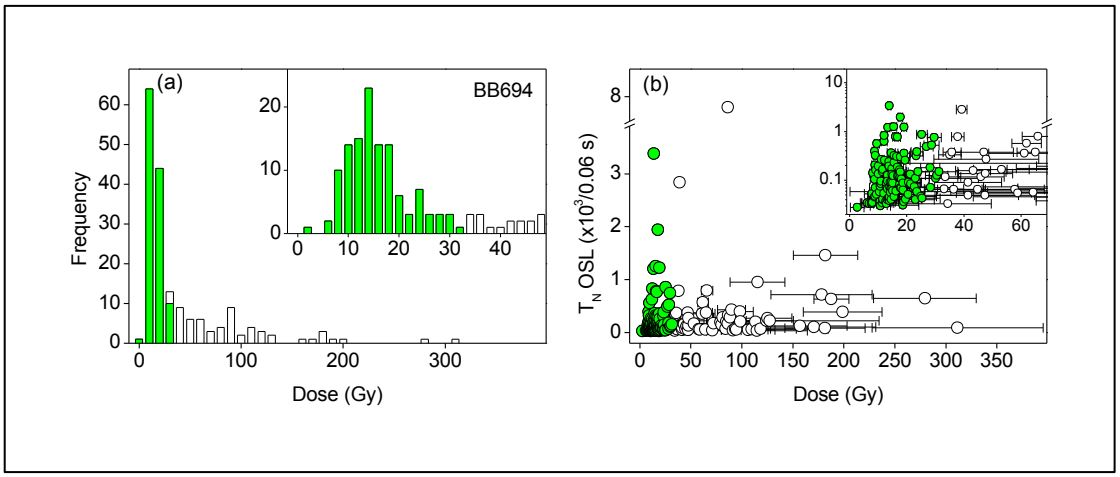

Figure 6.10: Natural single-grain dose distribution for sample BB694. a) dose histogram of all dose estimates irrespective of the precision with which they are known. b) natural test dose intensity as a function of dose. The insets show the lower parts of the dose distributions. Note the logarithmic ordinate axis in b). The shaded data represents the dose estimates identified by the IEU model to be well-bleached

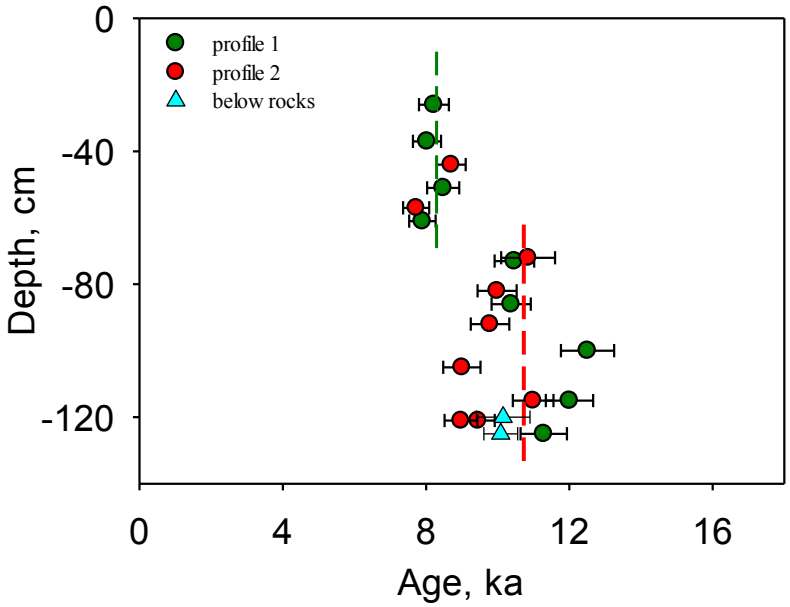

Figure 6.11: Ages distribution derived by Single Grain method, average age for the bottom layers is 10.7±0.3 ka

6.8 Discussion

Rock E24 is clearly part of the construction and it is the only sample that must have been laid down at the time the pit structure (and presumably the rest of the kite) was built. This sample represents incontrovertible evidence of human activity; its position cannot be attributed to natural causes. This is in contrast to the other two

the other two rock samples (E02 and E35) which could have been put in place by natural events after the pit was constructed.

In what follows, we use the ages based on directly measured SAR doses for individual slices (see above). These ages do not include the assumption that all slices have the same D_0, and so are considered the more accurate.

The inward facing surface of Rock E24 was last buried 9.7±1.2 ka ago. In contrast, the outward-facing surface appears to have been buried only 8.6±0.7 ka. Both dose estimates are equally reliable, but ~78% of the gamma dose rate to the outward-facing surface is based on a single sediment sample taken ~20 cm from the core location, towards a lower corner of the vertical rock slab (because the original sediment sample was lost in transport). (In contrast, this sediment sample only contributes 15% to the total gamma dose rate to the surface layers on the inward-facing surface). Because of this unavoidable uncertainty in dose rate, we consider the age of the inward-facing surface to be the more reliable.

The top surfaces of Rock E02 and Rock E35 give burial ages of 9.8±0.2 ka and 10.8±1.1 ka, respectively. These are indistinguishable from the age of the wall slab Rock E24, and suggest that the pit was certainly not maintained for more than a few hundred years after construction (Table 6-3). If the 'ramp' of large rocks on the right of the section shown in Figure 6.5c was put in place by human activity, (i.e. not by some extreme natural event) then it would appear that people did encounter the structure sometime after it fell out of use, and may have deliberately altered it to prevent it acting as an animal trap.

The sediment ages for the two profiles (Figure 6.11) suggest two depositional events, the bottom layers (up to 75 cm from the surface; n=12) were, on average, put in place 10.7±0.3 ka ago; these events are indistinguishable in age from the construction (E24) and abandonment (E35) ages, and imply natural back-filling very quickly after abandonment. There then appears to have been a period without much accumulation until about 8.3±0.2 ka ago (n=4), when the pit filled to at least within 15 cm of the modern surface.

6.9 Conclusion

The luminescence depth profiles for the rock samples examined from the Jibal al-Gadiwiyt kite contain surprisingly detailed information about burial and exposure history, and it proved possible to use the fitting parameters to calculate the depths to which the rocks were well bleached before deposition final burial. We suggest the ages derived by using D_e estimate directly from using a SAR protocol directly on individual aliquots are more reliable than those derived from the fitting model parameter, because the model makes use of an average D_o value for the entire profile, rather than the individual D_o values appropriate to each aliquot. Based on the model prediction of bleaching depth, and the SAR dose estimates from the bleached layers, the burial age of our three rocks are ~10.2±0.2 ka. In addition, this study has shown that the deposition of the back-fill sediments in the pit occurred following such short transport distances that the luminescence signal was not fully reset. Nevertheless, after allowing for incomplete bleaching, the single grain age for the bottom layers is 10.7±0.3ka, implying sedimentation occurred shortly after abandonment.

There seems little no doubt that these first instrumental ages from the Jibal al-Gadiwiyt kite suggest that construction took place ~10,000 years ago. This is considerably older than expected, and puts the use of this site firmly in the Neolithic period, considerably older than the anticipated Late Chalcolithic/Early Bronze Age.

"Mehr Licht!"
Goethe

7. Chapter 7: Conclusions

The aim of this study was to test the application of methods developed recently in luminescence dating to archaeological materials, and to use the methods to resolve some chronological problems for representative archaeological sites that are difficult to date by other radiometric methods, or in situations where luminescence ages can be used to support existing chronological information.

In the first case (*chapter 3*) we tested recent developments in the use of a more stable feldspar signal in luminescence dating. This new approach is used extensively in sediment dating and offered the possibility of obtaining accurate feldspar luminescence ages for ceramic artefacts; this is especially interesting for locations that do not provide suitable quartz extracts. This study reported on the first application to pottery samples of the stable infrared stimulated luminescence signal measured at elevated temperature (290^{o}C). A total of 52 potsherds were collected from three superimposed iron-age units at Pella (Jordan); based on ^{14}C dating, typology and seriation these units were deposited between 2700 and 2900 years ago. Sand-sized quartz extracts were unsuitable, and there was insufficient sand-sized feldspar, and so polymineral fine grains were chosen for dating. Various tests for reliability were undertaken (dose recovery, dependence of D_e on first stimulation temperature etc.). The pIRIR signals were weak, and 14 potsherds were rejected on this basis. Of the remaining 38, 3 were confidently identified as outliers. Based on those sherds for which IR signals were sufficiently intense, we used the ratio of the IR_{50} to $pIRIR_{290}$ signals to argue that these outliers do not arise from incomplete resetting during manufacture. The ages from each layer are considerably over dispersed (typically by ~25%) but average ages for each unit are consistent with each other and with the expected age range. The average OSL age for the site is 2850±220 years (n=35), with the overall uncertainty dominated by systematic uncertainties; this agrees with the range of ^{14}C ages from 2970 - 3270 cal. years BP reported from across the destruction horizon. We concluded that the $pIRIR_{290}$

signal is delivering accurate ages, but that the variability in age from shard to shard is much greater than would be expected. This demonstrates the need for site ages to be based on multiple samples; individual shard ages are unlikely to be sufficiently accurate. Although this could not be known in advance, the Pella potsherds did not represent a good test-case, because of the lack of quartz and the very weak feldspar signals. According, the next study investigated the use of the elevated temperature post-IR IR ($pIRIR_{290}$) SAR protocol for the dating of young heated artefacts from Denmark (*chapter 4*). Seven heated stones and seven potshards were collected from three different sites: one from the early Pre-Roman Iron Age 200 BC to AD 100, and two from the Viking period between AD 800 and 1200, no previous radiometric dating was available for these sites. Standard quartz OSL ages were first determined for these samples, to support the archaeological age control. The luminescence characteristics of the $pIRIR_{290}$ signal were then investigated; in particular the dose recovery ratios were shown to be close to unity. The performance of the feldspar $pIRIR_{290}$ protocol was then examined by comparing the $pIRIR_{290}$ ages with those based on the quartz OSL signal; the average ratio of $pIRIR_{290}$ to OSL ages was 1.14±0.05 (n=14) and there is some suggestion that the possible overestimation of the feldspar ages compared to quartz is only of significance for the heated stone samples.

The previous two studies tested the application of new feldspar dating methods to heated artefacts. In the third study, the application of OSL dating to arid sediment deposits resulting from human activity was investigated. OSL ages were measured for sediments associated with a well structure presumed to have been built by pastoralists in Qulbān Banī Murra, Jordan (*chapter 5*). The site is thought to belong to the Chalcolithic culture (5^{th} millennium BC). It partly includes megalithic burial fields related to a water management system. Two sediment samples from the well structure were dated using OSL (quartz OSL and feldspar post IR-IRSL). The good agreement between the two chronometers confirms that the sediment was fully reset at the time of burial, and so gives added confidence in the reliability of the chronology. The average age derived from quartz of the two samples is 6.6±0.2 ka, to be compared to an average of

6.8±0.3 ka for ages derived from feldspar. Both ages are in agreement with earlier assumptions. The investigation of such sites has previously been stalled by dating difficulties (due to the absence of suitable radiocarbon material). By using OSL signals from quartz and feldspar, this study provided some of the first instrumental ages for this widespread water-using culture.

In the final study described here (*chapter 6*), a very recently developed luminescence technique which determines the last time rock surfaces were exposed to light was investigated. The site selected for this investigation was one of the so-called kite structures found throughout the Near East. This particular structure (Jibal al-Gadiwiyt) is from southern Jordan. Three different rocks (one part of the construction, and two from infill) were sampled from a partly-excavated pit structure within the enclosed end of the kite. Both the construction (first human use of the kite) and the last exposure before infilling by wind-blown sand (last human use of the kite) could be identified in the luminescence profiles with depth in the three rocks. The time of last exposure based on the rock surfaces was also compared with quartz OSL dating of the sandy infill for the pit. It was shown that the luminescence profiles contained detailed information on the exposure and burial history of the rocks. The burial ages suggest that the rock wall was built ~10 ka, and the dating of surfaces covered by infill suggest the pit fell out of use ~10 ka ago. To confirm the reliability of the new surface ages, 18 samples were taken from two vertical profiles from the infill sediment were measured, together with two sediment samples more closely associated with the two rocks from the infill. Despite the expectation that the sediment had been blown into the pit, the quartz was clearly not completely reset to zero before deposition, and sand-sized quartz grains were measured using single grain analysis. Applying standard minimum-age modelling gave an average age of deposition of sediment at the bottom of the pit of ~10 ka, complexly consistent with the much simpler and less labour intensive rock surface ages.

Overall, this study has clearly demonstrated the great potential of OSL as a reliable independent chronometer for a variety of materials of archaeological

importance. It is clear that OSL can answer chronological questions that cannot be addressed by other methods (such as burial of light-exposed rock surfaces, or construction of structures based on sediment), and even in more traditional areas (potsherds and heated stones) OSL can be used to complement and support other dating methods.

These conclusions are all based on the individual cases presented in this study; the reliability of the IRSL signal at elevated temperature for young heated artefacts was demonstrated in *chapter 3* and *4*. Nevertheless, in the first case (Pella from Jordan, *chapter 3*) the effectiveness of the contribution of the method to ceramic dating must be discussed. Because of the lack of appropriate material (sand-sized feldspar and quartz) and the weak signal from the silt-sized grains that were available, only an average site age could be meaningfully derived from the processing of 52 sherds, although this average age agrees well with the range of ^{14}C ages available. In addition, luminescence dating was able to distinguish three otherwise unidentified reused sherds in the deposit. Nevertheless, in this case luminescence was time consuming, and in general other methods at such sites are likely to be more efficient. Studies of mound (Tell) sites are usually well constrained chronologically because of their well-defined stratigraphic structure, the abundance of organic matter suitable for radiocarbon dating and the well-established ceramic typology. Pella represents one of the sites in which a continuous settlement chronology has been identified using ^{14}C, and it is one of the triangle of sites in the Jordan Valley (along with Tell abu al-kharaz and Deir alla) that is used as a reference for building the chronology of the Bronze and Iron Age in the region. Nonetheless, this should not degrade the usefulness of luminescence dating for heated materials (quartz OSL or feldspar IRSL); not all sites have abundant organic matter, or a well-established typology. As was demonstrated using the Danish sites where there were no previous radiometric ages available, and dating relied only on the archaeological features of the site, the IRSL method could be used confidently on a standalone basis for the absolute dating for individual artefacts. Heated stones usually have no typological features (typified by the stones from Samsø and Århus) and luminescence dating

is almost the only possible method available for dating such material. The Levant has a wide diversity of ancient sites with pyrotechnic works. In Pre-Pottery Neolithic B (PPNB) (9th millennium B.C.) there was an extensive use of lime plaster production, and burnt limestone, sand and clay accumulations in pits and kilns hav been identified in different sites such as Jericho, 'Ain Gazal, Bouqras and Kafr Hahoresh (Goren & Goldberg, 1991; Kafafi, 1986; Frieman, 1971 and Goren & Goring-Morris, 2008). In addition mining sites like copper mines in Wadi Fidan (southern Jordan) and Timnna (Israel) ((Hauptmann, 2007; BEN-YOSEF *et al.*, 2010 and Tauxe & Levy, 2010) is rich with heated remains that have the potential to be dated using luminescence.

This study had also highlighted the potential of using luminesce dating for geo-archaeological landscapes (*chapter 5 and 6*). Recently, nomadic pastoral sites are receiving considerable attention from archaeologists, but the nature of these sites and the lack of organic matter had hindered the development of reliable chronologies. The study described in *Chapter 5* demonstrated that, despite the lack of a stratigraphic sequence, their deposition of sediments as a result of human activity was sufficient to reset the luminescence signal (as demonstrated by the agreement between feldspar and quartz ages). There are many sites in the region (presently considered in many cases undatable) for which it may now be possible to build a reliable luminescence-based chronology. In contrast the sediments infilling the Kite structure (*chapter 6*) did show a well-developed stratigraphic structure, and had previously been identified as mainly wind-blown; this should have provided ample opportunity for signal resetting before burial. Nevertheless, measurements clearly indicated incomplete bleaching, and it proved necessary to employ single grain measurements and minimum age modelling before a reliable age for the beginning of sediment infilling could be derived.

Chapter 6 applied rock-surface dating for the first time to the buried surfaces of a rock slab used in the construction of a stone-lined pit; this was part of a so-called kite in southern Jordan. It proved possible to reconstruct a complex burial and

exposure history by examining the resetting of OSL with depth and time. Kites and similar stone structures have been identified in large numbers in the Levant and central Asia, and have puzzled archaeological studies for some time. Most of the studies that attempted to date these structures relied on a presumed association with nearby prehistoric occupation sites (Betts, 1997 and 1998). Using rock surface dating it proved possible to date directly the time of emplacement of the main component in these structures – the rocks themselves. The derived ages were older than the archaeologically assumed age, but, from a comparison with another well-established luminescence dating methods, it was possible to argue for the accuracy of the rock-surface ages. Clearly it is now possible to date many if not all the kite structures, and this will undoubtedly lead to a reconsideration of the chronology of these sites and their relation to the other prehistoric sites. More generally, rock surface dating has many exciting potential applications addressing various archaeological problems. The method could be applied to rocks from megalithic landscape like stone circles, wheels and dolmens; these are widely diffused in the Levant and in Jordan (Kennedy, 2011 and 2012; Kempe & Al-Malabeh, 2012). The method can also be employed for field walls and cairns, building floors or reused rocks. It also has potential application to geological sites related to human existence, such as volcanic rocks, fault scarps and rock-falls.

In summary, this study has investigated the usefulness and potential application of recent developments in OSL dating to a variety of archaeological sites – in at least one case (pIRIR dating of heated materials) the approach had not been tested before. The study tested OSL dating by comparing it with other radiometric dating methods, and it was shown to provide accurate ages and other useful information (reused potsherds in Pella, description of burial/exposure history of rocks used in the kite) for the archaeological materials under investigation.

Recent technical developments (such as $pIRIR_{290}$ for heated materials and rock surface dating) have provided new perspectives in dating in archaeology. This

study has demonstrated the accuracy of these and other luminescence dating methods, and the ability of luminescence to address currently active archaeological questions that go beyond existing routine dating methods. It is the sincere hope of this author that, perhaps influenced by this work, archaeologists will become more aware of the considerable potential of luminescence dating, and move to take much more advantage of it in the future.

References

Abu-Azizeh, W., & Tarawneh, M. (in press). Out of the Harra: Desert Kites in Southeastern Jordan. New Results from the South Eastern Badia Archaeological Project. *Arabian Archaeology and Epigraphy* .

Abu-Azizeh, W. (2013). The south-eastern Jordan's Chalcolithic-Early Bronze Age pastrol nomadic complex: patterns of mobility and interaction. *Paléorient , 39* (1), 149-176.

Aitken, M. J. (1998). *An Introduction to Optical Dating: The Dating of Quaternary Sediments by the Use of Photon-stimulated Luminescence.* New York, United State: Oxford University Press.

Aitken, M. J. (1985). *Thermoluminescence dating .* London: Academic Press.

Akkermans, P., Fokkens, H., & Waterbolk, H. (1981). Stratigraphu, Architecture and Layout of Boukras. In P. Sanlaville, & J. Cauvin, *Prehistorie du Levant* (pp. 485-501). Paris: Editions du CNRS.

al khasawneh, S., al-Muheisen, Z., & Abd-Allah, R. (2010). Thermoluminescence Dating Of Pottery Objects From Tell Al-Husn, Northern Jordan. *Mediterranean Archaeology and Archaeometry , 11* (1), 41-49.

Albright, W. (1931). The Excavation of Tell Beit Mirsim. IA: The Bronze Age Pottery of the Fourth Campaign. *The Annual of the American Schools of Oriental Research* , 55-127.

Albright, W. (1932). *The Excavation of Tell Beit Mirsim: Vol. 1, The Pottery of the First Three Campaigns.* New Haven, CT:: Yale University Press.

Ankjærgaard, C., & Murray, A. S. (2007). Total beta and gamma dose rates in trapped charge dating based on beta counting. *Radiation Measurements , 42*, 352-359.

Arnold, L., Bailey , R., & Tucker, G. (2007). Statistical treatment of fluvial dose distributions from southern Colorado arroyo deposits. *Quaternary Geochronology , 2* (1), 162-167.

Auclair, M., Lamothe, M., & Huot, S. (2003). Measurement of anomalous fading for feldspar IRSL using SAR. *Radiation Measurements , 37*, 487-492.

Bøtter-Jensen , L., Andersen , C., Duller , G., & Murray, A. (2003). Developments in radiation, stimulation and observation facilities in luminescence measurements. *Radiation Measurements , 37*, 535-541.

Bøtter-Jensen, L., & Duller, G. A. (1992). A new system for measuring optically stimulated luminescence from quartz samples. *Nuclear Tracks and Radiation Measurements , 20*, 549-553.

Bøtter-Jensen, L., & Mejdahl, V. (1988). Assessment of beta dose-rate using a GM multicounter system. *nternational Journal of Radiation Applications and Instrumentation. Part D. Nuclear Tracks and Radiation Measurements , 14* (1), 187-191.

Bailey, R., & Arnold, L. (2006). Statistical modelling of single grain quartz De distributions and an assessment of procedures for estimating burial dose. *Quaternary Science , 25*, 2475-2502.

Bailiff, I. (2007). Methodological developments in the luminescence dating of brick from English late-medieval and post-medieval buildings. *Archaeometry , 49* (4), 827-851.

Bailiff, I. (2008). New developments in the scientific dating of brick. (7), 133-144.

Bailiff, I., & Barnett, S. (1994). Characteristics of infrared-stimulated luminescence from a feldspar at low temperatures. *Radiation Measurements , 23* (2-3), 541-545.

Bakraji, E. (2011). Study of Syrian archaeological pottery by the combined application of thermoluminescence (TL) dating, X-ray fluorescence analysis and statistical multivariate analysis. *uclear Instruments and Methods in Physics Research , 269* (19), 2052-2056.

Bakraji, E., Boutros, N., & Abboud, R. (2013). Thermoluminescence (TL) dating of ancient Syrian pottery from six different archaeological sites. *Geochronometria , 41*, 24-29.

Banerjee, D., Murray, A., Bøtter-Jensen, L., & Lang, A. (2001). Equivalent dose estimation using a single aliquot of polymineral fine grains. *Radiation Measurements , 33* (1), 73-94.

Barge, O., & Brochier, J. (2011). Visible from space, understood during the fieldwork: the example of "desert kites" in Armenia. *Conference on cultural heritage and new technologies.*

Barnett , S. (2000b). Luminescence dating pottery from later prehistoric Britain. *Archaeometry , 42*, 431-457.

Barnett, S. (2000a). Sampling pottery in luminescence dating studies. *Radiation Measurement , 32*, 467-472.

Barnett, S., & Bailiff, I. (1997). Infrared stimulation spectra of sediments containing feldspars. *Radiation Measurements , 27* (2), 237-242.

Bar-Oz, G., & Nadel, D. (2013). Worldwide large-scale trapping and hunting of ungulates in past societies. *Quaternary International , 297*, 1-7.

Bar-Oz, G., Melinda , Z., & Hole, F. (2011). Role of mass-kill hunting strategies in the extirpation of Persian gazelle (Gazella subgutturosa) in the northern Levant.". *Proceedings of the National Academy of Sciences , 108* (18), 7345-7350.

BEN-YOSEF, E., Tauxe, L., & Levy. , T. (2010). Archaeomagnetic dating of copper smelting site F2 in the Timna valley (Israel) and its implications for the

modelling of ancient technological developments. *Archaeometry , 52* (6), 1110-1121.

Betts, A. (1998). *The Harra and the Hamad, Excavations and Survey in Eastern Jordan. Archaeological Monographs.* Sheffield: Sheffield Academic Press.

Betts, A., & Helms, S. (1987). The Desert "Kites" of the Badiyat Esh-Sham and North Arabia. *13* (1), 41-67.

Betts, A., & Yagodin, V. (2000). A new look at desert kites. In L. Stager, J. Greene , & M. Coogan, *The Archaeology of Jordan and Beyond, Winona Lake, Indiana* (pp. 31-34). Eisenbrauns.

Blair, M., Yukihara, E., & McKeever, S. (2005). Experiences with single-aliquot OSL procedures using coarse-grain feldspars. *Radiation Measurements , 39* (4), 361-374.

Bourke, S. (2012, May 22). Exploring Pella's Bronze Age Temple Complex.

Bourke, S. J. (2011). Pella in Jordan 2003-2005: Further Explorations in the Bronze Age Temple Precinct. *Mediterranean Archaeology , 24*, 121- 130.

Bourke, S. J. (2014). Pella in Jordan 2013. *Near Eastern Arhaeology Foundation Bulletin , 57*, 17-21.

Bourke, S. J. (2000). Pella in The Early Bronze Age. In G. Philip, & D. Baird (Eds.), *Ceramics and Changes in the Early Bronze Age Southern Levant* (pp. 233-254). Sheffield: Scheffield Academic Press.

Bourke, S. J., Zoppi, U., Meadows, J., Hua, Q., & Gibbins, S. (2009). The Beginning of the Early Bronze Age in North Jordan Valley; New C14 Determinations from Pella in Jordan. *Radiocarbon , 51* (3), 905-913.

Bourke, S. (2012, Febrauary). Pella in Jordan 2011 Early Bronze Age Fortifications, a Late Bronze Age Palace and a Hellenistic Villa. *The Near Eastern Archæology Foundation BULLETIN , 55*, pp. 1-5.

Bourke, S. (2013, Summer). Preclassical Pella in Jordan: A Conspectous of Recent Work. *ACOR Newsletter , 25* (1), pp. 1-5.

Bourke, S., Sparks, R., & Shroder, M. (2006). Pella in the Middle Bronze Age. In P. Fischer (Ed.), *The Chronology of Jordan Valley.*

Boyle, R. (1664). *Experiments and Considerations Touching Colours.* London: Henry Herringham.

Burckhardt, J. (1831). *Notes on the Bedouins and Wahabys, collected during his travels in the east.* London: Colburn and Bently.

Buylaert, J., Jain, M., Murray, A. S., Thomsen, K., Thiel, C., & Sohbati, R. (2012). A robust feldspar luminescence dating method for Middle and Late Pleistocene sediments. *Boreas , 41*, 435–451.

Buylaert, J., Murray, A. S., Gebhardt, A. C., Sohbati, R., Ohlendorf, C., Thiel, C., et al. (2013). Luminescence dating of the PASADO core 5022-1D from Laguna Potrok Aike (Argentina) using IRSL signals from feldspar. *Quaternary Science Review , 71*, 70- 80.

Buylaert, J., Murray, A., Thomsen, K., & Jain, M. (2009). Testing the potential of an elevated temperature IRSL signal from K-feldspar. *Radiation Measurements , 44* (5-6), 560-565.

Buylaert, J., Thiel, C., Murray, A., Vandenberghe, D., Shuangwen, Y., & Huayu, L. (2011). IRSL and post-IR IRSL residual doses recorded in modern dust samples from the Chinese Loess Plateau. *Geochronometria , 38* (4), 432- 440.

Buylaert, J., Vandenberghe, D., Murray, A., Huot, S., De Corte, F., & Van den Haute, P. (2007). Luminescence dating of old (> 70ka) Chinese loess: a comparison of single-aliquot OSL and IRSL techniques. *Quaternary Geochronology , 2* (1), 9-14.

Chen, R., & McKeever, S. S. (1997). *Theory of Thermoluminescence and Related Phenomena.* World Scientific Publishing Co. Pte. Ltd.

Chen, R., & Pagonis , V. (2011). *Thermally and Optically Stimulated Luminescence: A Simulation Approach.* Chichester, UK: John Wiley & Sons, Ltd.

Crassard, R., Barge, O., Bichot, C., Chahoud, J., & al., e. (2014). Addressing the desert kites phenomenon and its global range through a multi-proxy approach. *Journal of Archaeological Method and Theory* , 1-29.

Cunningham, A., Wallinga, J., & Minderhoud, P. (2011). Expectations of scatter in equivalent-dose distributions when using multi-grain aliquots for OSL dating. *Geochronometria , 38* (4), 424-431.

Daniels, F., Boyd, C. A., & Saunders, D. F. (1953). Thermoluminescence as a research tool. *117*, 343-349.

Duller, G. A. (1991). Equivalent dose determination using single aliquots. *International Journal of Radiation Applications and Instrumentation. Part D. Nuclear Tracks and Radiation Measurements , 18* (4), 371-378.

Duller, G. (2003). Distinguishing quartz and feldspar in single grain luminescence measurements. *Radiation Measurements , 37*, 161-165.

Duller, G. (1994). Luminescence dating of sediments using single aliquots: new procedures. *Quaternary Science Reviews , 13* (2), 149-156.

Duller, G. (1995). Luminescence dating using single aliquots: methods and applications. *Radiation Measurements , 24* (3), 217-226.

Duller, G. (2008). Single-grain optical dating of Quaternary sediments: why aliquot size matters in luminescence dating. *Boreas , 37* (4), 586-612.

Edwards, P. (2013). *Wadi Hammeh 27, an Early Natufian Settlement at Pella in Jordan.* Brill.

Feather, J. K. (2003). Use of luminescence dating in archaeology. *Measurement Science and Technology , 149*, 1493-1509.

Fowden,, G. (1999). Desert kites': ethnography, archaeology and art. In H. Humphrey,, *The Roman and Byzantine Near East: Some Recent Archaeological Research* (Vol. 31, pp. 107-136). Journal of Roman Archaeology: Supplementary Series.

Freisleben, T., Sohbati, R., Murray, A., Jain, M., al Khasawneh, S., Hvidt, S., et al. (2015). Mathematical model quantifies multiple daylight exposure and burial events for rock surfaces using luminescence dating. *Radiation Measurements , in press*.

French Research Agency (ANR) . (n.d.). From Globalkites: http://www.globalkites.fr

Galbraith, R., Roberts, R., Laslett, G., Yoshida, H., & Olley, J. (1999). Optical dating of single and multiple grains of quartz from jinmium rock shelter, northern australia: part i, experimental design and statistical models. *Archaeometry , 41* (2), 339-364.

Galloway, R. B., & Hong, D. G. (1996). Concerning the normalisation of additive-dose optically stimulated luminescence data from quartz. *Ancient TL , 142*, 1-5.

Gebel , H., & Mahasneh, H. (2013). Disappeared by climate change: the shepherd cultures of Qulban Beni Murra (2nd half of the 5th millennium BC) and their aftermath." Syria. *revue d'art oriental et d'archéologie , 90*, 127-158.

Gebel, H. (2013). Arabia's fifth-millennium BCE pastoral well cultures: hypotheses on the origins of oasis life . *Proceedings of the Seminar for Arabian Studies , 43*, 111-126.

Gebel, H. (2010). Untergegangen im Klimawandel. Die paläo-beduinische Kultur von Qulban Beni Murra, Jordanien . *Antike Welt , 6* (10), 40-44.

Gebel, H., & Mahasneh, H. (2009). Petroglyphs and sepulchral contexts, Preliminary note on late Chalcolithic/early Bronze Age findings at Qulban Beni Murra, Wadi Sahab al-Abyad . *Journal of Epigraphy and Rock Drawing , 3*, 1-9.

Gebel, H., & Mahasneh, H. (2012). Qulban Beni Murra. Unknown Mid-Holocene Sepulchral Green Desert Landscapes, Pastoral Well Cultures, and the Origins of Arabia's Oasis Economies. In R. Eichmann, F. Klimscha, C. Schuler, & H. Fahlbusc (Eds.), *Wasserwirtschaftliche Innovationen im archäologischen Kontext. Von den prähistorischen Anfängen bis zu den Metropolen der Antike* (pp. 101-122). Rahden, Leidorf.

Gebel, H., Mahasneh, H., Keilholz , P., & Baumgarten, J. (2011). Life at the edge: Sepulchral, hydraulic and pastoral land use in Wādīs as-Sahab al-Abyad and al-Asmar, southeastern Jordan. Preliminary report of the Eastern Jafr J.A.P., 4th Season, 2010. . *Annual of the Department of Antiquities , 55*, 537-559.

Goren, Y., & Goldberg , P. (1991). Special Studies: Petrographic Thin Sections and the Development of Neolithic Plaster Production in Northern Israel. *Journal of Field Archaeology , 18* (1), 131-140.

Goren, Y., & Goring-Morris, A. (2008). Early Pyrotechnology in the Near East: Experimental Lime-Plaster Production at the Pre-Pottery Neolithic B Site of Kfar HaHoresh, Israel. *Geoarchaeology , 23* (6), 779-798.

Greilich, S., Glasmacher , G., & Wagner , G. (2005). Optical dating of granitic stone surfaces. *Archaeometry , 47* (3), 645-665.

Guérin, G., Benoit, C., Lahay, C., Thomsen, K., Tribolo, C., Urbanova, P., et al. (2015). Testing the accuracy of a Bayesian central-dose model for single-grain OSL, using known-age samples. *Radiation Measurements* .

Guérin, G., Mercier, N., & Adamiec, G. (2011). Dose-rate conversion factors: update. *Ancient TL , 29* (1), 5-8.

Hütt, G., & Jaek, J. (1989). Infrared stimulated photoluminescence dating of sediments. *Ancient TL , 7*, 48-51.

Habermann , J., Schilles , T., Kalchgruber , R., & Wagner, G. (2000). Steps towards surface dating using luminescence. *Radiation Measurements , 32* (5), 846-851.

Hansen, V., Murray, A., Buylae, J., Yeo, E., & Thomsen, K. (in press). A New Irradiated Quartz For Beta Source Calibration. *This preceedings* .

Harding, G. (1953). The cairn of Hani. *Annual of the Department of Antiquities of Jordan , 2*, 8-56.

Hauptmann, A. (2007). *The Archaeometallurgy of Copper: Evidence from Faynan, Jordan.* Springer Science & Business Media.

Helms , S., & Betts , A. (1986). Rock Art in Eastern Jordan : 'Kite' Carvings ? *Paléorient. , 12* (1), 67-72.

Herr, L. (2002). W.F. Albright and the History of Pottery in Palestine. *Near Eastern Archaeology , 65* (1), 51.

Holzer, A., Avner , U., Porat, N., & Kolska Horwitz, L. (2010). Desert kites in the Negev desert and northeast Sinai: Their function, chronology and ecology. *Journal of Arid Environments , xxx*, 1-12.

Hoyland, R. (2001). *Arabia and the Arabs: from the Bronze Age to the coming of Islam.* London: Routledge.

Hütt, G., Jaek, I., & Tchonka, J. (1988). Optical dating: K-feldspars optical response stimulation spectra. *Quaternary Science Reviews , 7*, 381-385.

Huntley , D., & Baril, M. (1997). The K content of the K-feldspars being measured in optical dating or in thermoluminescence dating. *Ancient TL , 15* (1), 11-13.

Huntley, D. J., Godfrey-Smith, D. I., & Thewalt, M. L. (1985). Optical dating of sediments. *Nature , 313*, 105-107.

Huntley, D. J., Short, M. M., & Dunphy, K. (1996). Deep traps in quartz and their use for optical dating. *Canadian Journal of Physics , 71* (3-4), 81-91.

Huntley, D., & Lamothe, M. (2001). Ubiquity of anomalous fadingin K-feldspars and the measurement and correction for it in optical dating. *Canadian Journal of Earth Science , 38*, 1093/ 1106.

Ivanovich, M., & Harmon., R. (1992). *Uranium-series disequilibrium: applications to earth, marine, and environmental sciences.*

Jacobs, Z., Duller, G., & Wintle, A. (2006). Interpretation of single grain De distributions and calculation of De. *Radiation Measurements , 41* (3), 264-277.

Jain, M., & Singhvi, A. (2001). Limits to depletion of blue-green light stimulated luminescence in feldspars: implications for quartz dating. *Radiation Measurements , 33* (6), 883-892.

Kafafi, Z. (1986). White objects from 'Ain Ghazal, Near Amman. *Bulletin of the American Schools of Oriental Research , 261*, pp. 51-56.

Kempe, S., & Al- Malabeh, A. (2010). Kites and other Archaeological Structures along the Eastern Rim of the Harrat (Lava Plain) of Jordan, Signs of Intensive Usage in Prehistoric Time, a Google Earth Images Study. *Proceedings 14th International Symposium on Vulcanospeleology* , 199-216.

Kempe, S., & Al-Malabeh, A. (2012). Distribution, Sizes, Function and Heritage Importance of the Harrat Al Shaam Desert Kites: The Largest Prehistoric Stoneworks of Mankind? *15TH INTERNATIONAL SYMPOSIUM ON VUCANOSPELEOLOGY* , 57-66.

Kendall, D. (1969). Incidence matrices, interval graphs and seriation in archeology. *Pacific Journal of mathematics , 28* (3), 565-570.

Kennedy, D. (2011). Kennedy, D., 2011: The “works of the old men” in Arabia: remote sensing in interior Arabia. *Journal of Archaeological Science , 38* (12), 3185-3203.

Kennedy, D. (2012). Kites —new discoveries and a new type. *Arabian archaeology and epigraphy , 23*, 145-155.

Kennedy, D. (2013). Remot sensing and 'Big Circles' - A new type of prehistory site in Jordan and Syria. *Sonderdruck aus Zeitschrift für Orient-Archälologie* , 44-63.

Kennedy, D., & Bishop, M. (2011). Google Earth and the archaeology of Saudi Arabia. A case study from the Jeddah area. *Journal of Archaeological Science , 38* (6), 1284–1293.

Kenyon, K. (1971). An Essay on Archaeological Technique: the Publication of Results from the Excavation of a Tell. *Harvard Theological Review , 64*, 271-279.

Kenyon, K. (1957). *Digging Up Jericho.* London.

Kook, M., Murray, A., Lapp, P., Denby, T., Ankjærgaard, C., Thomsen, K., et al. (2011). A portable luminescence dating instrument. *uclear Instruments and Methods in Physics Research Section B: Beam Interactions with Materials and Atoms , 269* (12), 1370-1378.

Lamothe, M. (2004). Optical dating of pottery, burnt stones, and sediments from selected Quebec archaeological sites. *Canadian Journal of Earth Sciences , 41* (6), 659-667.

Lamothe, M., Auclair, M., Hamzaoui, C., & Huot, S. (2003). Towards a prediction of long-term anomalous fading of feldspar IRSL. *Radiation Measurement , 37*, 493–498.

Lapp, P. (1961). *Palestinian Ceramic Chronology, 200 B.C.–A.D. 70.* New Haven, CT: American Schools of Oriental Research.

Libby, W., Anderson, E., & Arnold, J. (1949). *Age determination by radiocarbon content: world-wide assay of natural radiocarbon.* world-wide assay of natural radiocarbon.

Liritzis, I. (1994). A new dating method by thermoluminescence of carved megalithic stone building. *Comptes rendus de l'Académie des sciences. Série 2. Sciences de la terre et des planètes , 319* (5), 603-610.

Liritzis, I. (2013). Advances in surface luminescence dating : some new data from three selected Mediterranean sites. *Mediterranean Archaeology & Archaeometr , 13* (3), 105-115.

Liritzis, I., & Galloway, R. (1999). Dating implications from solar bleaching of thermoluminescence of ancient marble. *Journal of Radioanalytical and Nuclear Chemistry , 241* (2), 361-368.

Liritzis, I., Galloway, R., & Hong, D. (1997). IOANNIS LIRITZIS IOANNIS LIRITZIS Single aliquot dating of ceramics by green light stimulation of luminescence from quartz. *132* (3), 457-467.

Liritzis, i., Kitis, G., Galloway, R., Vafiadou, A., Tsirliganis, N., & Polymeris, G. (2008). Probing luminescence dating of archaeologically significant carved rock types. *Mediterranean Archaeology and Archaeometry , 8* (1), 61-79.

MacDonald, M. (2005). Of Rock-art, 'Desert Kites' and Mesayid. In A. Sedov, & I. Smulyanskaya (Eds.), *Arabia Vitalis: Arabskij Vostok, Islam, drevnyaya, Araviya: Sbornik Naychnykh statej, posvyashchennyj 60-letiyu V.V. Naumkina* (pp. 332-345). Moscow: Rossijskaya Akademiya Nauk.

Maitland, R. (1927). The 'works of the old man' in Arabia. *Antiquity, , 1*, 197–203.

McDougall, I., & Mark Harrison, T. (1990). *Geochronology and Thermochronology by the 40Ar/39Ar Method.* Oxford University Press.

McKeever, S. S. (1985). *Thermoluminescence of Solids.* New York: Cambridge University Press.

McNicoll, A., Henbury-Tenison, J., Hennessy, B., Potts, T., Smith, R., Walmsley, A., et al. (1992). *Pella in Jordan* (Vol. 2). Sydney: (Mediterranean Archaeology.

Murray, A. (1996). Incomplete stimulation of luminescence in young quartz sediments and its effect on the regenerated signal. *Radiation Measurements* (26), 221-231.

Murray, A. S., & Roberts, R. G. (1997). Determining the burial time of single grains of quartz using optically stimulated luminescence. *Earth and Planetary Science Letters , 152* , 163–180.

Murray, A. S., & Wintle, A. G. (2000). Luminescence dating of quartz using an improved single-aliquot regenerative-dose protocol. . *Radiation Measurements , 32*, 57-73.

Murray, A. S., Buylaert, J. P., Thomsen, K. J., & Jain, M. (2009). The effect of preheating on the IRSL signal from feldspar. *Radiation Measurements , 44*, 554-559.

Murray, A., & Wintle, A. (2003). The single aliquot regenerative dose protocol: Potential for improvements in reliability. *Radiation Measurements , 37*, 377-381.

Murray, A., Marten, R., Johnston, A., & Martin, P. (1987). Analysis for naturally occuring radionuclides at environmental concentrations by gamma spectrometry. *Journal of Radioanalytical and Nuclear Chemistry , 115* (2), 263-288.

Musil, A. (1928). The manners and customs of the Rwala Bedouins. In *Oriental Explorations and Studies* (Vol. 6). New York: American Geographical Society.

Naeser, C. (1979). Fission-track dating and geologic annealing of fission tracks. In *Lectures in isotope geology* (pp. 154-169.). Springer Berlin Heidelberg,.

Ollerhead, J., Huntley, D., & Berger, G. (1994). Luminescence dating of sediments from Buctouche Spit, New Brunswick. *Earth Sceince , 31*, 523-531.

Petrie, F. (1899). Sequences in prehistoric remains. *Journal of the Anthropological Institute , 29*, 295-301.

Petrie, W. (1891). *Tell El Hesy (Lachish).* London: Palestine Exploration Fund.

Porat, N., Avner, U., Holzer, A., Shemtov, R., & Horwitz, L. (2013). Fourth-millennium-BC 'leopard traps' from the Negev Desert (Israel). *Antiquity , 87*, 714-727.

Prescott, J. R., & Hutton, J. T. (1994). Cosmic ray contributions to dose rates for luminescence and ESR dating: large depths and long-term variations. *Radiation Measurements , 23*, 497-500.

Prescott, J. R., & Stephan, L. G. (1982). The contribution of cosmic radiation to the environmental dose for thermoluminescence dating. . *PACT , 6*, 17–25.

Ramsey, C. (1995). Ramsey, Christopher Bronk. "Radiocarbon calibration and analysis of stratigraphy; the OxCal program. *Radiocarbon , 37* (2), 425-430.

Rees, L. (1929). The Transjordan desert. *Antiquity , 3* (12), 389-407.

Rees-Jones, J. (1995). Optical dating of young sediments using fine-grain quartz. *Ancient TL , 13* (2), 9-14.

Reimann, T., Tsukamoto, S., Naumann, M., & Frechen, M. (2011). The potential of using K-rich feldspars for optical dating of young coastal sediments – A test case from Darss-Zingst peninsula (southern Baltic Sea coast). *Quaternary Geochronology , 6* (2), 207-222.

Renne, P., Sharp, W., Deino, A., Orsi, G., & Civetta, L. (1997). 40Ar/39Ar dating into the historical realm: calibration against Pliny the Younger. *Science , 277* (5330), 1279-1280.

Roberts , R. (1997). Luminescence dating in Archaeology: from origins to optical. *Rad Meas , 27*, 819-892.

Roberts, H., & Wintle, A. (2003). Luminescence sensitivity changes of polymineral fine grains during IRSL and [post-IR] OSL measurements. *Radiation Measurements , 37* (6), 661-671.

Sinclair, W., & Fergusson, D. (1902). *The travels of Pedro Teixeira: with his "Kings of Harmuz" and extracts from his "Kings of Persia.* London: Hakluyt Society.

Singarayer, J., & Bailey, R. (2003). Further investigations of the quartz optically stimulated luminescence components using linear modulation. *Radiation Measurements , 37* (4), 451-458.

Skriver, C. (2006). *FHM 4662 Sellekås.* Moesgård Museum.

Sohbati , R., Murray , A., Jain , M., Buylaert , J., & Thomsen, K. (2011). Investigating the resetting of OSL signals in rock surfaces. *Geochronometria , 38*, 249-258.

Spooner, N. A. (1994). On The Optical Dating Signal From Quartz. *Rodiarion Measurements , 23*, 593-600.

Spooner, N. (1992). Optical dating: preliminary results on the anomalous fading of luminescence from feldspars. *Quaternary Science Reviews , 11* (1), 139-145.

Templer, R. (1986). The localised transition model of anomalous fading. *Radiation Protection Dosimetry , 17* (1), 493-497.

Theocaris , P., Liritzis , I., Lagios , E., & Sampson, A. (1997). Geophysical prospection and archaeological test excavation and dating in two Hellenic pyramids. *Surveys in Geophysics , 17*, 593-618.

Thiel, C., Buylaert, J. P., Murray, A. S., Terhorst, B., Hofer, I., Tsukamoto, S., et al. (2011). Luminescence dating of the Stratzing loess profile (Austria) - Testing the potential of an elevated temperature post-IR IRSL protocol. *Quaternary International , 234*, 23- 31.

Thomsen , K., Jain , M., Bøtter-Jensen , L., & Murray , A. (2003). Variation with depth of dose distributions of single grains of quartz extracted from an irradiated concrete block. *Radiation Measurements , 37*, 315-321.

Thomsen , K., Bøtter-Jensen, L., Denby , P., Moska , P., & Murray, A. (2006). Developments in luminescence measurement techniques. *Radiation Measurements , 41*, 768-773.

Thomsen , K., Murray , A., & Bøtter-Jensen, L. (2005). Sources of variability in OSL dose measurements using single grains of quartz. *Radiation Measurements , 39* (1), 47-61.

Thomsen, K., Murray, A., Bøtter-Jensen, L., & Kinahan, J. (2007). Determination of burial dose in incompletely bleached fluvial samples using single grains of quartz. *Radiation Measurements , 42* (3), 370-379.

Thomsen, K., Murray, A., & Jain, M. (2011). Stability of IRSL signals from sedimentary K-feldspar samples. *Geochronometria , 38*, 1-13.

Thomsen, K., Murray, A., Jain, M., & Bøtter-Jensen, L. (2008). Laboratory fading rates of various luminescence signals from feldspar-rich sediment extracts. *Radiat.Meas. 43, 1474–1486 , 43*, 1474-1486.

Vafiadou, A., Murray, A., & Liritzis, I. (2007). Optically stimulated luminescence (OSL) dating investigations of rock and underlying soil from three case studies. *Journal of Archaeological Science , 34* (10), 1659-1669.

Vinter, M. (2012). *Søften Erhverspark, Gamma 5 og Omega 15.* Moesgaard Museum.

Visocekas, R. (1982). Tunnelling radiative recombination in labradorite: its association with anomalous fading of thermoluminescence. *Radiation Measurements (1982) 10.4 (1985): 521-529. , 10* (4), 521-529.

Wallinga, J., Bos, A., Dorenbos, P., Murray, A., & Schokker, J. (2007). A test case for anomalous fading correction in IRSL dating. *Quaternary Geochronology , 2*, 216–221.

Wallinga, J., Murray, A., & Wintle, A. (2000). The single-aliquot regenerative-dose (SAR) protocol applied to coarse-grain feldspar. *Radiation Measurements , 32* (5), 529-533.

Wild, E.-M., & Fischer, P. (2013). Chapter 4- Radiocarbon Dating. In P. Fischer, *Tell Abu Kharaz. Volume III. The Iron Age* (pp. 457-463). Vienna: Austrian Academy of Sciences Press.

Wintle , A. (2008). Fifty years of luminescence dating. *Archaeometry , 50* (2), 276-312.

Wintle, A. (1977). A thermoluminescence dating study of some Quaternary calcite: potential and problems. *Canadian Journal of Earth Sciences , 15* (12), 1977-1986.

Wintle, A. (1973). Anomalous fading of thermoluminescence in minerals. *Nature , 245*, 143-144.

Wright, W. (1895). *An account of Palmyra and Zenobia with travels and adventures in Bashan and the desert.* London: T. Nelson Edition.

Zeder, M., Bar-Oz, G., Rufolo, S., & Hole, F. (2013). New perspectives on the use of kites in mass-kills of Levantine gazelle: a view from northeastern Syria. *Quaternary International , 297*, 110-125.

Europass
Curriculum Vitae

For reasons of data protection, the curriculum vitae is not published in the electronic version

For reasons of data protection, the curriculum vitae is not published in the electronic version

For reasons of data protection, the curriculum vitae is not published in the electronic version